

Human interventions in river-estuary systems

A case study of the Loire, France

A. Kusters

Human interventions in river-estuary systems

A case study of the Loire, France

by

A. (Anna) Kusters

to obtain the degree of Master of Science
at Delft University of Technology,
to be defended publicly on Tuesday June 4, 2019 at 16:00.

Student number: 4247310
Thesis committee: Prof. dr. ir. Z.B. Wang, TU Delft/Deltares, chair
Dr. ir. E. Mosselman, TU Delft/Deltares
Dr. D.S. van Maren, TU Delft/Deltares

An electronic version of this thesis is available at <http://repository.tudelft.nl/>.

Cover photo: View over the Loire estuary. Courtesy: Comité Régional du Tourisme Centre-Val de Loire, 2018.

Preface

With this thesis I conclude my MSc studies in Hydraulic Engineering at the Faculty of Civil Engineering and Geosciences of Delft University of Technology. The great pleasure with which I have been working on this project is due not only to the challenging and complex subject of human interventions in river-estuary systems, but also to the enjoyable working environment at Deltares, where I carried out this research.

I would not have been able to carry out this project without the guidance and support of my supervisors. The broad expertise they offered helped me steer this research toward the result presented in this report.

I would like to express my gratitude to professor Zheng Bing Wang for chairing the committee and providing valuable feedback during the committee meetings. I also want to thank Erik Mosselman, who introduced me to the subject of this thesis. The conversations we had throughout the research period helped me time and again to see the project with new eyes and put it into a bigger perspective. Finally, I owe many thanks to Bas van Maren, who helped me discover and unravel the fine sediment dynamics in the Loire estuary. Your enthusiasm for the subject made our discussions always last much longer than anticipated, but they proved to be crucial to keep the project on track. In particular, I appreciate your help with the many modelling issues I encountered during the process.

Next to the members of the thesis committee, many other people at Deltares helped me with specific questions and modelling issues, among whom are Willem Ottevanger, Jan van Kester and Kees Sloff. Of course, many thanks go out also to the ever-growing group of graduate students at Deltares. Helping and motivating each other is such a valuable part of our projects and without you, the graduation process would not have been the same.

Finally, I want to thank my family and friends, who were always there to support me in every possible way.

*Anna Kusters
Delft, May 2019*

Summary

Like many rivers around the world, the Loire river in France has a history of human interventions in order to facilitate navigation and port development. Furthermore, large-scale extraction of sediment has taken place for construction purposes. Next to affecting bed levels directly, the heavy modification of the river-estuary has induced significant changes in the hydrodynamic and morphodynamic behaviour of the Loire. As a result, the Loire river is experiencing bed degradation, with lowering of bed levels of up to 4 m over the last century (Pérard, 2018). In the estuary, the interventions have led to an amplification of the tidal amplitude, a shift of the tidal and salt intrusion limit in upstream direction and a larger tidal asymmetry. According to Winterwerp and Wang (2013), this tidal deformation leads to an increased import of fine sediment in the estuary and a reduced hydraulic drag. This in turn enhances tidal deformation further. Due to this positive feedback mechanism the Loire estuary has evolved into a hyper-turbid state, associated with large suspended sediment concentrations and the formation of fluid mud.

To counteract bed degradation, several interventions are planned for implementation in the coming years. However, the behaviour of the river-estuary on large temporal and spatial scales and its response to historical and possible future interventions is not yet sufficiently understood. Therefore, an idealized, computationally efficient, three-dimensional morphodynamic model of the river-estuary is developed with the FLOW module of the Delft3D software suite (Deltares, 2014), in which the main processes influencing the morphology of the Loire river-estuary are included and interventions can be simulated. The system geometry is represented with one flow-carrying channel, with elevated floodplains and intertidal areas on both sides. Over the first 50 km from the river mouth, the width of the estuary converges exponentially, after which the width is kept constant up to the landward model boundary, at 115 km upstream of the mouth. The converging section is called the estuary in this research, whereas the part with constant width is referred to as the river section.

The current estuarine geometry, lacking the presence of large intertidal areas, induces a flood-dominant tidal signal. The river discharge introduces a mean seaward-directed velocity, but also enhances the flood-dominance of the tide by preferential damping of the ebb tide. In the mouth of the estuary, the baroclinic pressure gradient introduces a mean landward-directed velocity near the bed and amplifies the mean seaward-directed velocity near the surface. Only when this pressure gradient is included, net sand and mud transport in the estuary mouth are landward-directed for almost all considered discharges ($200 \leq Q \leq 6000 \text{ m}^3/\text{s}$). The gravitational circulation causes the formation of an Estuarine Turbidity Maximum (ETM) at the tip of the salt wedge, which is strengthened further by the flood-dominance of the tide. The ETM forms closer to the mouth and has a smaller extent for larger discharges. Model results confirm the feedback mechanism between tidal deformation, the import of fine sediment and the effective hydraulic drag as described above. However, next to tidal deformation, strengthening of the gravitational circulation also plays a large role in this mechanism for the Loire. Furthermore, model results indicate that historical deepening of the estuary has led to retrogressive erosion in the river section.

To mitigate bed degradation, several measures are simulated that decrease the transport capacity of the flow, increase the sediment supply or do both. Over the first 10 years, sediment nourishments are the most effective according to the model. However, after 100 years of simulation the removal of all groynes present in the river section leads to the most sedimentation relative to the reference scenario. On this centennial scale, it is important to account for the influence of climate change when assessing the effects of measures.

To decrease the import of mud into the estuary, two measures have been investigated. Increasing bed levels in the main channel of the estuary mainly leads to a decrease of the tidal range, whereas restoring tidal flats turns the tide from flood- into ebb-dominant. In both cases, a decrease of the salt intrusion length and a significant weakening of the gravitational circulation occurs, leading to a tidally averaged export of fine sediment and very low mud concentrations, in the water column as well as in the bed.

Model results appear sensitive to the schematization of the tidal motion at the downstream boundary. It is recommended to investigate further which simplifications of the tide are justified in situations where the interaction between river discharge and tide is significant. The sensitivity of model results to changes in morphological parameters and the configuration of measures should be tested as well. Furthermore, model results would benefit from an improved understanding and model representation of sand-mud interaction processes and fluid mud dynamics.

Contents

1	Introduction	1
1.1	Background	1
1.2	Problem statement	2
1.3	Objectives.	3
1.4	Research questions	3
1.5	Approach and limitations.	3
1.6	Reading guide.	5
2	Literature review	6
2.1	River bed degradation.	6
2.2	Bed degradation in the Loire river.	7
2.3	Measures to mitigate bed degradation	7
2.3.1	Sediment nourishments	7
2.3.2	Groyne modification	7
2.3.3	Longitudinal training dams	8
2.3.4	Fixed bed layer	9
2.3.5	Side channels	9
2.4	Residual sediment transport in estuaries	10
2.4.1	Overtides	10
2.4.2	River discharge	11
2.4.3	Mixing processes and ETM formation	11
2.5	Description of the Loire estuary.	12
2.6	Effects of historical interventions in the Loire estuary.	13
2.6.1	Tidal deformation and salt intrusion	13
2.6.2	Consequences	14
2.7	Measures in the estuary.	14
3	Approach and model set-up	15
3.1	Idealized modelling of river-estuary systems	15
3.2	Grid and bed topography	16
3.3	Boundary conditions	17
3.3.1	Flow	17
3.3.2	Transport of salt and sediment	19
3.4	Model settings for morphology	19
3.4.1	Sediment transport	19
3.4.2	Morphological acceleration factor	21
3.5	Hydrodynamic calibration	22
3.6	Simulation approach	25
3.6.1	Sediment nourishments	26
3.6.2	Groyne removal	26
3.6.3	Side-channel restoration	26
3.6.4	Energy loss structure	27
3.6.5	No maintenance dredging	27
3.6.6	Climate change	27
3.6.7	Historical deepening	28
3.6.8	Estuarine bed elevation	28
3.6.9	Tidal flat restoration	28
3.6.10	Combination scenarios	29
3.7	Computational efficiency	29

4	Model application	30
4.1	Hydrodynamic process analysis.	30
4.2	Sand transport	33
4.2.1	Influence of hydrodynamic processes	33
4.2.2	Reference situation	34
4.2.3	Measures to mitigate bed degradation	35
4.2.4	Combinations of measures	39
4.2.5	Sensitivity to changes in boundary conditions: climate change	40
4.3	Mud transport	41
4.3.1	Influence of hydrodynamic processes	41
4.3.2	Consequences of historical deepening	43
4.3.3	Measures to decrease turbidity	47
4.3.4	Sensitivity to changes in boundary conditions: tidal schematization	49
4.4	River-estuary interaction	52
5	Discussion	53
5.1	Simplifications	53
5.2	Consequences of numerical modelling approach.	54
5.3	Applicability to other river-estuaries	55
5.4	Relation to literature	55
6	Conclusions and recommendations	56
6.1	Conclusions.	56
6.2	Recommendations	58
6.2.1	Management of the Loire river-estuary	58
6.2.2	Further research	58
	Bibliography	60
A	Velocity under baroclinic forcing	65
B	Overview of measured SSC	67
C	Mud simulation results	68
C.1	Discharge	68
C.2	M2 component	71
C.3	M2, M4 and S2 component	76
D	Analysis of salt transport with sediment tracer simulations	77
D.1	Reference simulation: current situation.	78
D.2	Estuarine bed elevation	79
D.3	Tidal flat restoration	80

List of acronyms

CC	Climate change
CM	Cote Marine (FR)
EBE	Estuarine bed elevation
ELS	Energy loss structure
ETM	Estuarine Turbidity Maximum
GR	Groyne removal
HC	Hydrograph compression
HD	Historical deepening
HW	High Water
LW	Low Water
MF	Morphological factor
NMD	No maintenance dredging
R	Reference scenario
RCP	Representative Concentration Pathway
SC	Side-channel restoration
SN	Sediment nourishments
SSC	Suspended sediment concentrations
TFR	Tidal flat restoration

Introduction

1.1. Background

Like many rivers around the world, the Loire river in France (see Figure 1.1) has a history of human interventions in order to facilitate navigation and port development. These interventions include the construction of 700 groynes between Nantes and Angers to narrow the main channel, cutting off secondary branches, extensive dredging activities throughout the 20th century and the reclamation of intertidal areas in the estuary (Brière et al., 2011b). Upstream of Nantes a tidal basin, known as the *Bassin à Marée*, was created (1913-1920). This intervention comprised a lowering of the river bed, in order to increase tidal currents to improve navigation conditions (Brière et al., 2011b). Furthermore, over the past century more than 70 million m³ of sediment was mined upstream of Nantes for construction purposes.

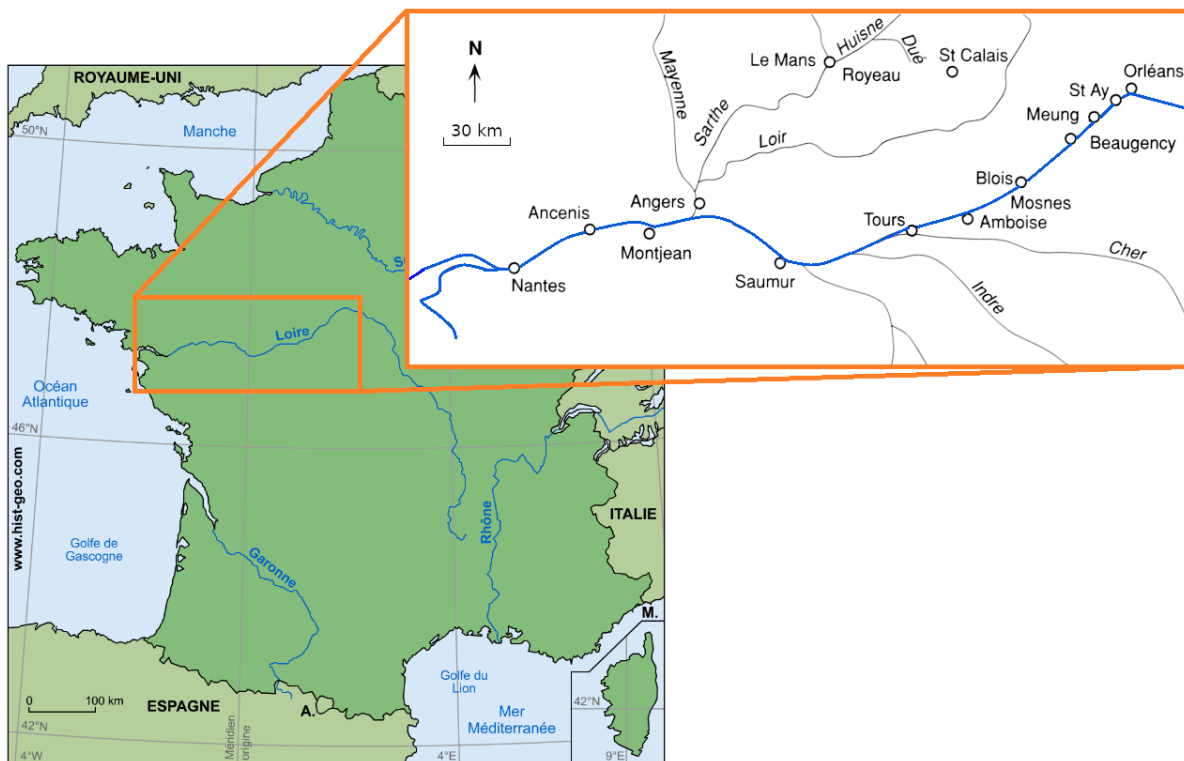


Figure 1.1: Lower Loire river and its tributaries. Sources: www.hist-geo.com and Larue (2004).

Next to affecting bed levels directly, the heavy modification of the river has induced significant changes in the hydrodynamic and morphodynamic behaviour of the Loire river. As a result, the Loire is experiencing an ongoing bed degradation, a process that has also been observed in other rivers such as the Rhine, Ems,

Elbe and Danube rivers (Koenig et al., 2012; Frings et al., 2014; Van Maren et al., 2015; Habersack et al., 2015). Between 1900 and 1990 the bed has lowered up to 4 m (Pérard, 2018). In the estuary, the interventions have led to an amplification of the tidal amplitude, a shift of the tidal limit in upstream direction and a larger tidal asymmetry (Brière et al., 2011a). Similar trends have been observed in other European estuaries (Van Maren et al., 2015). According to Winterwerp and Wang (2013), this tidal deformation leads to an increased import of fine sediment in the estuary and a reduced hydraulic drag. This in turn enhances tidal deformation further. Due to this positive feedback mechanism the Loire estuary has evolved into a hyper-turbid state, associated with large suspended sediment concentrations (SSC) and the formation of fluid mud.

The evolution of the Loire river-estuary has several adverse effects. In the historical centre of Nantes, many buildings have wooden pile foundations. Lowering of the river bed has led to lowering of groundwater levels, exposing these piles to decay processes (Brière et al., 2011a). Next to this, the stability of structures that are founded within the river bed can be compromised, a noteworthy example being the collapse of the Wilson Bridge at Tours in 1978 (Gasowski, 1994). As the bed degradation has mainly taken place in the main channel and secondary channels have not degraded equally, several channels have been cut off from the main channel and have closed as a consequence (GIP Loire Estuaire, 2003). More in general, bed degradation can expose non-erodible layers which can hamper navigation (Berkhof et al., 2018). This is less of an issue in the case of the Loire as commercial navigation does not play an important role anymore.

Furthermore, the interventions in the Loire river have decreased its ecological value as natural floodplains and wetlands have largely disappeared. The turbidity in the estuary has significantly increased, which leads to wear of ship propellers, clogging of water intakes and deoxygenation. The latter inhibits primary production and can ultimately affect the entire estuarine ecosystem. In the Loire estuary this process has led to increased mortality of fish, especially mullets (Le Hir and Thouvenin, 1992). The intake of fresh water from the river is hampered not only by the increased turbidity, but also because the salt intrusion length has increased and can nowadays reach up to 60 km upstream during low river flows (GIP Loire Estuaire, 2017).

Recognizing the negative consequences of the interventions, starting from 1995 a ban has been placed on sand extraction (Brière et al., 2011a) and under the authority of Voies Navigables de France (VNF) three strategic programmes have subsequently been put in place in order to counteract the bed degradation (Pérard, 2018). Within these programmes the causes of the degradation and the effects of interventions are investigated and several pilots and experimental measures have already been put in place. These measures include groyne remodelling, construction of sills and the removal of vegetation on sand bars (Pérard, 2018). So far, these measures have mainly been implemented on a local scale in order to study their effects. However, in the currently running, fourth programme for the Loire river, several larger interventions are prepared to be implemented. These include large-scale groyne remodelling, re-opening of the secondary channel on the north side of the île Neuve-Macrière near Ancenis and the construction of an energy loss structure at Bellevue. This structure consists of a fixed layer with a higher roughness than the river bed, aiming at counteracting further lowering of the bed and inducing sedimentation by backwater effects.

1.2. Problem statement

The river reach over which bed degradation occurs is several hundreds of kilometers long (Gasowski, 1994) and includes the estuary, which has a length in the order of 50 km (Winterwerp et al., 2013). Such a system is not only subject to the riverine supply of water and sediment, but also to marine influences such as the tidal motion and the import of marine sediment and saline water.

The studies that have been performed during the course of aforementioned programmes are each concentrated on a relatively small part of this system. An overview of these modelling studies is given in Figure 1.2. With these often detailed models, the local and short-term effects of interventions can be studied thoroughly, but only in an isolated way. The interactions between the different parts of the river are difficult to investigate, especially as there is not much consistency between the models in terms of assumptions and calibration. This also means that the mutual influence of riverine and estuarine processes remains poorly understood (Brière et al., 2011a, 2012). Furthermore, the timescale needed for a river-estuary system to reach a new equilibrium on the reach scale after an intervention depends on its specific characteristics, but is generally in the order of decades (Crosato, 2010). Such long-term simulations can only be carried out with models that cover a domain that is sufficiently large, in order to minimize the effect of boundary conditions. Thus,

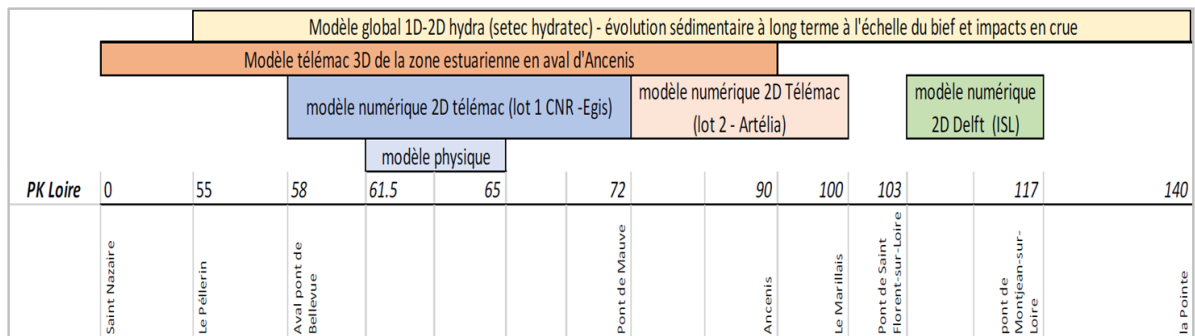


Figure 1.2: Overview of models for the Loire river and estuary (Pérard, 2018).

a model is required that includes important processes and their interactions and covers large spatial and temporal scales.

On the other hand, for an extensive assessment of measures to mitigate negative consequences of historical interventions, a large number of simulations must be carried out. Only a computationally efficient model can satisfy this requirement, which implies a high degree of schematization. This however bears the risk that important processes are not accurately represented. A balance between these conflicting demands remains to be found.

1.3. Objectives

The aim of this research is therefore twofold. The first objective is to develop a numerical schematization of the study area that is computationally efficient, but includes the main processes governing the morphological development of the river-estuary system. Subsequently, this model is used to investigate the morphological effects of human interventions, which forms the second research objective. In this investigation historical interventions are considered, but also possible future interventions that are meant to counteract negative consequences of previous measures.

1.4. Research questions

The main research question is posed as follows:

What are the effects of historical and possible future interventions in the Loire river-estuary, according to a computationally efficient morphodynamic model?

To answer the main research question, several subquestions need to be answered:

1. How can the main processes influencing the morphology of the Loire river-estuary be included in a computationally efficient morphodynamic model?
2. How do hydrodynamic processes affect the morphology of the Loire river-estuary, according to the developed model?
3. How did historical interventions affect the morphology of the Loire river-estuary?
4. Which types of measures can mitigate the negative consequences of historical interventions?
5. How sensitive are model results to changes in boundary conditions?

1.5. Approach and limitations

In order to provide answers to all abovementioned questions, the research is composed of several steps. Firstly a literature study is carried out, which already provides (part of) the answer to subquestions 1 to 4. Subsequently a model is set up in which both historical and future scenarios and strategies can be evaluated. Setting up this model will provide an answer to the first research question. The model is then used to further

explore question 2. Subsequently, a range of simulations representing historical and future scenarios and strategies is carried out. With the results of these simulations question 3 and 4 can be answered. To investigate the influence of boundary conditions on the model results, a sensitivity analysis is performed, which provides an answer to research question 5.

Model set-up

In order to explore the influence of a wide range of processes and interventions in a qualitative way, a highly schematized, idealized model representation is expected to be most suitable. This consideration is substantiated further in Section 3.1.

Because the model has to represent vertical gradients in salinity, sediment concentration and velocity, multiple layers are needed in the vertical. Furthermore, floodplains and intertidal areas must be represented as these geometrical features have a large influence on hydrodynamic processes. This requires multiple cells in the lateral dimension as well, resulting in a three-dimensional (3D) morphodynamic model. By keeping the grid resolution as low as possible, it is still possible to create a computationally efficient model, meeting the demands mentioned in Section 1.2. For the model set-up, the state-of-the-art Delft3D modelling software (Deltares, 2014) is used. This software has been tested and used for a wide range of applications and has been applied successfully to a large number of estuaries.

The Loire estuary has a macrotidal character with a tidal range at the mouth of 2.5 to 5 m (GIP Loire Estuaire, 2013) and an average river flow of 845 m³/s. Both tide and river discharge play an important role in sediment transport and therefore need to be represented in the model. Salinity-driven gravitational circulation plays a large role in Estuarine Turbidity Maximum (ETM) formation and must therefore be included in the model as well. As the Loire is a narrow, sheltered estuary with macrotidal conditions, waves only play a role in the mouth of the estuary (Dronkers, 2017). For simplicity, the influence of waves is excluded from our analysis, which is therefore not applicable to the estuarine mouth zone. The importance of the Coriolis force relative to inertia can be assessed with the Rossby number:

$$Ro = \frac{U}{fL} \quad (1.1)$$

with:

- U characteristic flow velocity [m/s]
- L characteristic length scale of the estuary [m]
- f Coriolis frequency, $f = 2\Omega \sin(\phi)$

with:

- Ω angular frequency of planetary rotation, $\Omega = 7.2921159 \times 10^{-5}$ [rad/s]
- ϕ latitude [°], $\phi = 47^\circ$ N for the Loire

For the Loire, Ro attains a value of about 10, indicating that inertia is more important than the Coriolis force. The Coriolis force is therefore neglected in this case, acknowledging that it can play a minor role in for example lateral sediment trapping (Burchard et al., 2018).

Data collection

Information needed for the model set-up is mainly retrieved from literature and technical reports issued by Groupement d'Intérêt Public (GIP) Loire Estuaire (GIP Loire Estuaire, 2011, 2013, 2014), Deltares (Brière et al., 2011a,b, 2012), VNF (Pérard, 2018; Voies Navigables de France, 2016a,b) and Hydratec (2013). From these reports information is retrieved regarding geometry, sediment transport and characteristics, historical development and planned interventions.

Hourly water level measurements are performed at 6 stations along the estuary, i.e. Saint-Nazaire, Donges, Paimboeuf, Cordemais, Le Pellerin and Nantes Usine Brûlée, by Service Hydrographique et Océanographique de la Marine (SHOM, data.shom.fr). Daily discharge and water level measurements are conducted by Direction Régionale de l'Environnement, de l'Aménagement et du Logement (DREAL) Pays de la Loire at six stations along the river (www.hydro.eaufrance.fr). The longest record of discharges is present at the station Montjean-sur-Loire (117 km upstream of the mouth), where measurements have been performed from 1863 onward. Furthermore, from 2007 onward continuous monitoring (measurements every 10 minutes) of dissolved oxygen, salinity, temperature and turbidity is performed at 6 stations (Donges, Paimboeuf, Cordemais, Le Pellerin, Trentemoult, Bellevue). This monitoring network is set up and maintained by GIP Loire Estuaire (www.loire-estuaire.org) and is called Système de Veille dans l'Estuaire de la Loire (SYVEL). Abovementioned data sources are used for model set-up and calibration.

1.6. Reading guide

In this research, a clear distinction can be made between mud and sand transport processes. Sand is mainly transported as bed load (see Section 3.4) and is important for the long-term development of the river bed. The effectiveness of measures to mitigate bed degradation will be assessed by looking at the development of the sandy bed profile. Mud transport mostly takes place in suspension and is important for the formation of turbidity zones and fluid mud in the estuary, processes that take place on a much smaller timescale than river bed degradation. The effectiveness of measures to decrease the turbidity in the estuary will be assessed by looking at SSC and the amount of mud deposited on the bed. Hence, both Chapter 2 (Literature review) and 4 (Model application) can be divided in two parts; one regarding mud transport and one regarding sand transport. As mud and sand simulations are performed with the same model, in which only sediment characteristics and simulation time differ, Chapter 3 (Model set-up) is valid for both types of sediment. Figure 1.3 gives an overview of the report structure.

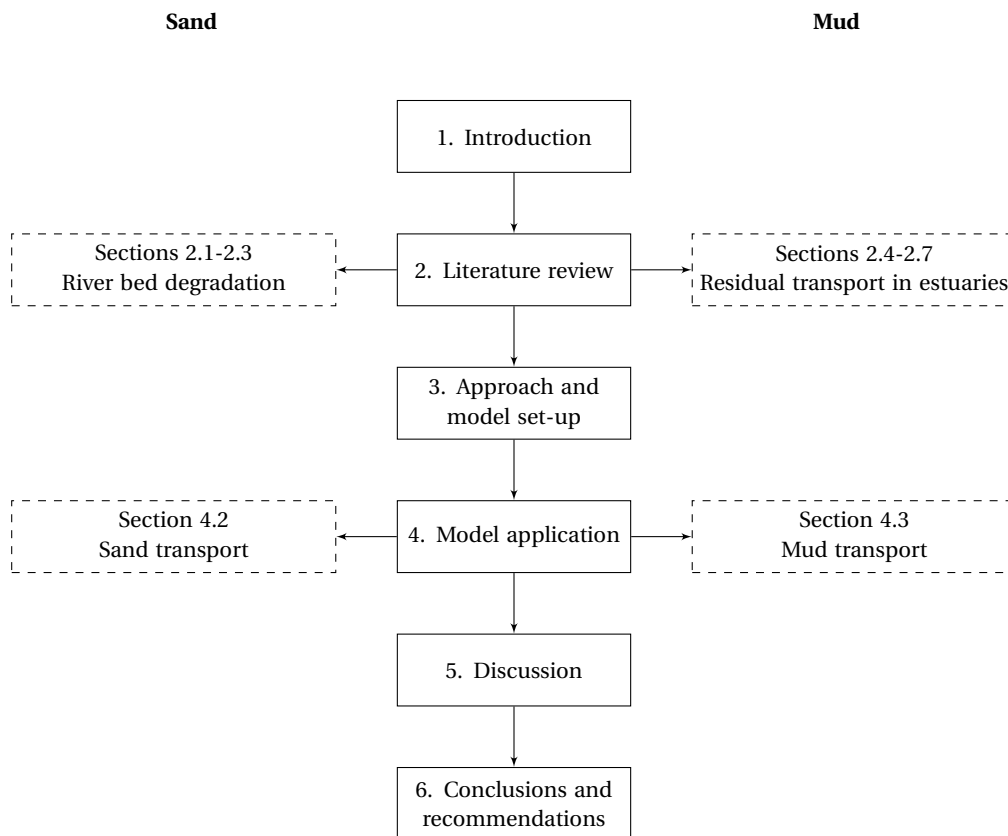


Figure 1.3: Reading guide.

2

Literature review

2.1. River bed degradation

A river is a dynamic system, formed by the interaction between water motion, sediment transport and bed elevation (De Vriend, 2006). If in these components no changes take place in time anymore, the system has reached an equilibrium situation. In this morphodynamic steady state, the river bed has adjusted such that all sediment supplied from upstream can be transported in downstream direction. In reality the discharge of water and sediment is always variable, for example due to seasonal changes. However, also under variable flow a river reach can find a dynamic equilibrium, if the timescale of changes in the channel slope is much larger than the timescale of changes in the discharge of water and sediment (Wright and Crosato, 2011).

If interference takes place in a river, the system needs to find a new equilibrium profile. Often human interventions are the cause of these transitions. Seeking to make optimal use of the services the river provides, we change the river system.

The evolution of the system towards a new equilibrium is marked by changes in the average channel slope. Bed degradation thus occurs in two types of situations (Galay, 1983):

1. Downstream progressing degradation is generally the result of changes in one or more independent variables, imposing a flattening of the channel slope. These independent variables comprise water discharge, sediment load and sediment characteristics.
2. Upstream progressing degradation is generally the result of an intervention downstream imposing a slope that is too steep. As the system seeks to return to a flatter slope, degradation occurs.

Galay (1983) notes that upstream progressing degradation generally proceeds at a much faster rate, as the steeper slope leads to an increase in bed material discharge. In the case of downstream progressing degradation the rate of slope flattening often decreases asymptotically. An example of bed degradation of the first type is the construction of a dam upstream of the considered reach, either in the river itself or in one of its tributaries, blocking the supply of sediment from upstream. An example of the second type is a decrease of the river length by a cutoff. Channelization can be seen as the creation of a long series of cutoffs. Often this is combined with regulation, which aims at creating a prismatic channel, using river training works. Also a lowering or shift in the base level or the removal of a control point can lead to degradation progressing upstream.

Some interventions may lead to both upstream and downstream progressing degradation. An example is the excavation of bed material, e.g. for construction purposes. If sediment is extracted at the same location on a regular basis, initially bed erosion will start at the extraction location and progress in downstream direction. A new equilibrium is found when the sediment transport capacity downstream of the extraction point reduces to the incoming sediment load minus the sediment extraction rate. This state is characterized by a decrease in bed slope and an increase in water depth downstream of the extraction location. Ultimately the lowering of the water level at the extraction location will lead to a lowering of the river bed upstream of the intervention as well (Crosato, 2010).

It is not uncommon that upstream and downstream progressing degradation occur within the same river reach. Also in the Loire river this is the case.

2.2. Bed degradation in the Loire river

Up till the 18th century, the lower Loire river and estuary formed a natural, meandering system, containing multiple islands and channels (Maquet, 1974). In 1859, construction of the first dikes and groynes started between la Martinière and Nantes (Brière et al., 2011a). From that moment onward, the Loire river has been characterized by large-scale river training. Brière et al. (2011a) and Maquet (1974) give detailed chronological overviews of interventions within the estuary from Saint-Nazaire to Nantes, comprising channelization and channel deepening, reclamation of intertidal areas, sediment extraction and the removal of a rocky sill at Bellevue. Also upstream of Nantes the river has been channelized with the construction of about 700 groynes. Furthermore, for the past century the Loire river has been a major source of sand and gravel for construction purposes. A total amount of more than 70 million m³ of sediment has been extracted upstream of Nantes in the period 1920-1993, whereas the natural riverine sediment supply is in the order of 0.5 to 0.8 million m³/y (Gasowski, 1994; Brière et al., 2011a). Dams have been constructed in the upper basin of the Loire, but these have only a small impact on the morphology of the lower river reaches (Gasowski, 1994).

From these interventions, a number of degradational processes can be deduced, referring back to Section 2.1. Firstly, the large-scale extraction of sediment has led to upstream and downstream progressing degradation. Channelization and regulation have led to narrowing of the cross-section and a decrease of the river length. These interventions mainly induce degradation along and upstream of the regulated reach. Channel deepening in the river mouth can be seen as a landward shift of the base level, which means the river is shortened. The bedrock outcrop at Bellevue formed a control point. Removal of a control point usually leads to upstream progressing degradation. One is referred to Galay (1983) and Crosato (2010) for schematizations of all abovementioned processes.

Gölz (1994) notes that the extent and course of degradation are controlled by the bed surface and subsurface characteristics, e.g. slope, sediment composition and the degree at which armouring takes place.

2.3. Measures to mitigate bed degradation

As bed degradation is such a commonly occurring process, several countermeasures have been investigated and implemented. A number of commonly proposed mitigating measures is discussed below, along with measures investigated specifically for the Loire river. It should be noted that, except for sediment nourishments, the proposed interventions cannot be adapted or reversed easily. Effects of these interventions should therefore always be investigated thoroughly before implementation is considered.

2.3.1. Sediment nourishments

With sediment nourishments, sediment is supplied artificially, aiming at bed stabilization at the nourished location and further downstream (Gölz, 1994). Due to backwater effects, nourishments can also promote sedimentation upstream (Mosselman et al., 2007). Important factors that influence the behaviour of nourishments are nourishment volume, location, and frequency. Furthermore, the grain size distribution of the nourished sediment is of importance. If the supplied sediment is coarser than the naturally present bed load, downstream of the nourishment degradation may occur due to the reduced sediment supply from upstream (Rudolph, 2018). An advantage of this measure is its flexibility and relatively low capital costs (Berkhof et al., 2018).

In the German Rhine, nourishment of coarse sediment has been used since 1978 as a measure to counteract bed degradation. Although this measure is effective in Germany, it might contribute to the bed degradation that is currently observed further downstream in the Dutch Rhine branches due to the abovementioned effect (Blom, 2016). On a larger timescale, however, downstream migration of the nourishment may lead to stabilization of the bed at these locations as well.

In the Netherlands, Rijkswaterstaat has started a pilot to test the applicability of sediment nourishments in the Rhine branches with a first nourishment carried out in 2016 and a second one planned for 2019 (Niessen and Becker, 2018). The effectiveness of this pilot is currently investigated.

2.3.2. Groyne modification

The modification of groynes, for example by shortening or lowering, may counteract bed degradation along the modified reach (Sloff et al., 2014). In river stretches where bed degradation goes on, groynes can increas-

ingly form an obstacle within the flow as these structures remain fixed at their original elevation. By decreasing the dimensions, the conveyance capacity of the river is increased and water levels are decreased. Groyne lowering only affects the conveyance capacity when water levels exceed the new crest level, whereas shortening increases the conveyance capacity at all times. An increase in the flow-carrying cross-section leads to a reduction of flow velocities in the main channel, such that sedimentation might occur here. In case of groyne lowering, erosion is expected to occur in the groyne fields as a larger part of the flow will be directed here in case of a high discharge event (Liefveld et al., 2011). However, the scour holes just downstream of each groyne tip will become shallower.

Downstream of the modified reach, erosion is expected to occur initially, but this effect may be compensated by the sedimentation wave travelling from the upstream end of the intervention in downstream direction (Sloff et al., 2014). Eventually, the steeper slope along the modified reach may lead to an increase in bed levels upstream of the intervention as well. However, this new equilibrium can only be reached after many decades.

In the Loire river, large-scale groyne remodelling is planned between Oudon and Anetz, as well as between Ingrandes and Montjean-sur-Loire (see Figure 2.1). Near Anetz, the interventions mainly consist of groyne lowering, whereas just upstream of Oudon a large number of groynes will be removed completely. Between Ingrandes and Montjean-sur-Loire, a combination of removal, lowering and shortening is applied (Voies Navigables de France, 2018). Groyne removal can be seen as an extreme case of groyne modification, with the largest effect on conveyance capacity. As commercial navigation is not important on the Loire river, the decrease in navigable depth as a consequence of this intervention might not present problems. Effects of the planned interventions on navigation are currently investigated (Voies Navigables de France, 2018).



Figure 2.1: Planned interventions in the Loire river between Ponts-de-Cé and Nantes. Source: Voies Navigables de France (2018).

Next to counteracting bed degradation at the location of the interventions, a main aim of the modifications is to release large volumes of sediment that are currently trapped in the groyne fields (Pérard, 2018). The increase in sediment supply is expected to lead to sedimentation further downstream. For the stretch between Ponts-de-Cé and Nantes (90 km long), the total trapped volume is estimated at 12.6 million m^3 (Hydratec, 2013), which is an order of magnitude larger than the annual riverine sediment supply (0.5 to 0.8 million m^3). However, groyne modification will not lead to a complete release of the trapped sediment volume. In a model study conducted by Hydratec (2013), a simulation in which all groynes between Ponts-de-Cé and Nantes are removed is compared to a reference scenario without interventions over a period of 40 years. Results show an erosion within the modified groyne fields of 1.5 million m^3 over the entire period, whereas in the reference scenario an additional 0.5 million m^3 would be trapped in these fields. Of this total sediment surplus of 2 million m^3 , 60% is estimated to be deposited further downstream, whereas the remaining 40% leaves the system without contributing to sedimentation. So, only a small fraction of the total trapped sediment volume within a groyne field will be released and deposited downstream if the groynes are removed. Groyne lowering or shortening will have an even smaller effect.

2.3.3. Longitudinal training dams

Within the Room-for-the-River programme in the Netherlands, groynes have been replaced with longitudinal dams at several locations. These dams are situated parallel to the bank instead of orthogonal to it, at about the same distance from the bank as the toes of the former groynes. Just like groynes, longitudinal dams nar-

row the channel cross-section at low water levels. During high discharges, however, the openings between the dam sections flow over and the channels behind the dams become part of the conveying cross-section. Compared to a situation with groynes, an increase in conveyance area is expected, as well as a decrease in flow resistance. In this way, water levels are lowered and flood risk is decreased, which is one of the principal aims of the Room-for-the-River programme (Mosselman et al., 2007). Another effect of this mechanism is that in the main channel, flow velocities and, consequently, sediment transport capacity are reduced. Therefore, replacing groynes with longitudinal dams has a potential to mitigate bed degradation in the main channel. Initially however, sedimentation might be preceded by an expanding erosion wave downstream of the intervention (Sloff et al., 2014). The local morphological response strongly depends on the specific configuration of the longitudinal dams (Rudolph, 2018). Besides these hydrodynamic and morphodynamic effects, longitudinal training dams aim at providing space for ecological development and recreation in the sheltered channels behind the dams (Rijkswaterstaat Oost-Nederland, 2016).

For the Loire river, the planned interventions do not include the replacement of groynes with longitudinal dams. This intervention is therefore not investigated further in this study.

2.3.4. Fixed bed layer

A natural rocky outcrop used to be present in the river near Bellevue, just upstream of Nantes. In the 1960s this sill was largely removed as it formed an obstacle for navigation (Voies Navigables de France, 2016a). In the period 1973-1976 the navigation channel was moved to the southern bank by dredging of the river bed south of the rocky outcrop (Brière et al., 2011a). These activities have contributed to the degradation of the bed at this location and further upstream. To counteract this process and partly restore the bed to its original situation, an energy loss structure will be implemented at the location of the rocky outcrop. Execution of the works is planned for 2020-2022. The structure consists of a fixed bed layer of more than 1 km long with a higher roughness than the river bed. The goal of the fixed layer is to stabilize the bed at Bellevue, while the increased roughness leads to backwater effects, inducing sedimentation upstream of the structure. An estimated amount of 1.5 billion kg (about 0.5 million m³) of sediment has been predicted to be deposited between Bellevue and Ancenis due to this effect (Voies Navigables de France, 2016a). However, it can be expected that downstream of the intervention (increased) erosion will occur due to the reduced sediment supply (Rijkswaterstaat Oost-Nederland, 2016). Additional measures are needed to prevent this.

2.3.5. Side channels

Another measure that is investigated for the Loire is re-opening side channels. Between Angers and Nantes, secondary branches cover an area of more than 2600 hectares. Discharge of water and sediment into these channels is often regulated by man-made structures. However, many of these channels are detached from the main channel for an increasing period of time each year, because they do not degrade at a rate equal to that of the main channel. This process does not only contribute to further erosion of the main channel, but also represents the loss of ecologically valuable areas.

Restoration of secondary channels can be a viable option to counteract bed degradation. When secondary channels start to carry flow (often only above a certain discharge), the conveyance area of the river increases, reducing flow velocities in the main channel. This can lead to sedimentation in the main channel, comparable to the effect of longitudinal training dams (see Section 2.3.3). Like in the case of longitudinal dams, erosion can be expected at the location where the secondary channel reattaches to the main channel, due to a sudden increase in flow velocities (Sloff et al., 2014).

Restoration of a side channel just downstream of Ancenis, the *Bras de l'Île Neuve-Macrière*, is planned for the period 2019-2022 (Pérard, 2018). Currently, sills are situated at both ends of this secondary branch to limit the discharge into the channel, see Figure 2.2. Due to the bed degradation of the main channel, which is particularly large at this location, the side channel is elevated with respect to the main channel, such that it starts to carry flow only for discharges above 800 m³/s (Voies Navigables de France, 2016b). As a result, the branch has largely silted up. By removing the sills, flow through the side channel will increase. Details of the intervention and complementary measures to keep the channel from closing, such as dredging activities within the secondary branch, are currently being investigated.

Next to a reduction of flow velocities in the main channel, restoring the secondary branch also aims at the release of sediment that is currently trapped here. Furthermore, a large amount of construction materials becomes available after the groyne removal that is also planned at this location (see Section 2.3.2 and Figure 2.2). The possibility to dump part of these materials in the main channel in order to increase the bed roughness, is being investigated as well.

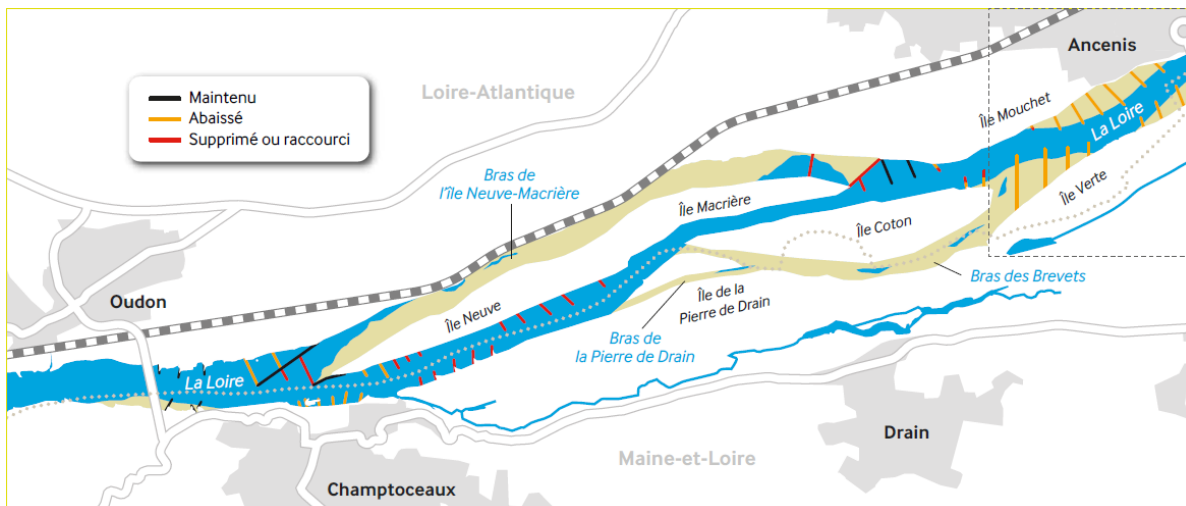


Figure 2.2: Planned interventions between Ancenis and Oudon. The black lines indicate groynes that will remain unchanged. Groynes that will be lowered are indicated in yellow, whereas the red-colored groynes will be removed completely. Source: Voies Navigables de France (2018).

2.4. Residual sediment transport in estuaries

Just as in the case of rivers, the morphology of an estuary is determined by the interaction between water motion, sediment transport and bed topography. However, while the water motion in the river is governed by the river discharge only, in the estuary the tidal motion is dominant (although in the case of the Loire, the influence of the river discharge is not negligible). The river discharge does not depend on the geometry of the channel itself, but the tidal motion is strongly influenced by the geometry of the estuary (Savenije, 2012; Dronkers, 2017). Furthermore, in the river sediment is generally transported in downstream direction, whereas in the estuary it is the difference between sediment import and export that determines morphological evolution. Many factors have an influence on this residual transport, of which several important ones will be treated here.

2.4.1. Overtides

As the tidal wave propagates up the estuary, it is deformed due to the varying basin geometry and friction. On the one hand, the exponentially decreasing width of the estuary leads to convergence of wave energy, thus to amplification of the tide. On the other hand, friction causes loss of energy and therefore a decrease of the tidal amplitude. As water depths and flow-carrying cross-sections are different for flood and ebb, the influence of basin geometry and friction also differs. As a result, the tidal wave becomes asymmetrical, meaning that the duration of the rising period is different from that of the falling period. Often, the tide is said to be flood-dominant if the rising period is shorter than the falling period. Vice versa, ebb-dominance means a shorter falling period. Ebb- or flood-dominance of the elevation signal will be translated into ebb- or flood-dominance of the velocity signal. However, this relation is non-linear and depends on the phase difference between the vertical and the horizontal tide. In alluvial estuaries, this phase lag is between 0 and 90°. Only asymmetry of the horizontal tide will lead to a residual sediment transport. A flood-dominant velocity signal implies that maximum flood velocities are larger than maximum ebb velocities. As sediment transport scales with the flow velocity to a certain power n (where n typically ranges between 3 and 5), this results in a net bed load transport in landward direction. Contrarily, an ebb-dominant signal leads to a net seaward transport (Wang et al., 1999). The same holds for suspended load, but here an additional effect plays a role as fine sediment does not react instantaneously to the flow conditions. It is found that residual transport of fine sediment depends on the duration of high and low water slack. During the slack periods, velocities are so small that fine sediment particles get the chance to settle. Generally, a longer high-water slack leads to a net landward transport of fines, whereas a longer low-water slack implies net export of fines (Wang et al., 1999).

The deformation of the tidal wave can be described by the inclusion of higher harmonics, i.e. tidal constituents of which the period is an integer fraction of the period of the basic astronomical constituents (Bosboom and Stive, 2015). The effect of varying basin geometry is accounted for by the inclusion of a wave with

twice the frequency of the basic harmonic. In this way, the M4 tidal constituent is generated from the M2 tide. Non-linear effects caused by the quadratic dependence of bottom friction on current speed are accounted for by tidal constituents with a frequency three times as high as the basic frequency. In case of the M2 tide, this leads to inclusion of the M6 tidal constituent. In the Loire, the M6 component is small compared to the M4 component and is therefore not considered further in this study.

Summation of the M2 and M4 tidal constituents leads to the following equation for the water surface elevation:

$$\zeta(t) = a_{M2} \cos(\omega_{M2}t - \varphi_{\zeta, M2}) + a_{M4} \cos(\omega_{M4}t - \varphi_{\zeta, M4}) \quad (2.1)$$

With a the amplitude [m], ω the frequency [°/s] and φ the phase [°]. Using $\omega_{M4} = 2\omega_{M2}$ and $t' = t - \varphi_{M2}/\omega_{M2}$, this can be written as:

$$\zeta(t') = a_{M2} \cos(\omega_{M2}t') + a_{M4} \cos(2\omega_{M2}t' + (2\varphi_{\zeta, M2} - \varphi_{\zeta, M4})) \quad (2.2)$$

Likewise, the velocity signal can be written as:

$$u(t') = \hat{u}_{M2} \cos(\omega_{M2}t') + \hat{u}_{M4} \cos(2\omega_{M2}t' + (2\varphi_{u, M2} - \varphi_{u, M4})) \quad (2.3)$$

As mentioned before, the asymmetry of the velocity signal is of importance for residual sediment transport. In this study the nature of the asymmetry, i.e. ebb- or flood-dominant, is indicated by the phase difference between the M2 and M4 velocity signals, $\Delta\varphi_u = 2\varphi_{u, M2} - \varphi_{u, M4}$. For $-90^\circ < \Delta\varphi_u < 90^\circ$, the maximum flood velocities are larger than the maximum ebb velocities, indicating flood-dominant transport. Maximum flood-dominance is reached for $\Delta\varphi_u = 0^\circ$. Furthermore, the duration of HW slack is longer than that of LW slack for $0^\circ < \Delta\varphi_u < 180^\circ$, leading to a net transport of fine sediment in flood direction.

However, it is often more convenient to use the water level signal, as water levels are easier to measure than current velocities. The M2-M4 phase difference of the horizontal and vertical tide can be related as follows:

$$\Delta\varphi_\zeta \approx \Delta\varphi_u + (\varphi_{\zeta, M2} - \varphi_{u, M2}) \quad (2.4)$$

For example, for $\varphi_{\zeta, M2} - \varphi_{u, M2} = 60^\circ$, a flood-dominant velocity signal is obtained for $-30^\circ < \Delta\varphi_\zeta < 150^\circ$, with maximum flood-dominance for $\Delta\varphi_\zeta = 60^\circ$ (Van Maren et al., 2015). Longer HW slack is reached for $60^\circ < \Delta\varphi_\zeta < 240^\circ$ (maximum at $\Delta\varphi_\zeta = 150^\circ$). However, the phase lag between surface elevation and flow velocity is not constant along the estuary. Hence, the boundaries for flood-dominance using the water level signal also vary.

Next to indicating flood- or ebb-dominance, the water level signal can also be used to indicate the strength of the asymmetry, which is expressed by the ratio between the water level amplitude of the overtide and that of the semi-diurnal tide, a_{M4}/a_{M2} .

2.4.2. River discharge

Depending on its magnitude relative to the tide, river discharge can have a significant impact on estuarine morphodynamics, but has not been studied as extensively as the effect of interactions between tidal constituents (Wang et al., 1999; Guo et al., 2014). The main impacts of a significant river discharge on estuarine morphodynamics are the supply of riverine sediment and an additional ebb-directed velocity superimposed on the tidal velocity signal (Guo et al., 2014). Furthermore, river discharge leads to an additional damping of the tidal wave through friction and influences salt intrusion and gravitational circulation (Savenije, 2012; Cai et al., 2014). In upstream converging estuaries, the influence of river discharge on tidal asymmetry decreases in down-estuary direction (Winterwerp, 2016).

Residual currents can also originate from other mechanisms than a fresh water discharge. Examples are a compensation for Stokes' drift (in case of an at least partly progressive tidal wave) or a bathymetry-induced circulation (Wang et al., 1999).

2.4.3. Mixing processes and ETM formation

Where fresh and saline water meet, horizontal density gradients induce a vertical flow circulation, resulting in a net landward flow along the bottom and a net seaward flow at the surface. In combination with the fact that suspended sediment concentrations are usually higher near the bed than near the surface, this circulation promotes a net import of sediment. Furthermore, salinity induces flocculation of particles present in the river flow near the head of the salt wedge. This process may lead to the formation of an ETM, characterized by large suspended sediment concentrations (Winterwerp and Wang, 2013).

Next to this gravitational circulation, tidal processes may also cause the formation of an ETM, which is not necessarily located at the salt intrusion limit (Burchard et al., 2018). The occurrence of such a secondary ETM, that can exist simultaneously with the salinity-induced ETM, has been described mostly for macrotidal, flood-dominant estuaries.

The strength of the gravitational circulation depends on the longitudinal salinity gradient. In strongly convergent estuaries, this gradient is usually largest in the central part of the salt intrusion length. Closer to the mouth the salinity gradient is small, and mixing of salt and fresh water is often dominated by tidal processes. The relative importance of gravitational circulation compared to tidal mixing is reflected in the Estuarine Richardson number (Savenije, 2012):

$$N_R = \frac{\Delta\rho}{\rho} \frac{gh}{u^2} \frac{Q_f T}{P_t} \quad (2.5)$$

with:

- $\Delta\rho$ density difference between sea and river water [kg/m³]
- ρ density of fresh water [kg/m³]
- g gravitational acceleration [m/s²]
- h water depth at the estuary mouth [m]
- u amplitude of the tidal velocity [m/s]
- Q_f river discharge [m³/s]
- T tidal period [s]
- P_t tidal prism [m³]

When this dimensionless number is large, gravitational circulation is more important than tidal mixing and the estuary is stratified. When it is small, the tide contains so much energy that a sharp interface between fresh and saline water cannot be maintained. The estuary is then called well-mixed.

However, within the tidal cycle the degree of stratification also varies. This process is referred to as internal asymmetry and may also lead to trapping of sediment within the estuary (Jay and Musiak, 1994). Differences in the degree of stratification within a tidal cycle may be the result of tidal velocity asymmetry, but also of tidal straining, which is explained as follows:

During flood, saline water is advected landward over slowly moving, less dense layers. This convective instability leads to increased vertical mixing and a more uniform, bottom-intensified velocity profile. During ebb on the other hand, fresh water at the surface moves over slow, dense bottom layers, leading to stable stratification and less mixing. The velocity profile is therefore strained and surface-intensified. Hence, near-bottom velocities are larger during flood than during ebb, leading to a net landward transport of sediment (Burchard and Baumert, 1998). An additional effect is that due to the decreased mixing during ebb, suspended sediment is kept near the bed, in the region of low velocities. This effect again leads to a net import of sediment.

Next to the abovementioned processes, several other, often secondary mechanisms can contribute to sediment trapping and ETM formation, such as topographic effects and spatial variation in sediment availability (Winterwerp, 2010). For simplicity, these processes are kept outside the scope of this research.

2.5. Description of the Loire estuary

The Loire estuary has a macrotidal character, with a tidal range at the mouth of 2.5 to 5 m (GIP Loire Estuaire, 2013). The average water depth is about 10 m throughout the estuary, whereas the width decreases rapidly from about 5 km at the mouth to about 300 m at a distance of 50 km upstream of the mouth. Further upstream, the width remains more or less constant. The estuary has a funnel shape, characterized by a convergence length of about 21 km (Dronkers, 2017). The tidal wave has a mixed character (partly standing, partly progressive) (Savenije, 2012). When the tidal wave propagates up the estuary, initially the tidal range increases in upstream direction because convergence is stronger than friction. The estuary can therefore be classified as amplified (Savenije, 2012). Around Nantes, 55 km upstream of the mouth, friction becomes dominant, such that the tidal range decreases from this point onward, until it is completely damped at Saint-Florent-le-Vieil, 103 km upstream of the mouth (GIP Loire Estuaire, 2013). Salt can intrude up to 60 km for low river flows (GIP Loire Estuaire, 2017).

With the Estuarine Richardson number (see Equation 2.5), the degree of stratification of the estuary can be assessed. It follows that the Loire can generally be described as a partially mixed estuary, with an Estuarine Richardson number of about 0.35 for a moderate river flow of $Q_f = 845 \text{ m}^3/\text{s}$. However, N_R varies between 0.08 during low river flows ($Q_f = 200 \text{ m}^3/\text{s}$) and 0.80 when the discharge is high ($Q_f = 2000 \text{ m}^3/\text{s}$). Hence, in periods with low discharges, when the salt intrusion length is large, the estuary is well-mixed, whereas the estuary is in stratified conditions for high discharges when the salt wedge intrudes only little.

2.6. Effects of historical interventions in the Loire estuary

2.6.1. Tidal deformation and salt intrusion

As mentioned in Section 2.4, the geometry of the estuary has a large influence on the distortion of the tidal wave. The geometry of the Loire estuary has been modified greatly over the past centuries, mainly by channel deepening and reclamation of intertidal areas. These changes have affected the tide within the estuary in several ways.

In the first place, the geometrical changes are likely the cause of the large increase of the tidal range in the estuary over the first half of the 20th century, see Figure 2.3 (Van Maren et al., 2015; Winterwerp and Wang, 2013). Although the precise mechanisms behind this process are not yet fully understood, the effects of channel deepening on effective hydraulic drag play an important role (Chernetsky et al., 2010; Winterwerp and Wang, 2013). Firstly, the effective drag decreases directly with the increase in depth. Furthermore, dredging activities may result in removal of bed forms, decreasing friction as well. Section 2.6.2 explains a third mechanism, in which hydraulic drag is reduced due to large SSC.

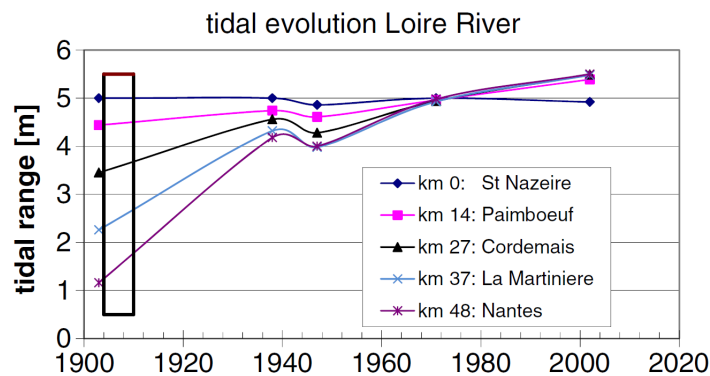


Figure 2.3: Evolution of the tidal range along the Loire river. The black box represents the period of channelization of the estuary. Source: Winterwerp and Wang (2013).

The tidal intrusion limit has also increased to 100 km upstream of the mouth. In this case, specific attention should be given to the *Bassin à Marée*, which was created upstream of Nantes by large-scale sediment extractions between 1913 and 1920. In 1906 and 1907, low river flows had led to an import of fine sediment into the estuary, hampering navigation. The *Bassin à Marée* was meant to create a larger ebb-tidal flow, such that fine sediment would not be able to settle (Maquet, 1974). Thus, this intervention was specifically designed to increase the tidal prism (Winterwerp et al., 2013).

Furthermore, the interventions have resulted in a stronger flood-dominance of the tide. Generally, it can be said that a large ratio of tidal amplitude over water depth (a/h) induces flood-dominance. A large intertidal storage volume as compared to the channel volume (V_s/V_c) enhances ebb-dominance (Friedrichs and Aubrey, 1988). The latter ratio has decreased in the Loire estuary, whereas the ratio a/h has increased in the upper part of the estuary (la Martinière - Nantes). Only here, the increase in tidal amplitude was larger than the increase in depth. At the mouth of the estuary the tide is already asymmetrical ($a_{M4}/a_{M2} \approx 0.11$, $\Delta\varphi_\zeta \approx 165^\circ$), but as the tide propagates up the estuary the signal becomes increasingly flood-dominant, both in strength and in nature (at Nantes, $a_{M4}/a_{M2} \approx 0.21$, $\Delta\varphi_\zeta \approx 125^\circ$). This deformation of the tide is larger than 50 years ago (Brière et al., 2011a).

Finally, the salt intrusion length has increased due to the interventions and can now reach values up to 60 km for small river flows.

2.6.2. Consequences

Winterwerp and Wang (2013) identified a feedback mechanism between this tidal deformation, the import of fine sediment and the effective hydraulic drag, as illustrated in Figure 2.4. Due to an asymmetry in both peak tidal velocities and vertical mixing (internal asymmetry), fine marine sediments are continuously transported up-estuary, or riverine sediments are being trapped. With increasing SSC, the hydraulic drag decreases as the vertical exchange of turbulent momentum is hampered. The lower hydraulic drag leads to further deformation of the tide, such that more sediments accumulate.

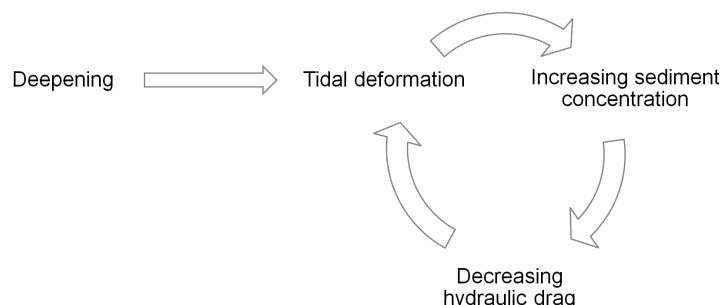


Figure 2.4: Feedback mechanism induced by estuarine channel deepening, after Winterwerp and Wang (2013).

Once SSC become very high, a hyper-turbid state may be reached (Van Maren et al., 2015; Winterwerp, 2010), which has been observed in the Loire as well as in the Ems river in Germany (Winterwerp et al., 2013). In this state an increase in concentration requires less energy to keep the sediment in suspension, due to hindered-settling effects. Therefore, this hyper-turbid state is stable and hard to reverse. The evolution of an estuary towards this state can be associated with the development of a second ETM, which may exist together or merge with the first ETM driven by gravitational circulation (see also Section 2.4). Furthermore, thick layers of fluid mud are observed in both the Ems and the Loire. Their location and extent vary with the magnitude of the discharge and the tide (Van Maren et al., 2015; GIP Loire Estuaire, 2014). In the Loire, the fluid mud is largely flushed from the estuary during high discharge events (Dronkers, 2017).

2.7. Measures in the estuary

Within the Loire estuary, considered interventions aim at decreasing tidal prism and asymmetry, salt intrusion and turbidity. Since these parameters are strongly dependent on estuarine geometry, proposed interventions focus on modification of this geometry. Several measures have been investigated in numerical modelling studies, including a significant reduction (about 40%) of the cross-sectional area over a length of more than 10 km and the creation of intertidal flats. Furthermore, the possibility to raise the bed upstream of Nantes (km 59-70) in order to limit the intrusion of tide and salinity was explored (Brière et al., 2011b).

Currently, the creation of tidal flats is considered the most promising option to reach the abovementioned goals. A strategy including creation of 340 ha of tidal flats between Paimboeuf and la Martinière has been developed. However, implementation of such an intervention is complicated, because it is a costly operation. Furthermore, tidal flat creation was found to have a significant effect only if applied on a large scale, such that results of a small-scale pilot study cannot be used to predict effectiveness on larger scales. Therefore, at this moment the main focus lies on preservation of the still existing tidal flats (GIP Loire Estuaire, 2018).

3

Approach and model set-up

3.1. Idealized modelling of river-estuary systems

In order to further study the behaviour of the Loire river-estuary system, an idealized, process-based numerical model is developed. An idealized model has several advantages compared to a precise model representation. Firstly, one of the principal aims of the model is to obtain a better fundamental understanding of the coupling of riverine and estuarine processes. An idealized, process-based model is eminently suited for this goal (Huijts et al., 2006). As the different processes can relatively easily be switched on and off, their effect can be investigated in both an isolated and a coupled manner. Furthermore, interventions in the Loire river have been ongoing since the beginning of the last century and the bed topography and planform of the river have undergone major changes. As data concerning these interventions, such as the large-scale sediment extractions, are scarce (Winterwerp et al., 2013), it is difficult to isolate the effects of certain interventions. When setting up a model with the aim of being as realistic as possible, the same problem will occur. Inaccurate or incomplete data regarding already implemented interventions will introduce uncertainties in the outcomes of such a model. The third reason that an idealized model is preferred over a precise representation is that the time it takes both to build the model (including data collection, pre-processing and calibration) and to run a simulation is generally shorter. A short computational time gives the possibility to simulate a large number of configurations and to analyze the sensitivity of the results. Finally, the results of an idealized model may be more generally applicable, such that conclusions can be drawn not only for the Loire, but also for comparable river-estuary systems.

Idealized models, both numerical and analytical, have been used extensively in order to study estuarine morphodynamics. While analytical models can provide an even clearer insight in the governing physical laws, numerical models present the possibility to easily consider the feedback mechanisms between bed level changes and hydrodynamics (Guo et al., 2014). In this way, the long-term morphological evolution of estuaries can be assessed. Furthermore, in order to construct an analytical model, non-linear processes need to be approached with linearized equations. Using a numerical model, such approximations are not necessary. As precisely these nonlinear processes often determine the development of estuarine systems, this difference is of importance.

Although it is known that river discharge has an important influence on estuarine morphodynamics, its effect is studied to a much lesser extent than the influence of the tide (Guo et al., 2014, 2015b; Canestrelli et al., 2014). In this research, a deliberate choice is made to focus on an area where both river discharge and tide have an important influence. Over the area of more than 100 km long that is considered, the influence of the river discharge diminishes as the cross-sectional area increases in downstream direction, whereas the tidal influence decreases in opposite direction. The relative influence of river discharge and tide, which thus varies along the channel axis, is an important parameter for morphodynamic development (Guo et al., 2015b).

Within the limited amount of studies concerning river-estuaries the discharge is often assumed to be constant (Guo et al., 2014; Canestrelli et al., 2014). Such an assumption is too crude for the Loire, where the discharge shows a significant seasonal and inter-annual variability (see also Section 3.3). Hence, in this case a varying discharge boundary condition must be applied when assessing long-term development, which has implications for the model set-up and the interpretation of the results.

Another distinguishing feature of this study is the modelling of turbidity in the estuary. As the hyper-turbid state that characterizes the estuary is most likely an unwanted effect of human interventions, it is deemed important that this characteristic is represented in the model. In order to achieve this, vertical gradients in salinity, sediment concentration and flow velocities need to be resolved. Usually these gradients are not resolved in idealized modelling studies of estuarine morphodynamics. In these studies, often a choice is made for a 1D or 2DH model representation for reasons of computational efficiency (Lanzoni and Seminara, 2002; Schuttelaars and De Swart, 2000; Guo et al., 2014).

Furthermore, a cohesive sediment fraction must be introduced next to the sand fraction that is characteristic for the riverine sediment discharge. However, even with these additional features the fine sediment dynamics in the estuary cannot be simulated accurately. Especially for the representation of fluid mud, as well as the interaction between sand and mud, many processes are lacking. A much higher level of detail and complexity would be needed in order to include these processes (Van Maren et al., 2015).

3.2. Grid and bed topography

The study area is represented by a total of 2320 active cells in the horizontal plane, with 464 cells in the longitudinal m -direction and 5 cells in the transverse n -direction. This configuration makes it possible to model the main flow-carrying channel, as well as two elevated areas on either side of the main channel, representing floodplains in the river section and tidal flats in the estuary. These elevated areas are connected to the main channel by means of a transitional cell, representing a steep slope between them. For the main channel as well as the elevated areas, cell sizes decrease from 600×2500 ($m \times n$) m^2 in the estuary to 200×330 m^2 in the river section. The transitional cells are much smaller, with sizes ranging from 600×500 m^2 at the estuary mouth to 200×66 m^2 in the river. The vertical direction is discretized with 10 equidistant σ -layers. With this number of grid cells, a compromise is made between computational speed and accuracy. The grid resolution is high enough to represent important hydrodynamic features, but low enough to allow for long-term computations. In Section 5.2 the grid features are discussed further.

The total length of the computational domain is 115 km, covering the river section between Saint-Nazaire (downstream boundary) and Montjean-sur-Loire (upstream boundary). This length is computed along the river axis, which is assumed to be a straight line in the model. In accordance with many studies of tidally dominated estuaries (e.g. Friedrichs et al., 1998; Lanzoni and Seminara, 1998; Dronkers, 2017; De Jonge et al., 2014), the channel width is modelled as exponentially converging:

$$b_c = b_0 \exp(-x/L_b) \quad (3.1)$$

with:

- b_c width of flow-carrying cross-section [m]
- b_0 width of flow-carrying cross-section in the estuary mouth [m]
- x longitudinal coordinate, positive in landward direction [m]
- L_b convergence length [m]

According to Dronkers (2017), $L_b \approx 20$ km for the Loire, but the exponential convergence does not apply to the first 10 km (Saint-Nazaire to Paimboeuf). In this study, a convergence length of 25 km is assumed, and applied to the first 50 km of the model domain (Saint-Nazaire to Nantes). Throughout the report, this section of the model is indicated as the estuary. Upstream of the estuary, the remaining 65 km of the main channel is assumed to have a constant width, equal to the width at the upstream end of the estuary. This section is called the river section (although there is a tidal influence in this area as well).

The elevated areas on either side of the main channel are assumed to have the same width as the main channel at that location, whereas the width of the transitional cells is 20% of the main channel width throughout the model domain. Figure 3.1 gives an overview of the geometrical features of the model.

In the estuary section, both main channel and tidal flats are assumed to have no bottom slope. In the river section, the main channel and floodplains have a constant slope, of 2.46×10^{-4} and 1.69×10^{-4} respectively. The schematization of the main channel slope is based on a longitudinal bottom profile of the estuary measured in 1990, see Figure 3.2. The representation of other geometrical features, such as the elevation of floodplains and tidal flats, the width of the main channel and the width of the transitional areas mainly results from the hydrodynamic calibration as described in Section 3.5. Furthermore, the groynes that are currently present in the river section are schematized within the bed topography, by adjusting the elevation of the transitional areas over the entire length where groynes are present, between 56 and 106 km upstream

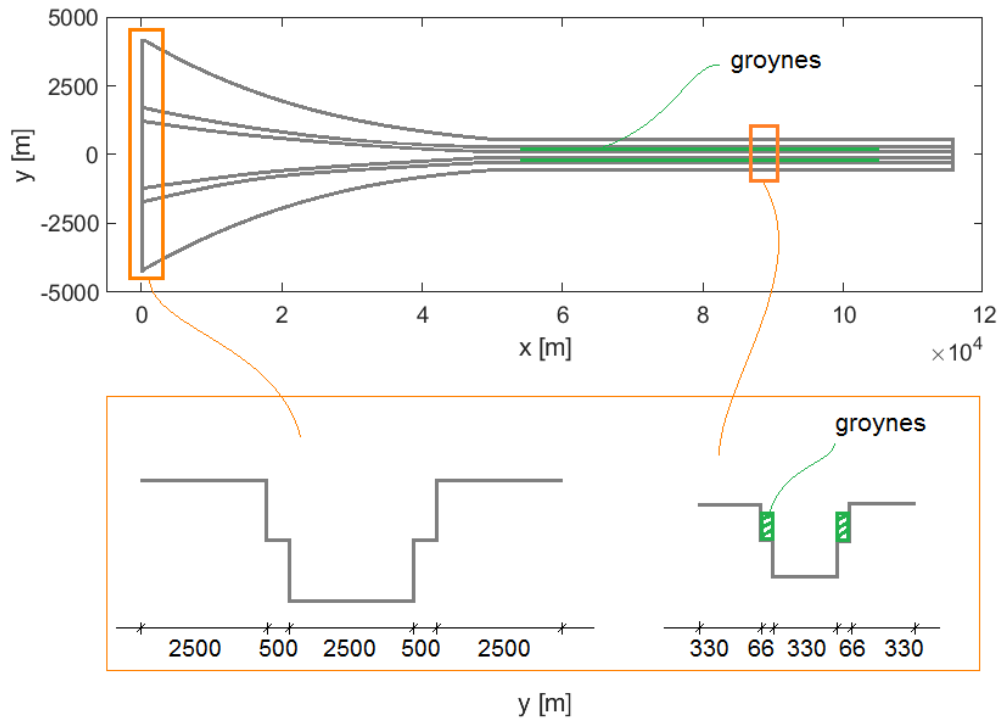


Figure 3.1: Sketch of the model geometry. Above, a top view of the model domain. For clarity, grid lines in y -direction are not shown. The lower figure shows two cross-sections, one at the estuary mouth and one in the river section.

of the mouth. Representation of the groyne fields is not necessary, since these fields do not carry flow and their morphological development does not have to be taken into account explicitly (but is included implicitly, see Section 3.6.1). The elevated section becomes submerged for a discharge of about $2500 \text{ m}^3/\text{s}$, which is exceeded 5% of the time. This is roughly in accordance with reality, because although the groynes were originally almost always submerged, due to the bed degradation they now usually emerge from the flow.

3.3. Boundary conditions

3.3.1. Flow

At both ends of the model, boundary conditions need to be prescribed for the flow and the transport of salt and sediment. At the landward end a discharge boundary condition is used to prescribe the inflow of water, whereas the seaward end is a water level boundary. The landward model boundary is located at Montjean-sur-Loire, where daily discharge measurements have been performed from 1863 onward. Only for the period 1894-1899 no data are available. Thus, a 150-year-long record of discharges is present at this location. During this period, the average river discharge was $845 \text{ m}^3/\text{s}$, whereas yearly averages ranged between 282 and $1958 \text{ m}^3/\text{s}$. Extreme values were as high as $6200 \text{ m}^3/\text{s}$ and as low as $50 \text{ m}^3/\text{s}$. Hence, the river discharge shows large seasonal and interannual variability. In comparable model studies of river-estuary systems, often a constant river discharge is prescribed (Canestrelli et al., 2014; Guo et al., 2014). In this case, however, the discharge variability is too large to be completely neglected, especially as the discharge is expected to have a significant influence on the morphodynamic development of the river-estuary system. On the other hand, prescribing the raw discharge time series at the model boundary complicates our analysis of the long-term development of the system, as river flood events can alter the bed topography significantly in a short period of time. Taking these considerations into account, a representative daily discharge time series of one year is calculated by averaging each daily value over all years. In this way, the seasonal variation of discharges is taken into account, whereas the influence of extreme events is diminished. The resulting hydrograph, as shown in Figure 3.3, is repeated each year for the entire duration of the model simulations of long-term morphological development.

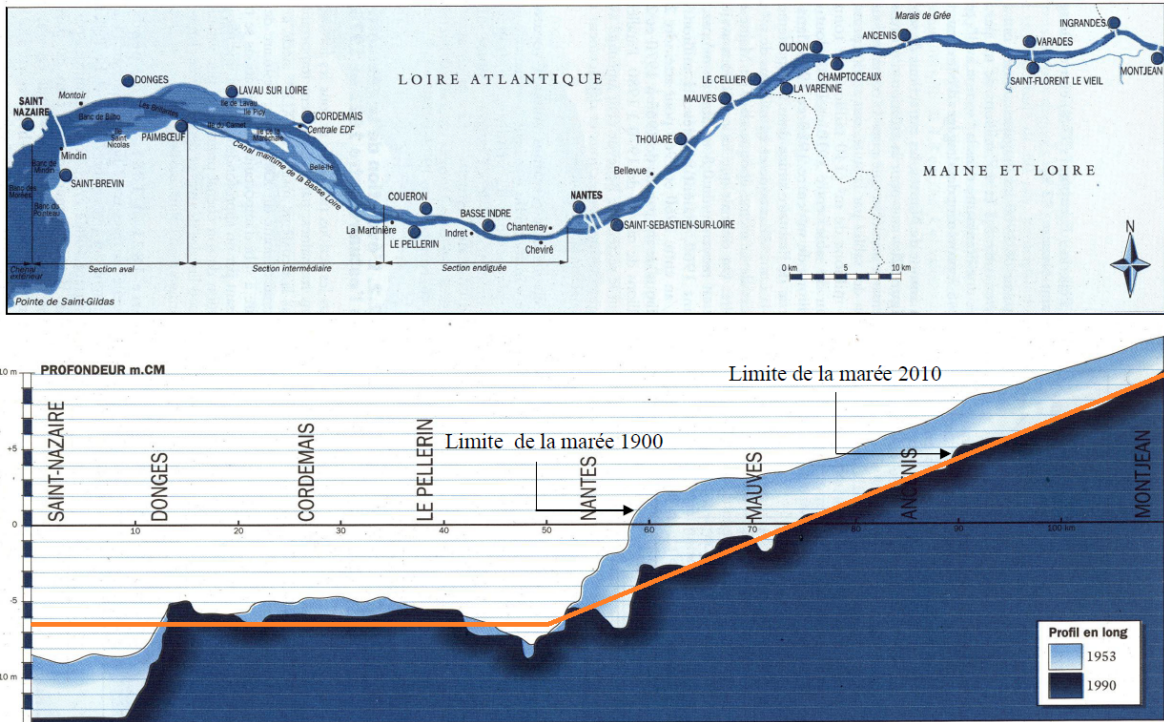


Figure 3.2: Schematization of the bottom topography (indicated in orange), based on a longitudinal profile measured in 1990. Note that the (historical) reference level used in the figure is +0.40 m CM96. After Migniot (1993) and Brière et al. (2011a).

The water level imposed at the downstream boundary consists of a constant value equal to mean sea level, with tidal variations superimposed. In this study, the tidal forcing consists of the M2 tidal constituent, which is the principal component at this location, and its first higher harmonic, the M4 constituent. Amplitudes and phases are taken from the Saint-Nazaire gauging station (Ferret et al., 2018), giving the following condition:

$$\zeta(t) = 3.63 + 1.75 \cos(28.984t - 105) + 0.20 \cos(57.968t - 45) \tag{3.2}$$

with:

- ζ water elevation [m]
- t time [hour]

Van de Kreeke and Robaczewska (1993) showed that in case of bed load, the influence of other constituents on net sediment transport is of a lesser order of magnitude, when the M2 component is dominant. For fine sediment, however, the spring-neap tidal cycle (resulting from the interaction between the M2 and S2 component), can have a significant influence on residual transport (Allen et al., 1980; Fettweis et al., 1998). This is investigated further in Section 4.3.4.

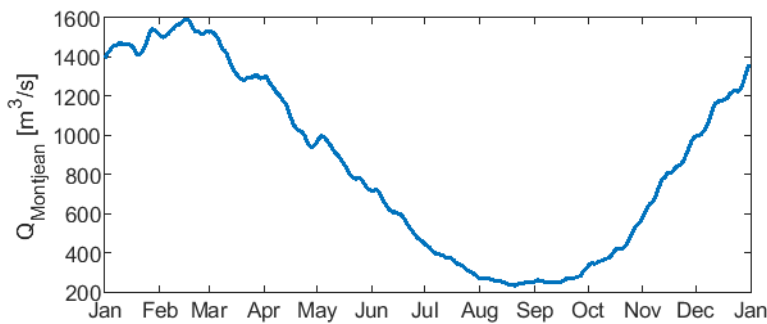


Figure 3.3: Representative discharge year as imposed at the upstream model boundary.

3.3.2. Transport of salt and sediment

At the landward boundary, a salinity of 0 ppt is prescribed (fresh water). The salinity at the seaward boundary is set to 35 ppt, equal to that of sea water. Use is made of two sediment fractions: a cohesive mud fraction and a non-cohesive sand fraction. For sand a grain size of $D_{50}=1.2$ mm is used, based on measurements taken in 1998, 2006 and 2011 (Hydratec, 2013). The distinction between these two fractions is made in order to model the turbidity in the estuary as well as the long-term development of the bed topography. For both fractions sediment concentrations need to be prescribed at the boundaries. Mud concentrations at the landward and seaward boundary are set to 0.05 and 0.1 kg/m³ respectively, based on observations from the SYVEL measurement campaign (GIP Loire Estuaire, 2017), see Section 1.5.

For the sand fraction, boundary conditions are more complicated to deduce. As taking measurements of especially bed load transport is complicated and expensive, no reliable data are available for this parameter (Bagnold, 1977; Hu et al., 2009). In modelling practice, use is often made of the equilibrium sand concentration profile just inside the model domain, in combination with a Neumann boundary condition with which a zero concentration gradient is specified at the boundary. In this way, sediment concentrations at the boundary are set equal to those just inside the domain, leading to very little accretion or erosion at the boundary. In this case, however, the use of this method cannot be justified as it is known that sediment transport at the landward boundary is not in equilibrium. At Montjean-sur-Loire, the river bed is subject to ongoing degradation, which is, next to large-scale river training, also caused by the extensive sand and gravel mining that took place upstream of the model boundary over the past century. When sediment supply is reduced while the sediment transport capacity of the flow remains unaltered, the flow becomes what can be called sediment-starved. By eroding the river bed, the flow regains some of its former sediment load. Although sediment extraction was put to a halt in the '90s, the consequences of the mining activities are still being felt.

In order to account for this effect in the model, a method is adopted in which a constant fraction of the equilibrium sand transport, as calculated by the model, is prescribed at the boundary. To this extent, as a first step a simulation is performed in which the equilibrium transport functionality is switched on, but bed level updating is switched off. From the output of this simulation, the time series of equilibrium sediment transport at the upstream boundary can be read. Subsequently, a constant fraction of each record in the time series is taken. The resulting time series can be used as input for a new simulation in which bed level updating is switched on. Following the first step of this method, an equilibrium transport of 0.77 million m³/y is obtained, which is in the same range as the values of 0.5 to 0.8 million m³/y reported in literature (Gasowski, 1994; Brière et al., 2011a). By varying the fraction with which the equilibrium transport values are multiplied, the final simulations show varying amounts of aggradation and degradation, as transport rates within the model adapt to the sediment supply from upstream. Because the same average hydrograph is repeated every year, the yearly averaged sand transport at the upstream boundary remains constant. In reality, however, the sediment supply from upstream changes over the years, for example because sand mining has ceased. As this variation is unknown, the transport boundary condition chosen within the model is rather arbitrary. It is decided to choose the boundary condition such that the bottom topography that is reached at the end of the simulation remains as close as possible to the topography of the initial situation, as only for the initial situation the hydrodynamic behaviour can be calibrated. Thus, a fraction of 0.5 of the equilibrium transport is selected, which amounts to 0.39 million m³/y.

3.4. Model settings for morphology

3.4.1. Sediment transport

For the calculation of sand transport, the total load formulation of Engelund-Hansen is used (Engelund and Hansen, 1967), which was calibrated on data from flume experiments with grain sizes ranging from 0.19 to 0.93 mm. In contrast with many other transport formulae, the relation of Engelund-Hansen does not include a critical bed shear stress, indicating applicability to conditions with large mobility. The conditions for which initiation of motion occurs are often indicated with the Shields parameter, which, for $D = 1.2$ mm, has a value of about $\psi_c = 0.037$ (based on the assumption of uniform flow). Model results show that in the section unaffected by the tide, these conditions are indeed exceeded at all times. However, in the section where the flow direction alternates, the bed shear stress shows an oscillating motion and can reach values smaller than the critical value.

In this context it should be noted that, although the Engelund-Hansen transport relation has been applied successfully in a large number of studies of rivers, as well as estuaries and tidal basins (e.g. Van der Wegen

et al., 2010; Guo et al., 2015a,b), its derivation was based on unidirectional flow data only. The applicability of the Engelund-Hansen formulation and comparable transport relations (such as the Meyer-Peter-Müller formula) to tidal environments requires further investigation (Lanzoni and Seminara, 2002), that falls outside the scope of this study.

To investigate if sand is mainly transported as bed load or as suspended load, the ratio u_* / w_s can be used, in which u_* is the shear velocity [m/s] and w_s the sediment settling velocity [m/s]. The shear velocity is defined as $u_* = \sqrt{\tau / \rho}$, with τ the bed shear stress [N/m²] and ρ the water density [kg/m³]. Within the model domain and for average discharge conditions, the maximum value of this ratio is 0.56. Critical values for the initiation of suspension that have been derived in literature range between 0.25 and 1 (Van Rijn, 1984). Hence, it is assumed that sand is transported mainly as bed load, but partly as suspended load as well.

For the cohesive mud fraction, Partheniades' equation for erosion is used, whereas the deposition flux is set independent of the shear stress (Sanford and Halka, 1993; Van Maren et al., 2015):

$$E = M \left(\frac{\tau}{\tau_{cr}} - 1 \right) \quad (3.3)$$

$$D = w_s c \quad (3.4)$$

with:

- M erosion parameter [kg/(m²s)]
- τ bed shear stress [N/m²]
- τ_{cr} critical bed shear stress for erosion [N/m²]
- w_s settling velocity [m/s]
- c sediment concentration [kg/m³]

The bed stratigraphy is not explicitly included in the model. In this study, sand and mud transport are considered separately, but they can also be combined in one simulation. In that case, erosion rates are affected by the availability of each sediment fraction at the bed surface. Hence, an assumption must be made regarding the composition of the bed (well-mixed or stratified). Since sediment dynamics in the Loire estuary are dominated by entrainment and deposition of mud and the formation of fluid mud layers (Cheviet et al., 2002), it is assumed that the cohesive fraction, when deposited, forms a layer covering the sand present in the bed. Hence, the erosion rate of mud is not reduced due to the presence of sand. Although this assumption might lead to an overestimation of the mud erosion rate, assuming a well-mixed bed will most probably lead to a much larger underestimation of this rate.

Hindered settling is taken into account through the formulation of Richardson and Zaki (1954):

$$w_s = \left(1 - \frac{c}{c_{ref}} \right)^5 w_{s,0} \quad (3.5)$$

with:

- w_s settling velocity [m/s]
- c sediment concentration [kg/m³]
- c_{ref} reference concentration [kg/m³]
- $w_{s,0}$ clear water settling velocity [m/s]

Furthermore, the effect of flocculation in salt water is taken into account by specifying different settling velocities for fresh and salt water. The exact implementation of this feature can be found in the Delft3D-FLOW manual (Deltares, 2014).

In order to preserve the shape of the channel cross-section, which is modelled as a compound channel, the elevated and transitional areas are modelled as non-erodible. As our interest lies in the morphological development of the main channel only, this does not present limitations. At the beginning of the simulation, a 5 m thick sand layer is available for erosion in the main channel. The river-estuary planform is assumed to be fixed, such that interventions only affect bed morphology.

In the navigation channel, maintenance dredging is carried out from 55 km upstream of Saint-Nazaire up to 15 km downstream of this location. The largest volumes are dredged in the section between km 3 and km 18. Dredged material mainly consists of mud, but also contains some sand. On average, about 10 million m³/y was dredged between 1984 and 2010 (GIP Loire Estuaire, 2011). To represent the current situation, these dredging activities are included in simulations of long-term bed development.

3.4.2. Morphological acceleration factor

To enable long-term simulations, a morphological factor (MF) is used. In Delft3D, bed levels are updated every hydrodynamic time step. Using the MF approach, the computed erosion and deposition fluxes at the bed surface are multiplied with the user-defined MF, such that bed level changes are accelerated. This approach can only be used under the assumption that the morphological timescale is much larger than the hydrodynamic timescale, such that disturbance of the feedback between flow and morphology is negligible (Roelvink, 2006).

The implications of the use of an MF are different for tidal and river environments. For the periodic tidal motion, the morphological development simulated during one tidal cycle with $MF = n$, can be interpreted as the development that would occur after n tidal cycles. This interpretation is allowed if the hydrodynamics are not significantly affected by the bed level changes (Deltares, 2014). This modelling technique has been used and validated extensively for tide- and wave-dominated systems (Guo, 2014). However, for applications where river discharge plays an important role, the interpretation of the MF approach is not so straightforward. River hydrographs can be highly irregular, with extreme events of short duration occurring between longer periods of moderate discharge. High discharge events may have a significant impact on bed level changes, disproportionate to the duration of these events. To account for this effect in morphodynamic models, several methods have been proposed to schematize the discharge boundary condition.

Firstly, a constant river discharge may be applied, that leads to the same sediment influx at the upstream boundary as the full hydrograph. This morphologically representative discharge is larger than the arithmetic mean river discharge, because sediment transport scales nonlinearly with the discharge (such that high discharges have a relatively larger contribution). This method is straightforward, but may lead to significant deviations in model outcomes if the full hydrograph shows large variability (Guo et al., 2015a).

In a second approach, the seasonality of the river discharge is accounted for explicitly by applying a (schematized) hydrograph. In this case, the use of an MF is problematic, because it leads to distorted relations between the timescales of different processes (Mosselman and Le, 2016). When an MF is applied while the discharge time series remains unaltered, the hydrograph is effectively stretched on the morphodynamic timescale with a factor equal to the MF. This means excess water volumes (for discharges higher than bankfull discharge) are also multiplied with that same factor, leading to a distortion of the dynamics of filling and emptying of storage areas. A solution would be to compress discharge time series on the hydrodynamic timescale. It makes sense to choose the hydrograph compression (HC) factor equal to the MF, such that the compressed time series contains the same number of seasons as would occur in reality during the morphological time represented by the model. However, also HC should be applied with the greatest consideration for the resulting hydrodynamic behaviour. In reality, discharge variations are usually sufficiently small to consider the river flow as quasi-steady (De Vries, 1959). When compressing hydrographs in time, the resulting discharge variations on the hydrodynamic timescale should not become so large that this approximation is no longer valid. Furthermore, when considering a discharge hydrograph as a single flood wave, its diffusive behaviour should be correctly represented. The larger the curvature of the free surface, or in other words, the sharper the peak of the flood wave, the stronger the attenuation of the wave. Hence, compressing the hydrograph too much distorts the dynamics of flood wave propagation (Mosselman and Le, 2016). Furthermore, when subsequent flood peaks follow each other up too closely, they might start interfering with each other due to their dispersive behaviour, leading to a single elongated flood stage in the downstream part of the domain (Guo et al., 2015a). A correct representation of flood wave diffusion becomes more important as the length of the domain increases. It can be concluded that both an unchanged and a compressed hydrograph lead to an incorrect representation of the riverine hydrodynamics. This poses limitations on the MF that can be applied.

Finally, a temporally varying MF could be applied such that events leading to large bed level changes are combined with a small MF and vice versa. However, in Delft3D a time-varying MF presents problems when modelling suspended sediment transport, due to the delay between erosion and deposition. When the entrainment and deposition of suspended sediment occurs at time steps governed by a different MF, this leads to errors in the sediment mass balance (Deltares, 2014).

An appropriate river discharge schematization and selection of MF and HC remains location- and problem-specific and based on judgement and sensitivity analysis by the modeller. For the Loire, the discharge variability is judged as too high to justify the application of a constant morphologically representative discharge. Hence, the decision is made to apply an average discharge year, as reported in Section 3.3. With this averaging procedure extreme events are already omitted, which is expected to be beneficial for the application of HC

Table 3.1: Sensitivity scenarios for MF and HC.

Simulation	MF	HC
1	1	1
2	30	1
3	30	30
4	60	15
5	60	30
6	60	60
7	120	60
8	120	120
9	240	120
10	240	240

and MF. For simplicity, a constant MF is applied. In order to select the most appropriate combination of MF and HC, a sensitivity analysis of these parameters is performed. In total, 10 different combinations of MF and HC are applied, as reported in Table 3.1. For all simulations, the morphodynamic time is 100 years.

On the basis of the simulation results several remarks can be made. In general, both an increase of MF and HC leads to higher equilibrium bed profiles with respect to the reference scenario (MF = HC = 1). However, the bed level is much more sensitive to changes in HC than in MF for values higher than 60. For example, simulations 6 and 7 show comparable bed profiles, whereas simulation 8 shows relatively large deviations with respect to simulation 7. Both these results are in agreement with Guo (2014), who finds an increasing sediment influx at the head and a decrease in outflux at the mouth for increasing HC, which indeed leads to a higher profile throughout the domain. The increasing influx is attributed to the larger inertia of the river flow when the hydrograph is compressed more, whereas the decreasing outflux is explained by the overlap of discharge peaks in the downstream part of the domain.

However, for the current model set-up the sensitivity to halving HC decreases for lower HC values, whereas the sensitivity to halving MF remains constant. Hence, the difference between simulations 3 and 5 is larger than between 5 and 6. Furthermore, it is found that the difference between MF and HC should not become too large. The results from simulation 2 deviate more from the reference scenario than the results of simulation 3. Simulation 4 and 5 have a comparable performance. In the last 30 years of the simulation the profile resulting from simulation 4 lies slightly closer to the reference profile, but simulation 5 performs slightly better over the first 70 years.

To still be able to obtain results for morphological development on a century-timescale within reasonable computation time, an MF of 60 in combination with HC = 30 is selected for the model simulations outlined in Section 3.6. In this case, the maximum deviation in bed level with respect to the reference scenario is 35 cm. In the selection of HC, attention is also paid to the timing of the yearly hydrograph with respect to the tidal cycle: the hydrograph duration should not be an integer factor larger than the duration of the tidal cycle to avoid river stages coinciding with the same stage of the tide every few cycles.

3.5. Hydrodynamic calibration

An accurate representation of the hydrodynamic behaviour is important to obtain a reliable morphodynamic development. As simulation results represent either a historical or a future situation, data needed to calibrate these results are scarce or non-existent. Therefore only a calibration of the initial situation is performed. As idealized models are not meant to precisely reproduce measurements, this calibration is qualitative and meant to check whether important processes are represented. However, the parameters following from calibration of the initial situation are probably not valid for the final result. An extensive sensitivity analysis is therefore recommended to investigate the influence of model parameters on the solution (Schuttelaars et al., 2013). A start with this analysis is made in this study, see Section 4.2.5 and 4.3.4.

Calibration is performed by comparing modelled water levels at the upstream boundary, tidal range, tidal asymmetry and salt intrusion length with observations. Geometrical features (width of main channel and transitional areas, elevation of tidal flats and floodplains) and bottom roughness (imposed in terms of Chézy coefficients) are used as calibration parameters. Results of the hydrodynamic calibration are shown in Figures 3.4 to 3.7. These results were obtained for a Chézy coefficient of $60 \text{ m}^{1/2}/\text{s}$ in the estuary section and $30 \text{ m}^{1/2}/\text{s}$

in the river, with a linear transition over a distance of 6 km between them. Due to the high level of geometrical schematization, flow resistance due to bars, islands and bends is also incorporated in the roughness coefficient, which explains the relatively low values. The value in the estuary is in agreement with the analysis of Winterwerp et al. (2013), who investigated the evolution of the effective hydraulic drag in the Loire estuary over the past century. Where in 1900, this value ranged between $63 \text{ m}^{1/2}/\text{s}$ near the mouth to $30 \text{ m}^{1/2}/\text{s}$ near Nantes (km 50), in 2004 the effective hydraulic drag had increased to around $65 \text{ m}^{1/2}/\text{s}$ throughout the estuary. It should be noted that in these values the damping of turbulence due to large sediment concentrations is included, whereas in Delft3D this is taken into account separately. Thus, the effective hydraulic drag within the model will be lower (represented by a higher Chézy value) than the prescribed Chézy coefficient of $60 \text{ m}^{1/2}/\text{s}$.

Calibration of the tidal range (see Figure 3.5) is performed for two different conditions, the first being a spring tide with a low discharge and the second a neap tide with a high discharge. The tidal conditions are simulated by modifying the amplitude of the M2 component such that the tidal range at the seaward boundary of the model is equal to the measured range at this location. For the spring tide condition, model results agree well with measurements in the region where the tide is amplified, but show an overestimation of the tidal range further upstream. The deviation is largest at Mauves (km 72.5), where the range is overestimated by 1.4 m. For the neap tide condition the model overestimates the range both in the amplification and in the damping region, the largest deviation being 1.2 m at km 66.5.

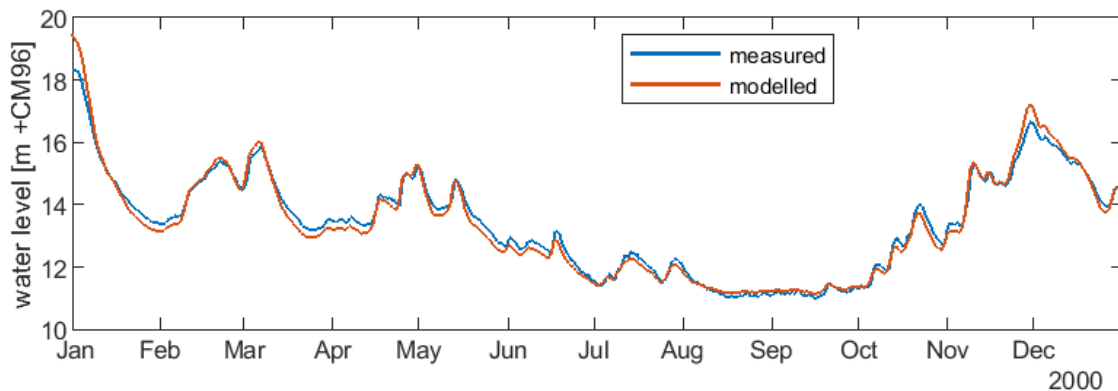


Figure 3.4: Modelled and observed water level at Montjean-sur-Loire (km 115) in the year 2000.

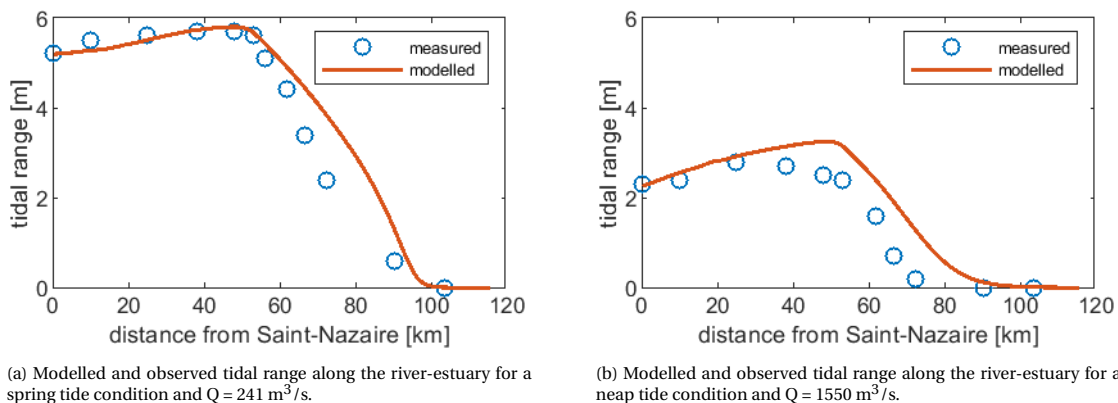


Figure 3.5: Modelled and observed tidal range along the river-estuary for (a) a spring tide condition, measured September 26, 2000 and (b) a neap tide condition, measured April 25, 2000.

In order to investigate the development of tidal asymmetry within the estuary, Fourier analysis is performed on model results to obtain amplitudes and phases of the M2 and M4 component. Furthermore, tidal analysis is performed on records of hourly water level measurements for the year 2000 at 5 locations along the estuary, using the UTide Matlab functions by Codiga (2011). From this analysis only the M2 and M4 components are used for calibration. In general, the chosen tidal analysis method performs well for the M2 and M4 component. The 95% confidence intervals for amplitudes and phases of these components increase slightly for stations located further landward. Nevertheless, the interval is never more than $\pm 0.925 \text{ cm}$ for amplitudes and

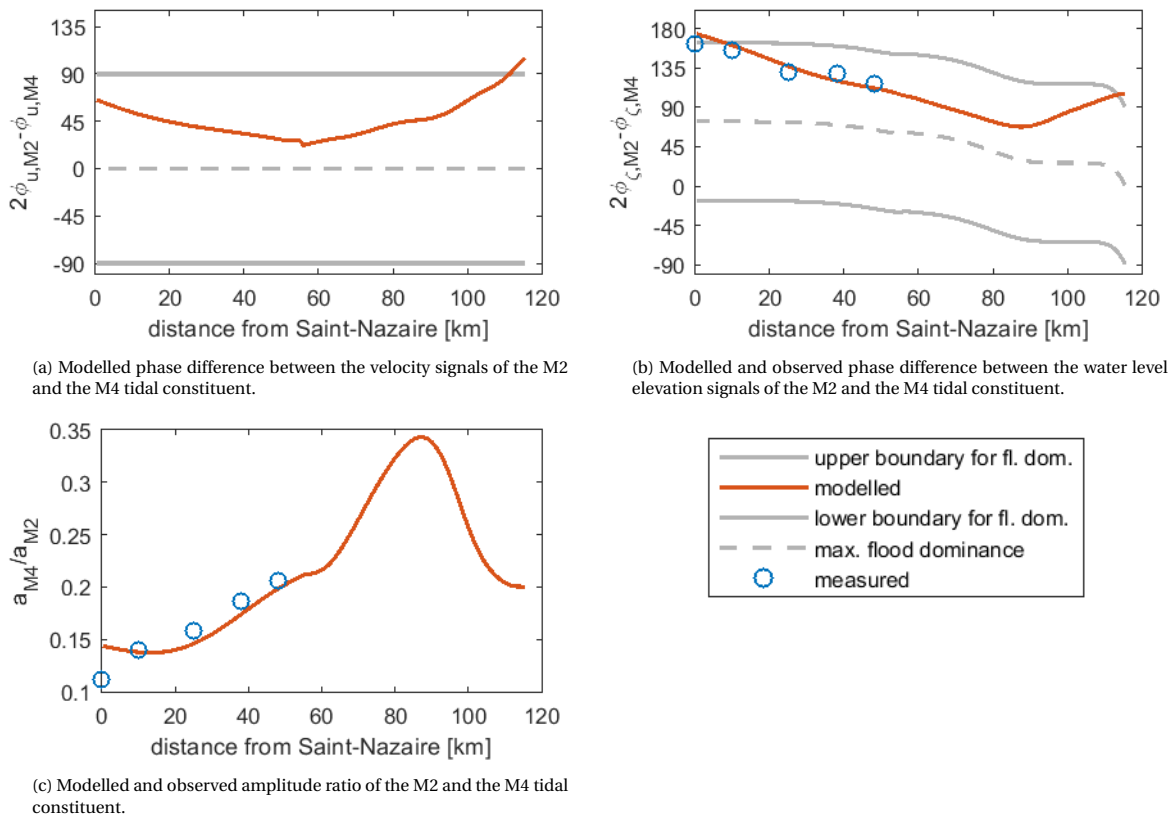


Figure 3.6: Indicators of the nature (Figures 3.6a and 3.6b) and strength (Figure 3.6c) of the tidal asymmetry, with $Q = 845 \text{ m}^3/\text{s}$.

$\pm 1.59^\circ$ for phases. The results obtained from analysis of model output and observations are used to calculate several indicators for tidal asymmetry, as explained in Section 2.4.1. Figure 3.6 shows the resulting comparison. Model results show increasing flood-dominance as the tide propagates up the estuary (Figures 3.6a and 3.6b), as well as an increase in the strength of the asymmetry (Figure 3.6c). Both are in good agreement with observations in the estuary.

Figure 3.7 shows salt intrusion lengths for different discharges, but comparable tidal conditions. Where the intrusion length is slightly overpredicted by the model for the two largest discharges, the intrusion is underpredicted for the lower discharges. Especially for $Q = 100 \text{ m}^3/\text{s}$ the deviation (10 km) is large. This underestimation for lower discharges is attributed to the unrealistically smooth geometry of the schematized estuary, lacking the presence of distinct ebb, flood and connecting channels (Kuijper and Van Rijn, 2011). Such an irregular geometry is believed to contribute to large-scale mixing processes and therefore enhance salt dispersion (Savenije, 2012). For high discharges this effect may be compensated by the high salinity (35 ppt) imposed at the downstream boundary during inflow, without using a Thatcher-Harleman timelag (that would smooth the transition between outflow and inflow conditions). In reality, the salinity at Saint-Nazaire during flood is not equal to that of sea water, especially when the river discharge is high.

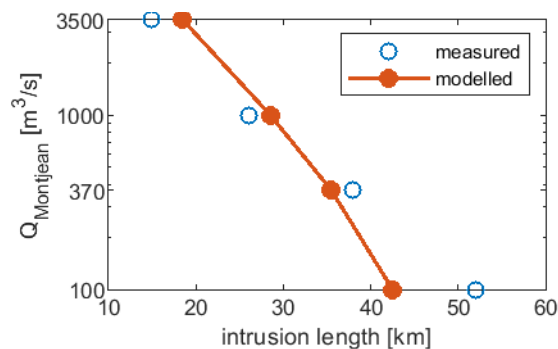


Figure 3.7: Modelled and observed salt intrusion length for 4 different discharges, but comparable tidal conditions (modelled with $a_{M2} = 2.5 \text{ m}$). Note that the dependent variable is plotted on the horizontal axis, because it denotes a length in the horizontal plane.

3.6. Simulation approach

With the model set-up as described so far, simulation results are obtained that represent a reference situation. By applying changes to the model set-up and comparing the results to this reference situation, effects of human interventions can be investigated. As the reference situation is based roughly on the current state of the Loire, the assessment of future interventions is relatively straightforward. However, the interpretation of model results becomes more complicated if the goal is to investigate effects of historical interventions. As these historical interventions are, either explicitly or implicitly, already included in the reference situation, their influence can only be studied in isolation by reversing the interventions. An example is the large-scale construction of groynes that has taken place in the past. As these groynes are already included in the model, only the effect of removing the groynes can be studied. Of course the effects of groyne removal will not be the exact opposite of groyne construction, if only because the present situation from which the groynes are removed is not the same as the historical system in which the groynes were constructed. Still, general tendencies can be deduced from reversing interventions. For example, if groyne removal leads to sedimentation, it is likely that groyne construction in the past has led to erosion. The effect of historical interventions can thus be studied in a qualitative way.

The simulations selected for investigation are listed in Table 3.2. In the following subsections, the choice for each scenario is motivated and the schematization of each intervention is explained. In general, the dimensions of the tested measures are chosen relatively large, in order to obtain a clear view of the effects. Although in reality implementation of such extreme cases is often not feasible, the results of these extreme scenarios can be used for a qualitative assessment of the effects of different measures.

Depending on the location and the intended effect of the intervention, the simulations are carried out with either sand or mud transport. The main reason to decouple these processes is because the interaction between sand and mud morphodynamics is not included sufficiently accurately in the current model set-up. For reasons of computational efficiency, bed composition and temporal and spatial variations therein are not taken into account explicitly. However, erosion behaviour of sand-mud mixtures can change suddenly and dramatically from non-cohesive to cohesive for a certain critical clay content (generally 5-10%) (Van Ledden et al., 2004). As this behaviour is not represented well in the model, resulting bed level changes in simulations where sand and mud transport are combined are unreliable in the regions where both sediment types can be found in the bed, which is mainly the case in the estuary section. Long-term (century-scale) bed evolution of the system is therefore simulated with non-cohesive sediment only. Subsequently, results are interpreted knowing that sand-mud interaction processes are lacking.

However, next to long-term bed development we are also interested in the fine sediment dynamics and ETM formation in the estuary, for which mud simulations are needed. In this case the decoupling of mud and sand transport can be justified, considering that the timescale needed to adapt to a disturbance is generally much smaller for mud than for sand (Van Ledden et al., 2004). Hence, on the mud timescale bed level changes due to sand can be assumed small. Furthermore, as a consequence of using the Engelund-Hansen transport formulation as implemented in Delft3D, suspended sediment transport is not modelled explicitly. The total load transport is simulated as bed load transport, such that sediment cannot be found in suspension within the model simulations (although in reality, the sand is transported partially in suspension). For these reasons, excluding sand transport does not introduce large errors when simulating the development of SSC.

Hence, the interventions specifically aimed at counteracting bed erosion are simulated with sand transport only, for a period of 100 years (morphological time, $MF = 60$, $HC = 30$). After this timespan an equilibrium situation is often not reached yet, but a significant percentage of the final bed level change already occurs in the first century. The effectiveness of a measure depends not only on the difference with the reference scenario at the end of the simulation, but also on the morphological development towards this result. Furthermore, as in reality external forcings and interventions within the domain never remain constant over the course of a century, it is unlikely that the final model result will be reached in reality. It is however much more likely that forcings will remain approximately constant over the course of one or two decades. The initial response of the system to a change in conditions is therefore at least as important as the final response when the system has reached a new equilibrium.

The interventions aiming at a decrease in turbidity in the estuary are represented with mud transport only, for a period of up to 5 months (depending on the simulation). Because the simulation time is so short and bed level changes due to deposition and erosion of mud are relatively large, a morphological factor of 1 is used in these simulations.

Table 3.2: Overview of model simulations.

Simulation	Abbreviation	Description	Sand/Mud	Results
0	R	Reference	S	4.2.2
1	SN	Sediment nourishments	S	4.2.3
2	GR	Groyne removal	S	4.2.3
3	SC	Side-channel restoration	S	4.2.3
4	ELS	Energy loss structure	S	4.2.3
5	NMD	No maintenance dredging	S	4.2.3
6	CC	Climate change	S	4.2.5
7	HD	Historical deepening	M	4.3.2
8	EBE	Estuarine bed elevation	M	4.3.3
9	TFR	Tidal flat restoration	M	4.3.3
Combinations				
10	GR + NMD	Groyne removal, no maintenance dredging	S	4.2.4
11	EBE + NMD	Estuarine bed elevation, no maintenance dredging	S	4.4
12	N + NMD	Sediment nourishments, no maintenance dredging	S	4.4
13	GR + SN	Groyne removal and sediment nourishments	S	4.2.3
14	SC + SN	Side channel and sediment nourishments	S	4.2.3

3.6.1. Sediment nourishments

Addition of sediment to the domain represents the reversal of a historical intervention (large-scale extraction of sediment), but has also been applied as a measure to counteract bed degradation in other rivers, such as the Rhine (see Section 2.3). Furthermore, both groyne removal and side-channel restoration are expected to lead to the release of sediment trapped in the groyne fields and disconnected side channels. This effect is represented with sediment nourishments (SN) as well.

Sediment nourishments are implemented as periodically recurring events, using the dredging and dumping feature within Delft3D. For the isolated investigation of nourishments, a volume of 100.000 m^3 (including pores) per morphological year is supplied, consisting of sediment with the same grain size as present in the system ($D_{50}=1.2 \text{ mm}$). The annually nourished volume is comparable to that of the pilot nourishment carried out in the Rhine in 2016 (Rudolph, 2018) and comprises about 10% of the annual riverine sediment load. Nourishment occurs each year at the same location, over a period of 1 day (morphological time) and a length of 1 km. The location is chosen in the middle of the river section (30 km downstream of the landward boundary), such that effects in both upstream and downstream direction can be assessed. When simulating the release of sediment trapped in groyne fields and side channels the schematization of the nourishment differs, as will be explained in Subsection 3.6.10.

3.6.2. Groyne removal

Partial removal, lowering or shortening of groynes is planned between Nantes and Montjean-sur-Loire (km 50 - 115). To investigate the influence of this measure, the most extreme case of complete removal of all groynes is simulated. Hence, the effect that will be achieved in reality will be much smaller. Furthermore, this simulation represents the reversal of the historical intervention of groyne construction.

The presence of groynes was schematized in the reference situation by elevating the transition cells up to a level where they are emerged for a discharge lower than $2500 \text{ m}^3/\text{s}$ (initially). Hence, groyne removal is schematized by adjusting the elevation back to the original level of the transitional area, which is on average 2.2 m lower and emerges for discharges lower than $1200 \text{ m}^3/\text{s}$.

3.6.3. Side-channel restoration

Re-opening side channels that have been disconnected from the main channel could be a viable option to counteract bed degradation in the Loire. Near Ancenis (km 85), a side channel of about 5 km long will be restored in the coming years.

In the model, the side channel is schematized as a discharge intake and outlet. For $Q > 500 \text{ m}^3/\text{s}$, 10% of the discharge is removed from the domain at the intake location, 6 km downstream of the landward boundary, and released 20 km further downstream at the outlet location. Hence, in the model schematization the side channel is located somewhat further upstream than in reality, in order to stay within the river section

unaffected by the tide. In a tidal area, schematizing the side channel as an inlet/outlet structure would not be justified as there could be inflow of water at the downstream end of the channel during part of the tidal cycle.

With this schematization, the effect of re-opening a side channel on the hydrodynamics and morphodynamics of the main channel can be investigated, without considering the evolution of the side channel itself. In reality, the morphology of the side channel will develop, such that the discharge distribution at the side channel entrance does not remain constant. The schematization represents a situation in which the morphological development of the side channel is negligible, either due to the naturally occurring circumstances or due to regular maintenance. The discharge withdrawal is distributed uniformly over the vertical layers and retains the concentration of constituents. However, there is no withdrawal of bed material load. In reality, it depends on the configuration of the side channel whether withdrawal of bed material load takes place or not. As it is often desired that side channels accrete as little as possible, they are usually designed such that no or very little bed material load is transported into the side channel. This can be achieved by locating the channel entrance in an outer bend, or by construction of a sill or sediment trap at the entrance. It is assumed that also in the case of the Loire such design considerations are made.

Another consideration is the discharge capacity of the side channel. In the Netherlands, this capacity is, according to a rule of thumb, restricted to only a few percent of the total river discharge. As the navigable depth in the main channel should remain sufficient for the commercial navigation that takes place on the Dutch Rhine branches, the effect of the side channel on the main channel should remain negligible, both in terms of hydrodynamics and morphology. In the case of the Loire, commercial navigation is virtually absent upstream of Nantes, such that strict draught limitations are not necessary. Besides, one of the principal reasons to re-open side channels is to promote sedimentation in the main channel. As this effect is expected to increase for increasing discharge withdrawal, an intake of 10% of the total discharge is selected. The schematized length of the side channel is also much larger than that of the channel that will be restored. Again, an extreme case is chosen in order to investigate the effects of this measure qualitatively.

3.6.4. Energy loss structure

A fixed bed layer with an increased roughness, indicated as an 'energy loss structure', will be constructed at Bellevue (km 62). Schematization of this measure in the model is problematic, because in the reference situation this part of the river does not undergo erosion, but sedimentation. The need for bed stabilization is therefore absent in the model. However, the effect of an increased roughness can still be investigated. Hence, the structure is schematized by changing the Chézy value from 30 to 15 m^{1/2}/s over a length of 3 km.

3.6.5. No maintenance dredging

About 10 million m³ of sediment is dredged annually in the estuary, to maintain the necessary depth for navigation. This intervention is represented in the reference situation with the dredging and dumping feature of Delft3D. In this way, the bed level in the estuary between 30 and 50 km upstream of the mouth is kept fixed at its initial elevation. By comparing this situation to a simulation where no maintenance dredging is carried out, the influence of this activity can be assessed.

3.6.6. Climate change

For all intervention simulations, external forcings have been assumed constant on an interannual scale, as it is unknown how these forcings will change. One future development that will most probably have a significant influence on the development of the Loire is climate change, of which two main impacts will be a change in the hydrograph and an increase of the mean sea level. For the Representative Concentration Pathway 8.5 (RCP8.5) scenario, which represents the most severe increase in radiative forcing of all RCP scenarios, the discharge of the Loire is expected to decrease in both winter and summer, with an average decrease of 20% ($\pm 15\%$ with a 90% confidence interval) at Montjean at the end of the 21st century (Dayon et al., 2018). Assuming a sea level rise of 0.80 m/century at the river mouth under RCP8.5 (Grinsted et al., 2015), mean sea level will increase to +4.43 m CM96 in 2100.

In the model, this scenario is schematized by imposing gradually varying hydrodynamic boundary conditions, both at the seaward and at the landward end. At the seaward boundary, mean sea level is increased by 8 mm every year. Although the tide at Saint-Nazaire will also undergo changes due to sea level rise, the tidal condition is left unchanged for simplicity. At the landward boundary, daily imposed discharges are reduced by 0.2% of the initial hydrograph every year, until a decrease of 20% is reached after 100 years. The incoming supply of sand at the upstream boundary is decreased with the same percentage.

3.6.7. Historical deepening

In Section 2.6, it was hypothesized that the human-induced deepening of the estuary led to tidal deformation, which in turn might have set a positive feedback mechanism in motion, leading to increasingly larger SSC.

A key relation in this mechanism is the decrease in hydraulic drag due to the presence of mud. Within the model, this relation is taken into account in several ways. Damping of turbulence by sediment that is suspended in the water column is taken into account through the effect of sediment on fluid density. Due to the non-uniform distribution of sediment over the water column, vertical density gradients arise. The damping effect of such vertical gradients (which may also be due to salinity or temperature) on turbulence is represented by a buoyancy flux in the $k - \epsilon$ turbulence closure model. Next to sediment suspended in the water column, the presence of fluid mud on the bed also leads to a decrease in hydraulic roughness in the estuary. As both the resolution and the complexity of the model are insufficient to accurately represent fluid mud layers, this effect is taken into account through the bed roughness coefficient.

The historical deepening of the estuary is therefore investigated using a two-phased approach, moving increasingly further back in time. First, the effect of the decrease in hydraulic roughness due to fluid mud and SSC is investigated. This is done by decreasing the Chézy coefficient to its historical value in the period just after deepening and by switching off the effect of sediment on fluid density. In the second phase, the deepening itself is also reversed, by increasing the bed level in the main channel of the estuary by 3 m, meaning a reduction of the cross-section of about 38% at LW and about 26% at HW. In the model set-up, the Chézy coefficient is prescribed by the user and is not set dependent on the water depth. In reality, however, an increase in water depth already in itself leads to a decrease of the hydraulic drag. In order to account for this relation, the Chézy coefficient is reduced further in the second phase.

Roughly based on the analysis by Winterwerp and Wang (2013), a Chézy coefficient of $C = 50 \text{ m}^{1/2}/\text{s}$ is chosen to represent the situation before deepening occurred (around the year 1940). Supposing the water depth of the thalweg increased by 3 m due to the deepening, the direct effect on the Chézy coefficient is an increase of about $3 \text{ m}^{1/2}/\text{s}$ (using the White-Colebrook formulation). The situation just after deepening (phase I), is therefore represented with $C = 53 \text{ m}^{1/2}/\text{s}$. Table 3.3 provides an overview of the different simulations.

Table 3.3: Simulations representing historical deepening.

Simulation	Situation	Bed elevation main channel [m CM96]	Chézy value estuary [$\text{m}^{1/2}/\text{s}$]	Effect of sediment on fluid density
Reference	Current	-6	60	on
Phase I	Just after deepening	-6	53	off
Phase II	Just before deepening	-3	50	off

3.6.8. Estuarine bed elevation

If historical deepening has indeed caused the current hyper-turbidity, the question remains if this state can be reversed by elevating estuarine bed levels in the current situation. This possibility is investigated with the model, by implementing the topography used in Phase II of the historical deepening scenario in the current situation, without changing the Chézy coefficient and keeping the effect of sediment on fluid density switched on. However, the simulation is carried out without an initial sediment concentration in the domain. The hypothesis that the high sediment concentrations currently present in the estuary would prevent reversal of the hyper-turbid state, even if the geometry is changed, can therefore not be tested with this simulation.

3.6.9. Tidal flat restoration

Restoration of tidal flat areas, that have been reclaimed on a large scale for agricultural purposes, is considered for the Loire estuary. Reclamation of intertidal areas has likely been a cause for the increased flood-dominance of the tide within the estuary, as explained in Section 2.6. Thus the aim of this intervention is mainly to decrease the flood-dominance of the tide and consequently also the SSC.

In order to investigate the effects of tidal flat restoration, the elevated areas on either side of the main channel in the estuary are lowered by 4 m to a level of +3 m CM96, such that they are flooded during approximately 67% of the tidal cycle (depending on the river discharge).

3.6.10. Combination scenarios

In the abovementioned simulations, possible interventions are assessed individually. In reality a combination of measures is planned for implementation. It is expected that these measures will influence each other, such that the effect of a combination of certain measures will not be the same as the sum of effects of the individual measures. This hypothesis is tested with a simulation in which groyne removal (GR) is combined with no maintenance dredging (NMD) (simulation 10 in Table 3.2).

Furthermore, the individual interventions are often intended to impact either the river or the estuary section of the domain. However, the influence of measures in the estuary can reach further upstream into the river section, whereas measures in the river can influence the morphology of the estuary. The current model set-up gives an opportunity to gain more insight in this interaction, as the entire estuary and tidal river, from Saint-Nazaire to Montjean-sur-Loire, are included in the domain. Hence, two simulations are carried out in which the influence of a riverine measure on the estuary is assessed, and vice versa (simulations 11 and 12 in Table 3.2). As maintenance dredging at the transition between river and estuary limits the interaction between the two sections (as it keeps the bed level fixed over a large part of the estuary), these simulations are carried out with NMD.

Finally, GR and side-channel restoration (SC) are both combined with sediment nourishments (SN) (simulations 13 and 14 in Table 3.2). This is done because it is expected that both GR and SC will lead to the release of sediment that is trapped in groyne fields and abandoned side channels. In these cases, the schematization of SN is adapted to the situation that is to be represented. As the side channel is schematized such that it carries flow only during part of the year, nourishment is active continuously during this period, whereas it is inactive when there is no flow in the side channel. For simplicity, the nourishment rate is set constant during the active period and independent of the flow rate in the side channel, such that cumulative nourished volumes are easily determined. Nourishment is carried out in the main channel just downstream of the discharge outlet that represents the point where side and main channel reconnect.

For the GR simulation, nourishment is carried out continuously throughout the area where groynes are removed. In Section 2.3, GR is estimated to lead to an additional sediment supply of 1.2 million m³ over a period of 40 years. When for simplicity, a constant sediment supply rate is assumed, this leads to a nourishment of 30.000 m³/y. In order to compare the effect of including SN between the GR and the SC simulation, the same supply rate is used for the SC simulation. As in the latter case nourishment is active only during 2/3 of the year, the supply rate per time step is 1.5 times larger than for the GR case.

Within the secondary branches and groyne fields the sand is finer than in the main channel, with an estimated D₅₀ of 0.8 mm (versus 1.2 mm in the main channel) (Hydratec, 2013). The nourishments representing release of this sediment are therefore carried out with D₅₀ = 0.8 mm as well, while keeping D₅₀ = 1.2 mm for all other morphological processes.

3.7. Computational efficiency

Now that the simulations to be carried out with the model have been defined, the computational effort it takes to run these simulations can be assessed. All simulations are run on a single processing unit¹. The simulations regarding morphological development of the sand profile over a century (morphodynamic time) take about 1 day to run. Depending on the specific features used in the simulation, the computation time can vary between 18 and 32 hours. As the mud dynamics can be assessed on a much smaller timescale (months) and bed level changes are disregarded, these simulations are much shorter and take only a few (up to 7) hours to run.

Comparing this performance to that of other three-dimensional morphodynamic models covering similar temporal and spatial scales (through personal communication and experience), the developed model can indeed be called computationally efficient.

¹Specifications: Intel Xeon CPU E3-1276 v3 @ 3.60GHz.

4

Model application

4.1. Hydrodynamic process analysis

In order to obtain insight in the model behaviour, the influence of different hydrodynamic processes on velocities throughout the domain is investigated. First, the effects of adding a constant river discharge and, subsequently, the baroclinic pressure gradient on horizontal velocities in the main channel are shown. In Sections 4.2 and 4.3, the influence of these hydrodynamic processes on the transport of sand (mainly bed load) and mud (suspended load) in the main channel is explored. Mud and sand transport are investigated separately, neglecting interaction processes between these two types of sediment.

In the following simulations, sediment transport is switched off. Figure 4.1 shows the mean and peak components of the horizontal velocity signal for the tide only. The lower plot in this figure shows the difference between peak flood and peak ebb velocity, which is an indicator for tidal asymmetry. Evidently the tide is flood-dominant according to this parameter, which is partly due to the flood-dominant tidal signal imposed at the boundary, and partly due to deformation of the tidal wave inside the domain. Due to a small bathymetry-induced residual current, the tidally averaged velocity is in seaward direction, while the flow in the more elevated transitional areas on both sides of the main channel is slightly landward-directed (not shown in the figure).

Figure 4.2 shows the same decomposition, but now for a simulation where the average discharge of the Loire is added. Naturally this leads to a seaward-directed mean velocity component, which decreases in magnitude as the channel diverges towards the estuary mouth. Next to the mean velocity, the peak flood and ebb velocities also change. The seaward-directed river flow leads to an additional contribution to the friction term, which scales with the flow velocity squared. Hence, especially in the most landward region of the domain, where the river flow velocity is relatively large, the tide is damped significantly. Furthermore, a preferential damping of the ebb tide can be observed, leading to a more flood-dominant peak flow asymmetry. This preferential damping may again be explained by the quadratic dependence of friction on flow velocity: during ebb river and tidal flow are both directed seaward, leading to much larger flow velocities than during flood, when river and tidal flow, with similar magnitudes, are in opposite direction. Friction is therefore larger during ebb than during flood, leading to preferential damping of the ebb tide (Godin, 1985).

When including the baroclinic pressure term in the equations, the hydrodynamics change completely. Figure 4.3 shows tidally averaged flow velocity and salinity for this situation. In the region of horizontal salinity gradients gravitational circulation occurs, leading to net landward-directed flow velocities near the bed and net seaward velocities near the surface. The baroclinic pressure gradient also leads to a change in shape of the velocity signal, as can be seen in Figures 4.4 and 4.5. In Section 2.4.3 it was explained how velocity profiles during ebb and flood are expected to change due to gravitational circulation and tidal straining. Model results agree only partly with this theory.

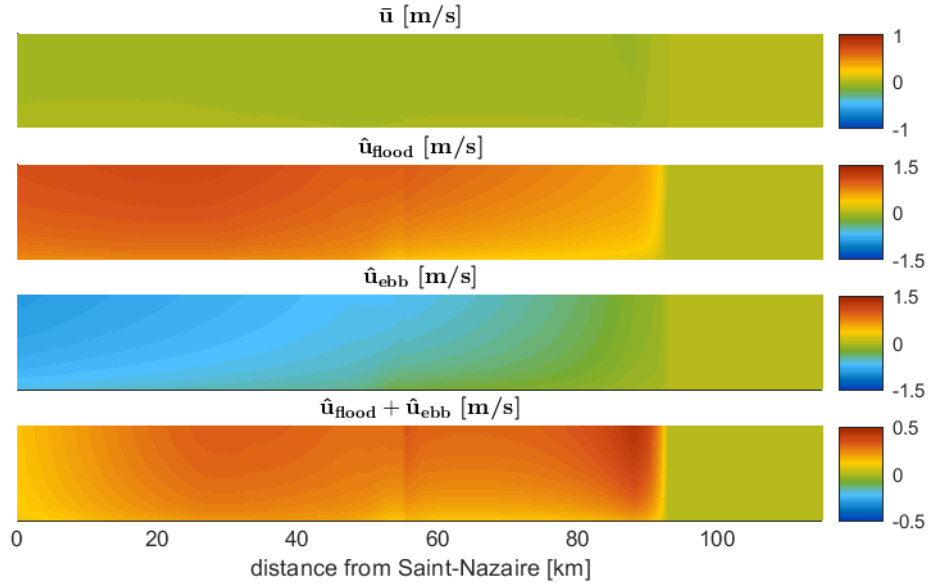


Figure 4.1: Horizontal velocity mean and peaks for an external M2 and M4 tide, along the main channel. No information on water depth is included in the figure; the time-varying vertical layer thickness is replaced by an arbitrary constant throughout the domain in order to create a rectangular plot.

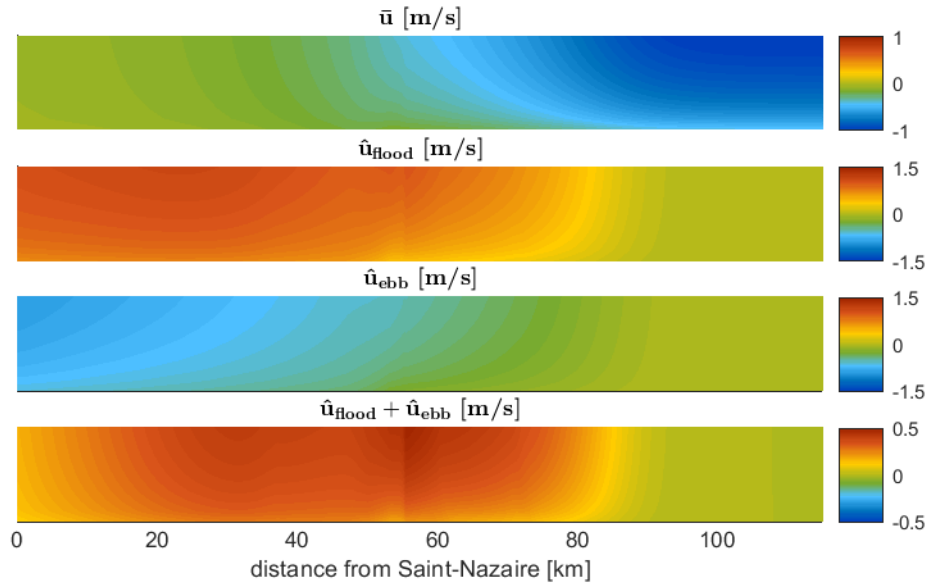


Figure 4.2: Horizontal velocity mean and peaks for an external M2 and M4 tide and a constant river discharge of $Q = 845 \text{ m}^3/\text{s}$. Note that the peak flood and ebb velocities are corrected for the mean.

Figure 4.4 shows the velocity signal at a location close to the tidally averaged end of the salt wedge. The change in the mean velocity is caused by an amplification of the ebb velocities near the surface and a damping of ebb velocities near the bed, which is in line with expectations. During flood, however, the baroclinic profile shows almost no difference with the barotropic one. Looking at a location more in the middle of the salt wedge, the resulting velocity signals deviate even more from the classical picture. During ebb, a strong increase in velocities can be seen at the surface and a strong decrease at the bed, again in line with expectations. However, also during flood velocities are amplified at the surface and slightly damped at the bed, whereas according to theory the opposite would be expected. Hence, not only the mean velocity changes between a barotropic and a baroclinic situation, but also the variation: the latter becomes much larger at the surface and smaller near the bed. In Appendix A this effect is investigated and explained further by relating it to salinity gradients during flood.

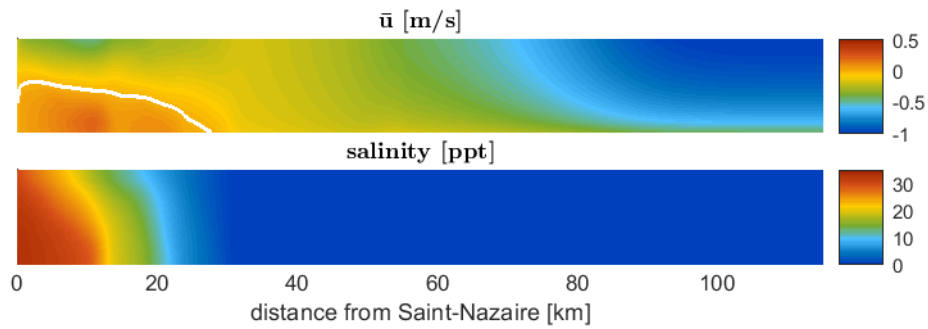


Figure 4.3: Mean horizontal velocity for an external M2 and M4 tide, a constant river discharge of $Q = 845 \text{ m}^3/\text{s}$ and a salinity of 35 ppt imposed at the seaward boundary. The zero-velocity contour is indicated in white. The lower plot shows tidally averaged salinity.

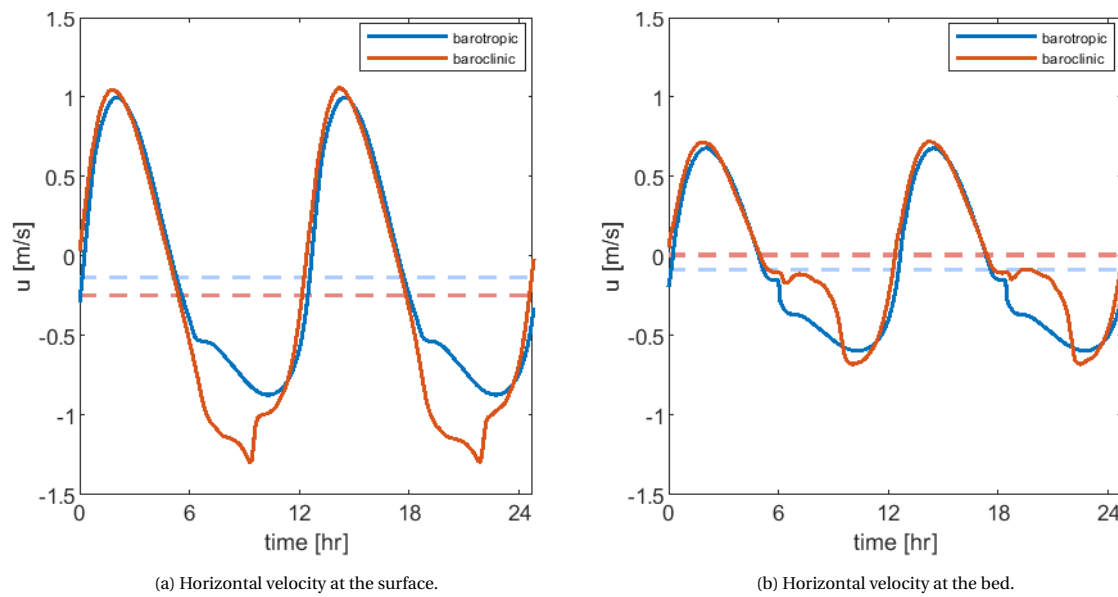


Figure 4.4: Horizontal velocity signals with and without the baroclinic pressure gradient for a constant river discharge of $Q = 845 \text{ m}^3/\text{s}$, at a distance of 27 km from Saint-Nazaire. Dashed lines indicate the mean of the displayed signals.

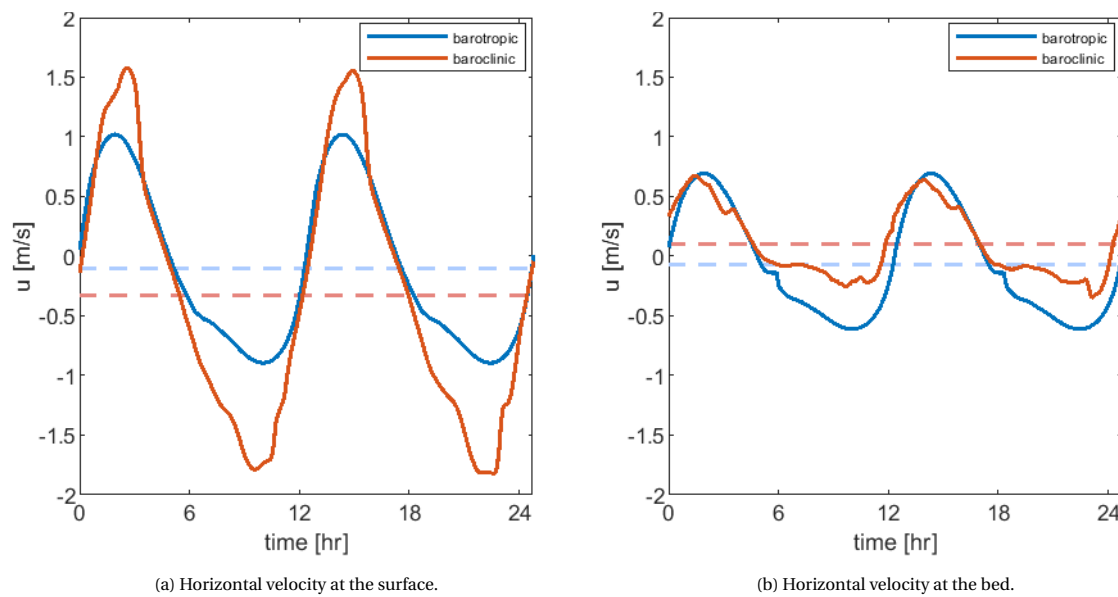


Figure 4.5: Horizontal velocity signals with and without the baroclinic pressure gradient for a constant river discharge of $Q = 845 \text{ m}^3/\text{s}$, at a distance of 18 km from Saint-Nazaire. Dashed lines indicate the mean of the displayed signals.

4.2. Sand transport

4.2.1. Influence of hydrodynamic processes

In the previous section it was seen that velocities in the estuary are highly affected by the gravitational circulation. It is therefore expected that this will also be the case for the transport of sand, which is calculated with the total load formulation of Engelund-Hansen. Figure 4.6 shows that in barotropic conditions, total load transport close to the mouth is flood-dominant for an average discharge of $Q = 845 \text{ m}^3/\text{s}$, due to the flood-dominance of the tide. For discharges higher than $1375 \text{ m}^3/\text{s}$, transport becomes ebb-dominant throughout the estuary.

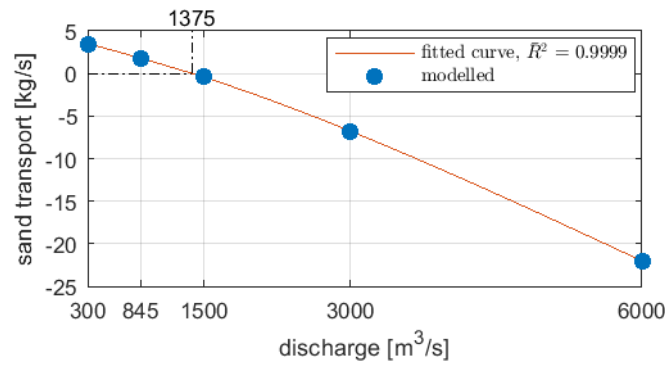


Figure 4.6: Tidally averaged sand transport (total load) at a distance of 10 km from Saint-Nazaire for different discharges in barotropic conditions. Positive values indicate landward transport. A distance of 10 km is chosen as closer to the mouth sediment transport slightly decreases again (see dashed lines in Figure 4.7).

However, if the baroclinic pressure gradient is included, the estuary mouth becomes flood-dominant in terms of sand transport for all simulated discharges, see Figure 4.7. The larger the discharge, the shorter the length over which the net transport becomes landward-directed, but the larger the difference in transport at the mouth compared to the barotropic case. This is understandable as a large discharge limits the salt intrusion, but strengthens the gravitational circulation through stratification.

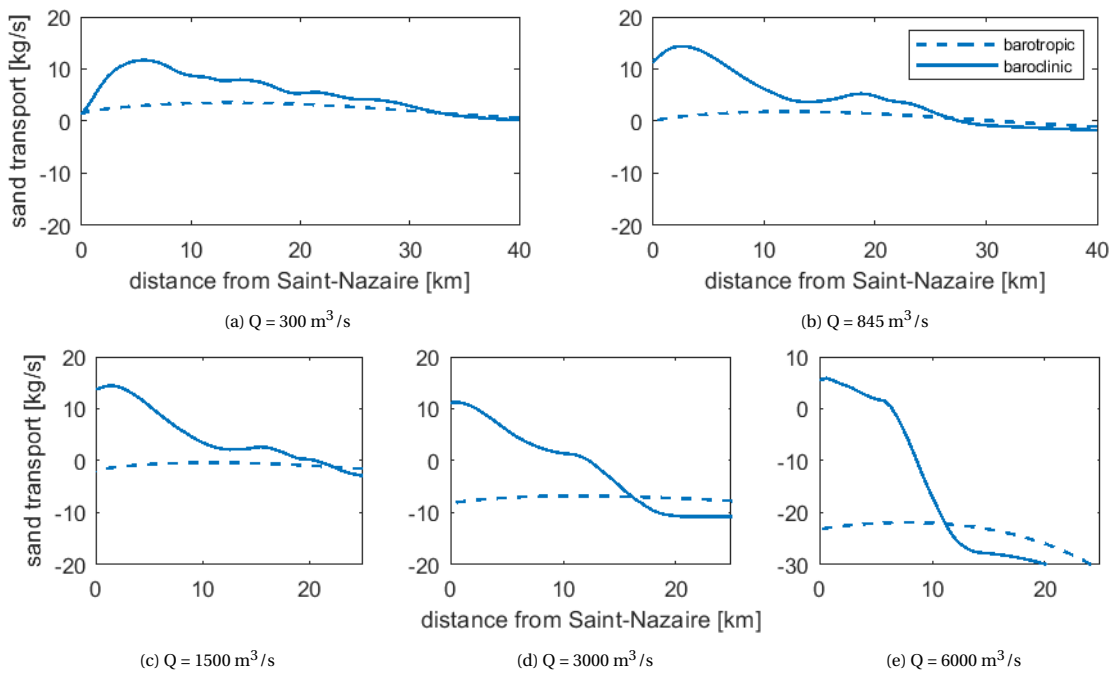


Figure 4.7: Tidally averaged sand transport in the estuary mouth for different discharges. Note the different y-limits in Figure 4.7e.

4.2.2. Reference situation

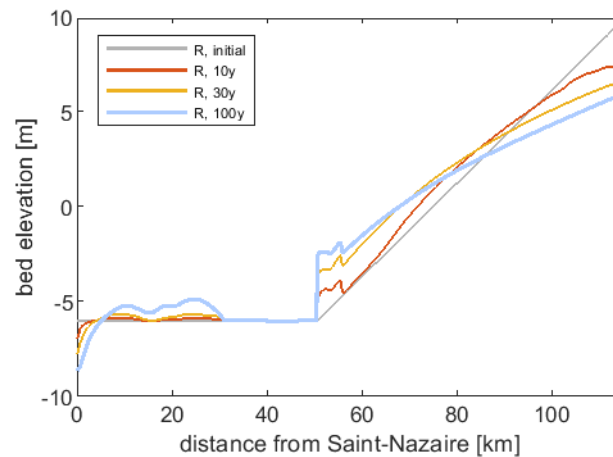


Figure 4.8: Bed level in the main channel for the reference scenario at $T = 0, 10, 30$ and 100 yr.

Looking at the evolution of the sand profile without any interventions (Figure 4.8), several remarks can be made. In the river section a continuous flattening of the slope occurs, with progressive erosion in the upstream part of the domain and deposition closer to the estuary section. This is in line with the theory of Section 2.1 and 2.2, in which it was explained how historical interventions have increased the channel slope, while the equilibrium bed slope was decreased due to sediment extraction. It is therefore not surprising that the river-estuary system responds to these interventions with slope flattening, seeking to return from the imposed steep slope to a new equilibrium bed slope that is more gentle.

However, it is unexpected that bed degradation does not occur throughout the domain, but only in the upstream part of the river section. The initial bed profile is based on a survey from 1990, after which in reality bed degradation continued throughout the river section for another 20 years. Only in 2009 this autonomous degradation came to a halt at most locations.

This mismatch between model and reality is caused by the high degree of schematization of the study area within the model. However, due to the large number of simplifying assumptions that have been made in order to arrive at this schematization, it is difficult to pinpoint which assumption led to the observed discrepancy. A first likely cause is the simplified representation of the geometry, with a river channel with constant width and an exponentially diverging estuary. In reality, the width of the main channel actually decreases from the upstream boundary towards the downstream end of the river section, before it diverges again towards the sea. Secondly, it is probable that the representation of sand transport in the model is inaccurate. The sediment transport formula that is used has not been calibrated for this situation and sand characteristics are described with one sand fraction only, which might not do justice to the variability in sediment characteristics throughout the domain.

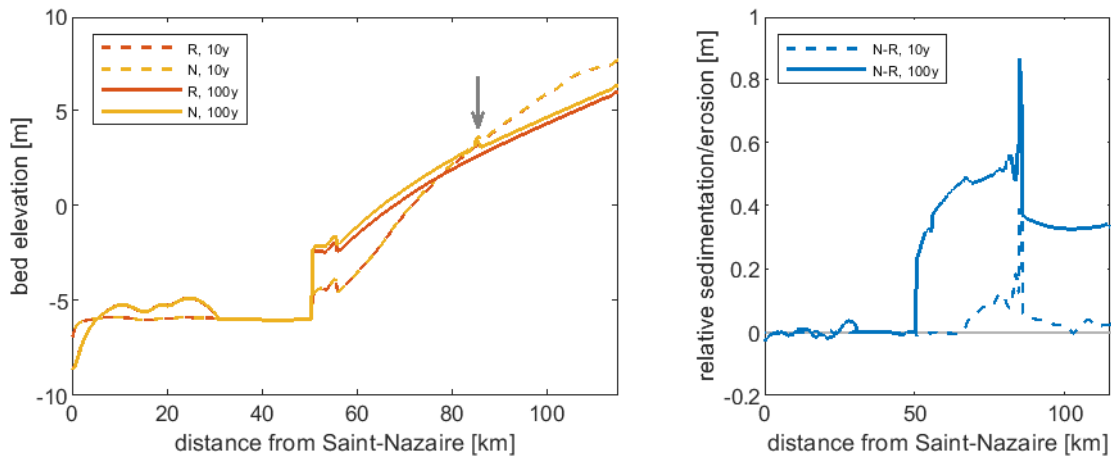
Furthermore, it is noted that a ban on sand mining was put in place in 1995, 5 years after the survey that has been used to define the initial bottom profile in this study. The sand mining that occurred after the survey contributed to the bed degradation during and after that period, but is not included in the model. This could explain part of the deviation from reality.

In the region between 30 and 50 km upstream of the mouth, the effect of maintenance dredging is visible, fixating the bed level at its initial value. Between 5 and 30 km from Saint-Nazaire, a net import of sand due to gravitational circulation (see also Figure 4.7) leads to an increase in bed level. Over the first few kilometers net export occurs due to the transport condition imposed at the downstream boundary during inflow.

In the following section, five interventions that could mitigate the ongoing bed degradation in the Loire are compared with this reference scenario. By looking at the difference in bed level after 10 and 100 years of morphological development between an intervention scenario and the reference situation, the effectiveness of each intervention to counteract bed erosion can be assessed. A positive bed level difference is indicated as relative sedimentation, whereas a negative bed level difference indicates relative erosion.

4.2.3. Measures to mitigate bed degradation

Sediment nourishments



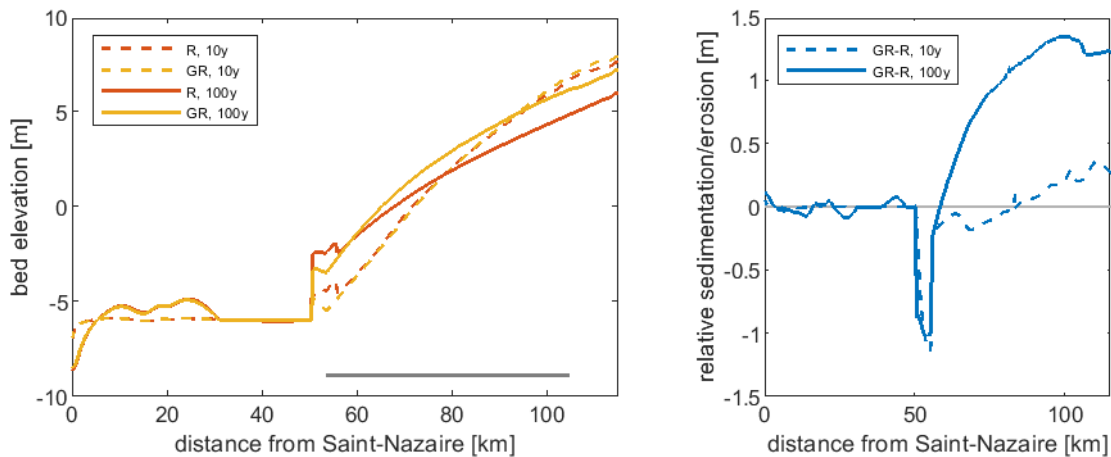
(a) Bed level in the main channel.

(b) Sedimentation/erosion relative to the reference scenario.

Figure 4.9: Effect of nourishment (N) on bed level after $T = 10$ yr and $T = 100$ yr compared to the reference scenario (R). The grey arrow indicates the location of the nourishments.

Annually repeated sediment nourishment in the river section leads to relative sedimentation both downstream and upstream of the nourishment location, although the effect in upstream direction is somewhat smaller (Figure 4.9). The effect is largest just downstream of the intervention, where a relative sedimentation of about 0.5 m is reached after 100 years. Figure 4.9b shows a peak at the nourishment location, which is due to the nourishment carried out at the end of the 10th and the 100th year. At the moments shown in the figure, this last nourishment has not had time yet to spread out and move in downstream direction.

Groyne removal



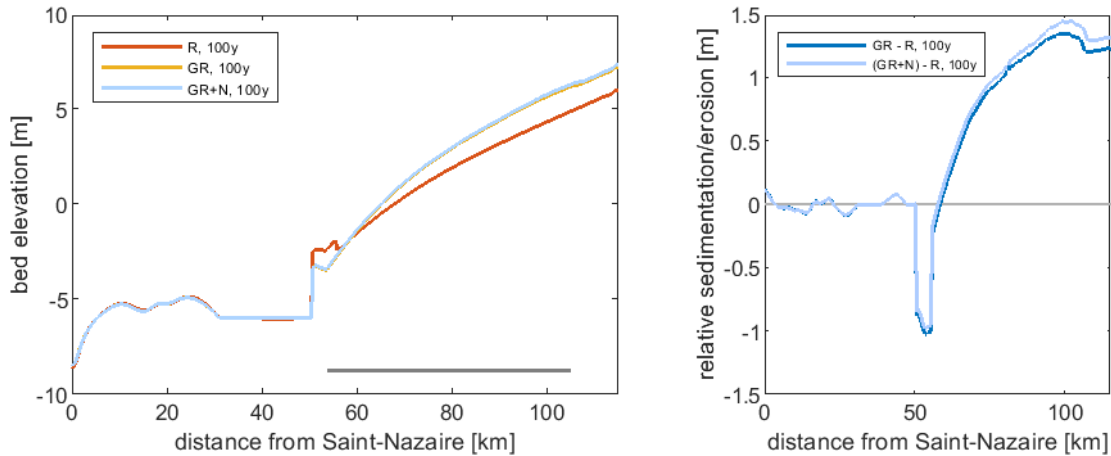
(a) Bed level in the main channel.

(b) Sedimentation/erosion relative to the reference scenario.

Figure 4.10: Effect of groyne removal on bed level after $T = 10$ yr and $T = 100$ yr compared to the reference scenario. The grey line indicates the location where groynes are removed.

Removal of all groynes in the river section leads to significant sedimentation along and upstream of the modified reach, as well as a steeper slope relative to the reference scenario (Figure 4.10). The effect is largest at the upstream end of the section where groynes used to be present. Here, a relative sedimentation of more than 1.3 m is reached after 100 years. However, in the first 10 years relative erosion occurs downstream of km 84 due to steepening of the channel slope. Relative erosion also occurs downstream of the modified reach,

between km 50 and 55. In the reference scenario heavy sedimentation occurs here due to the abrupt channel widening downstream of the groyne section, an effect that is absent in the scenario where groynes are removed. Figure 4.11 shows the results of a scenario where next to groyne removal, the release of sediment that was trapped in the groyne fields is simulated. Compared to groyne removal only, the effect of this increase in sediment supply is small, leading to an additional relative sedimentation of at most 0.1 m after 100 years.

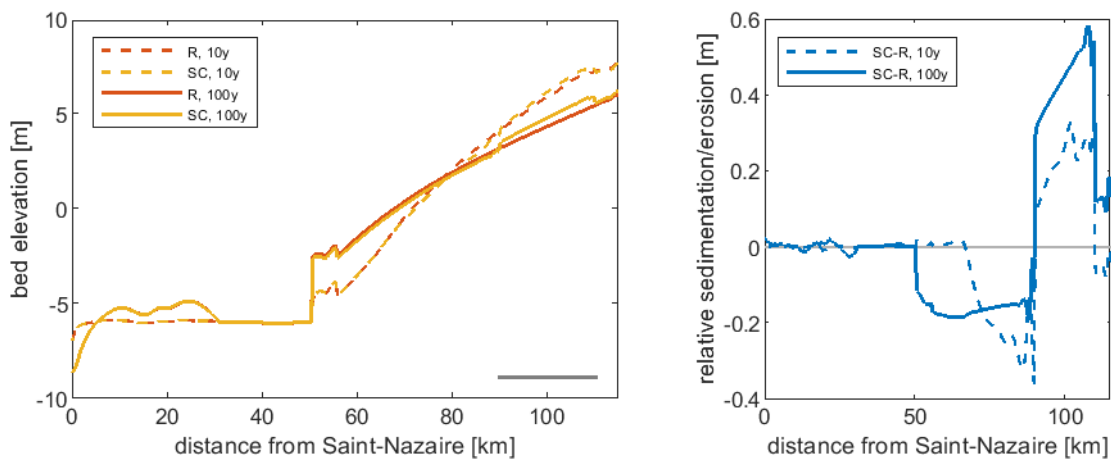


(a) Bed level in the main channel.

(b) Sedimentation/erosion relative to the reference scenario.

Figure 4.11: Effect of groyne removal and release of trapped sediment on bed level after $T = 10$ yr and $T = 100$ yr compared to the reference scenario. The grey line indicates the location where groynes are removed and sediment is added.

Side-channel restoration



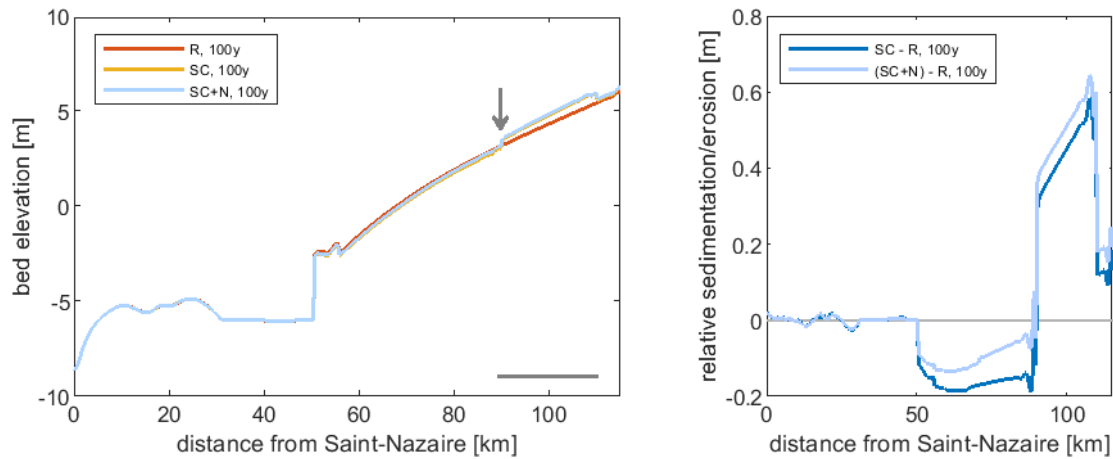
(a) Bed level in the main channel.

(b) Sedimentation/erosion relative to the reference scenario.

Figure 4.12: Effect of re-opening a side channel on bed level after $T = 10$ yr and $T = 100$ yr compared to the reference scenario. The grey line indicates the location of the side channel.

Re-opening a side channel leads to relative sedimentation in the main channel between the in- and outlet, up to 0.6 m after 100 years (Figure 4.12). Initially, relative erosion occurs downstream and upstream of the intervention. In downstream direction, the erosion wave expands and has reached the end of the river section after 100 years, leading to a relative erosion of up to 0.2 m downstream of the side channel. Upstream of the side channel, relative sedimentation occurs after some time, following the sedimentation in the side channel reach. After 100 years a relative sedimentation of about 0.1 m is reached upstream of the intervention.

The additional effect of the release of sediment that was trapped in the abandoned side channel is shown in Figure 4.13. As in the groyne removal simulation, this effect is only little, leading to a maximum increase in bed levels of 0.1 m after 100 years.

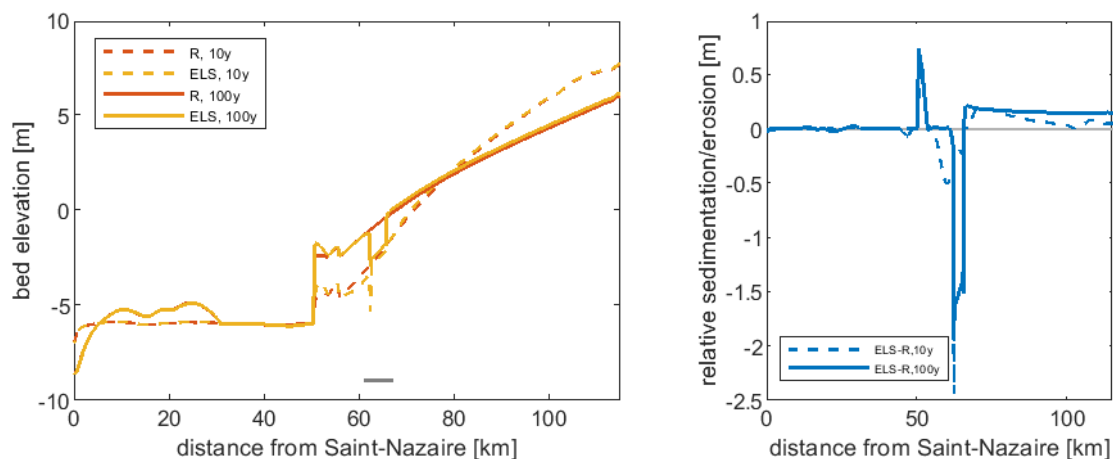


(a) Bed level in the main channel.

(b) Sedimentation/erosion relative to the reference scenario.

Figure 4.13: Effect of re-opening a side channel and release of trapped sediment on bed level after $T = 10$ yr and $T = 100$ yr compared to the reference scenario. The grey line indicates the location of the side channel, the grey arrow indicates the location where sediment is added.

Energy loss structure



(a) Bed level in the main channel.

(b) Sedimentation/erosion relative to the reference scenario.

Figure 4.14: Effect of energy loss structure on bed level after $T = 10$ yr and $T = 100$ yr compared to the reference scenario. The grey line indicates the location of the structure.

The energy loss structure that is planned for implementation in the Loire has significant morphological effects on a local scale and a much less pronounced effect on the scale of the entire reach (Figure 4.14). As was explained in Section 3.6.4, the results at the location of the intervention have no physical interpretation. In reality, the bed is fixated at the location of the structure, such that no bed level change should occur here. However, the results can be interpreted upstream and downstream of the intervention. The most important local effect is the deep erosion pit that occurs immediately at the beginning of the simulation just downstream of the energy loss structure. The erosion does not extend further downstream in the remainder of the simulation, but remains fixed at the downstream end of the structure. This is because the structure is situated just upstream of the groyne section end, where the bed accretes due to the sudden flow expansion. The intervention leads to slight relative sedimentation (0.2 m) throughout the reach upstream of the structure, due to the backwater effects induced by the increased roughness of the fixed layer.

No maintenance dredging

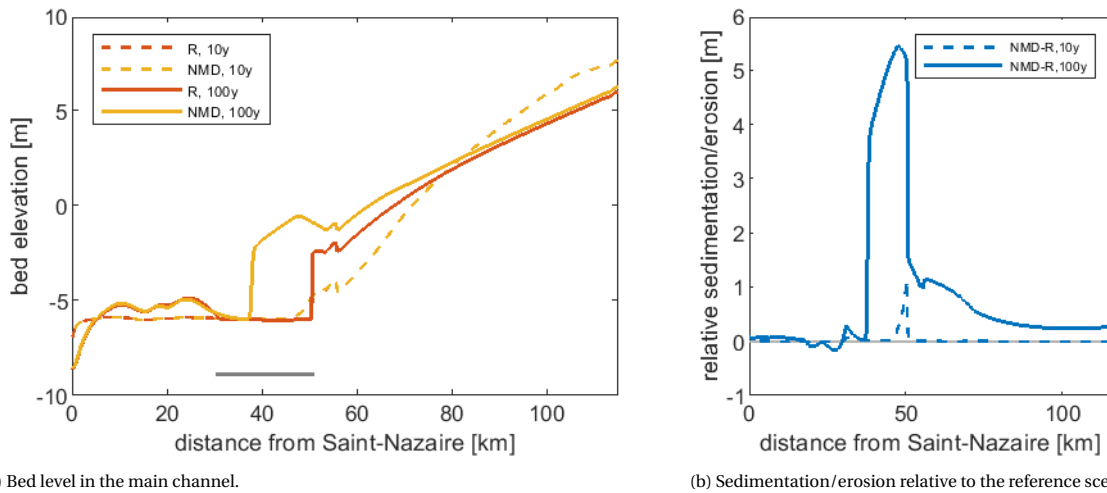


Figure 4.15: Effect of cessation of maintenance dredging in the estuary on bed level after $T = 10$ yr and $T = 100$ yr compared to the reference scenario. The grey line indicates the location of the intervention.

Evidently, cessation of maintenance dredging in the estuary (between km 30 and 50) affects the bed level not only in the estuary, but also throughout the entire river section (Figure 4.15). Although the effect diminishes when moving further upstream from the estuary, the intervention still leads to a sedimentation of 0.25 m relative to the reference scenario at the landward end of the domain. Furthermore, a steep sedimentation front propagates in downstream direction, leading to large bed level changes of up to 5.5 m in the estuary after 100 years. It is remarkable that this front does not diffuse in downstream direction, but maintains such a steep interface. Initially, sedimentation occurs downstream of the groyne section, 55 km upstream of the mouth, due to the sudden increase in cross-sectional area. Also at the transition between the river and estuary section, 50 km upstream of the mouth, sedimentation occurs due to the sudden change in bed slope and roughness. Just downstream of this initial discontinuity sedimentation is promoted due to the decrease in flow velocities, such that the hump grows in both downstream and upward direction. In this way the sedimentation front becomes steeper, which leads to an even more sudden decrease in flow velocities and further deposition downstream of the front. In the estuary, residual landward sand transport occurs roughly over the first 30 km upstream of the mouth due to gravitational circulation, whereas residual transport in barotropic conditions is close to zero for average flow conditions (see Figure 4.7). Hence, between the salt intrusion limit and the edge of the sedimentation front little bed level change occurs, such that the steep transition is maintained.

Assessment of individual measures

Using the results as described above, the interventions aimed at counteracting bed degradation can now be compared to each other in their effectiveness.

When focusing on the development within the first 10 years after the intervention, SN seem to be most effective in generating relative sedimentation throughout the river section. GR, SC and ELS all lead to relative erosion in the downstream part of the river section. For ELS, the relative deposition upstream of the structure is small, while immediately downstream of the fixed layer a deep erosion pit arises. For SC, upstream deposition and downstream erosion are about equal, and for GR the deposition is somewhat larger than the erosion when the discontinuity around km 50 is disregarded. NMD has little effect within the first 10 years.

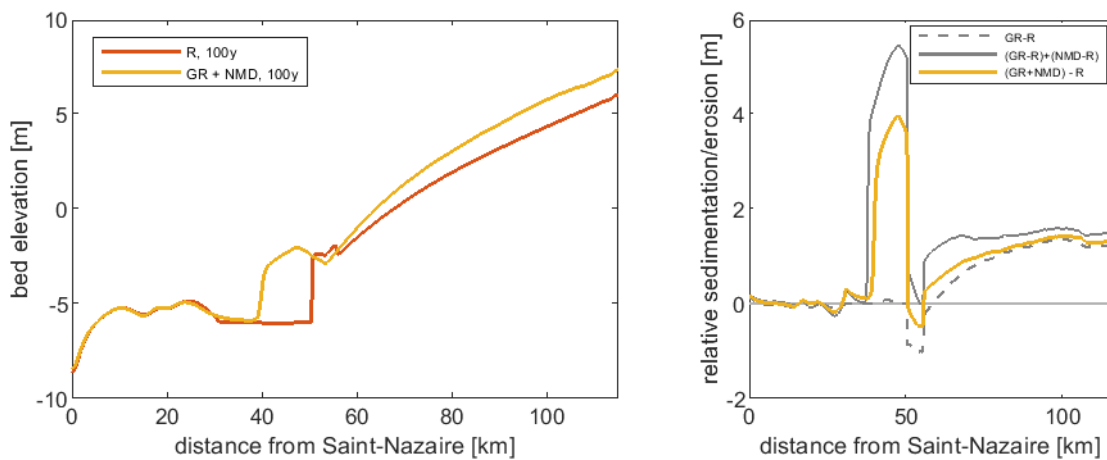
For the long-term response of the system to the interventions, the picture looks somewhat different. GR now has the largest aggrading effect, which increases in landward direction due to slope steepening. NMD has also reached considerable sedimentation throughout the river section and in the upper estuary. The effect of SN remains positive, but moderate throughout the river section. In the SC case, relative erosion downstream of the intervention has spread out, whereas the relative sedimentation along the modified reach and further upstream has only increased mildly compared to the 10-year result. The erosion pit downstream of the ELS remains deep, but does not move in downstream direction, while the upstream sedimentation due to back-water effects remains small.

On the basis of this qualitative analysis, the interventions could be ranked as presented in Table 4.1. Of course, this ranking can change completely when other evaluation criteria, such as costs or ecological benefits, are taken into account.

Table 4.1: Assessment of effectiveness of interventions against bed degradation.

Ranking	10 years	100 years
1	SN	GR
2	GR	NMD
3	NMD	SN
4	SC	SC
5	ELS	ELS

4.2.4. Combinations of measures



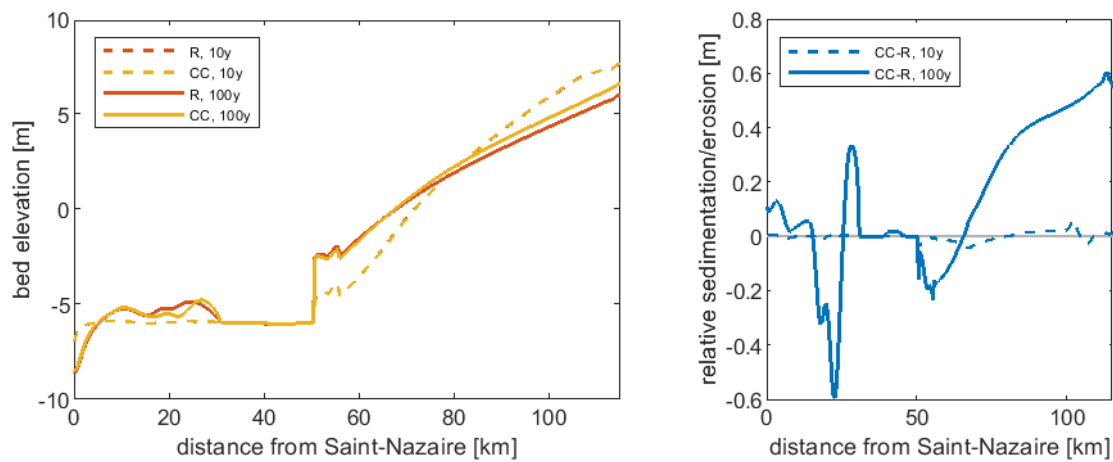
(a) Bed level in the main channel.

(b) Sedimentation/erosion relative to the reference scenario.

Figure 4.16: Effect of a combination of groyne removal and no maintenance dredging on bed level compared to the reference scenario. In the right figure, the dashed grey line shows the result of groyne removal only. The dark grey line indicates linear addition of the separate results of groyne removal and no maintenance dredging. The yellow line shows the result of the combination scenario. All results are given at $T = 100$ yr.

So far the effects of individual measures were assessed. In reality, however, a combination of different measures will be implemented. It is highly unlikely that a certain measure will lead to the same amount of sedimentation or erosion when applied in combination with another measure, as it leads to when it is applied individually. As the number of individual measures is too large to assess the effect of every possible combination, one combination is simulated to serve as an example. Figure 4.16 shows the results of this simulation, in which groyne removal is applied in combination with no maintenance dredging. Figure 4.16a shows the bed level of this scenario after 100 years, which indeed bears similarities with both the GR and the NMD simulation, see Section 4.2.3. In Figure 4.16b the bed level change with respect to the reference scenario can be seen for the combination scenario, as well as the added effect of both measures when applied individually. It turns out that the effect of a combination of GR and NMD is significantly smaller than the added effect of GR and NMD when applied individually. This result marks the importance of a combined assessment of measures that are planned to be implemented simultaneously.

4.2.5. Sensitivity to changes in boundary conditions: climate change



(a) Bed level in the main channel.

(b) Sedimentation/erosion relative to the reference scenario.

Figure 4.17: Effect of a climate change scenario under RCP 8.5 on bed level after $T = 10$ yr and $T = 100$ yr compared to the reference scenario.

As was explained in Section 3.6.6, the climate change scenario is simulated with a gradual increase in water level at the downstream boundary and a gradual decrease of the water and sediment discharge at the landward end. Hence, the effects of this scenario are noticed both in the upstream and in the downstream part of the domain, see Figure 4.17. The decrease in discharge leads to a steeper slope in the river section, which can be expected as the equilibrium bed slope is more sensitive to a decrease in discharge (leading to a steeper slope) than to a decrease in sediment load (leading to a flatter slope), if river width and sediment characteristics stay the same. Remarkably, part of the slope steepening is also caused by the increase in downstream water level.

In the estuary, relative erosion occurs between km 15 and 25, and relative sedimentation occurs between km 25 and 30. This could be explained by a larger salt intrusion length due to the increase in water depth, which leads to sand being transported further into the estuary.

The effect of this climate change scenario is of the same order of magnitude as the effects of planned human interventions, see Section 4.2.3. It is therefore important to take this process into account when assessing the effects of measures on a century-timescale.

4.3. Mud transport

4.3.1. Influence of hydrodynamic processes

For a barotropic situation with an average discharge (Figure 4.18), a net export of suspended sediment takes place (4.18a) and mud concentrations in the water column (4.18b) as well as in the bed (4.18c) are close to zero. The estuary approaches a morphodynamic equilibrium after about three months, at which point the mud availability in the bed remains constant (4.18c). In fact, for all considered discharges (the lowest being $Q = 200 \text{ m}^3/\text{s}$) the entire estuary remains ebb-dominant for suspended sediment transport in barotropic conditions, despite the flood-dominance of the tide.

An ETM only arises when the baroclinic pressure gradient is taken into account (Figure 4.19). For the same discharge, the estuary now starts to import mud up to the end of the salt wedge (4.19a), where transport from upstream and downstream converge and an ETM is formed (4.19b). The estuary is now not in morphodynamic equilibrium anymore: the mass of mud within the bed keeps steadily growing when the bed level is not updated (4.19c).

The large tidally averaged import of mud is mainly caused by the decrease of ebb velocities in the lower layers of the water column due to gravitational circulation. A large fraction of the suspended sediment resides in these lower layers and is not exported anymore during ebb. The bed shear stress stays below the critical value for erosion during almost the entire ebb duration, such that the mud that is imported during the previous flood and deposited at HW slack is not resuspended during ebb. Residual sediment import increases towards the end of the salt wedge and suddenly changes to residual export landward of this point, such that sediment accumulates here.

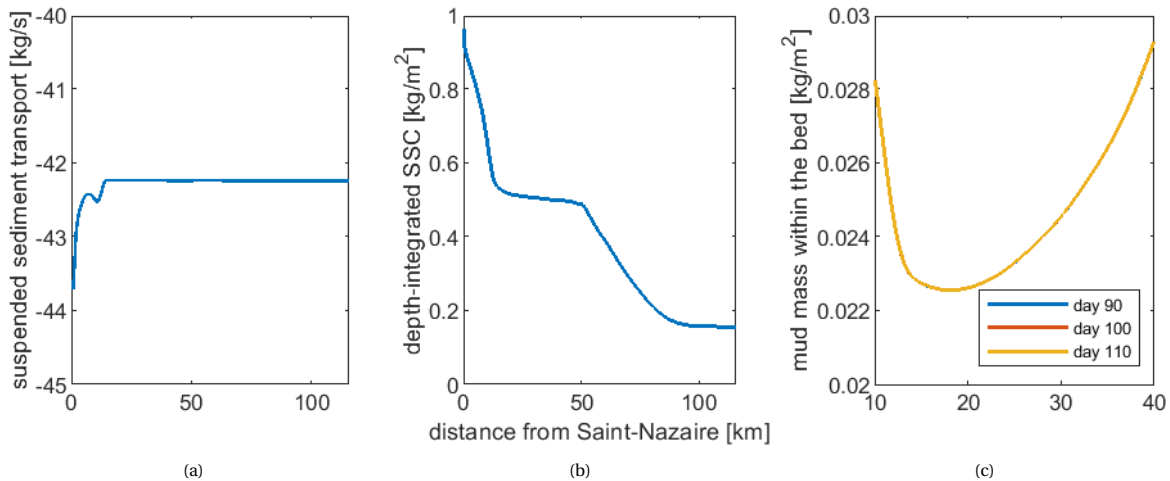


Figure 4.18: Mud transport for a barotropic situation with $Q = 845 \text{ m}^3/\text{s}$. All parameters are tidally averaged.

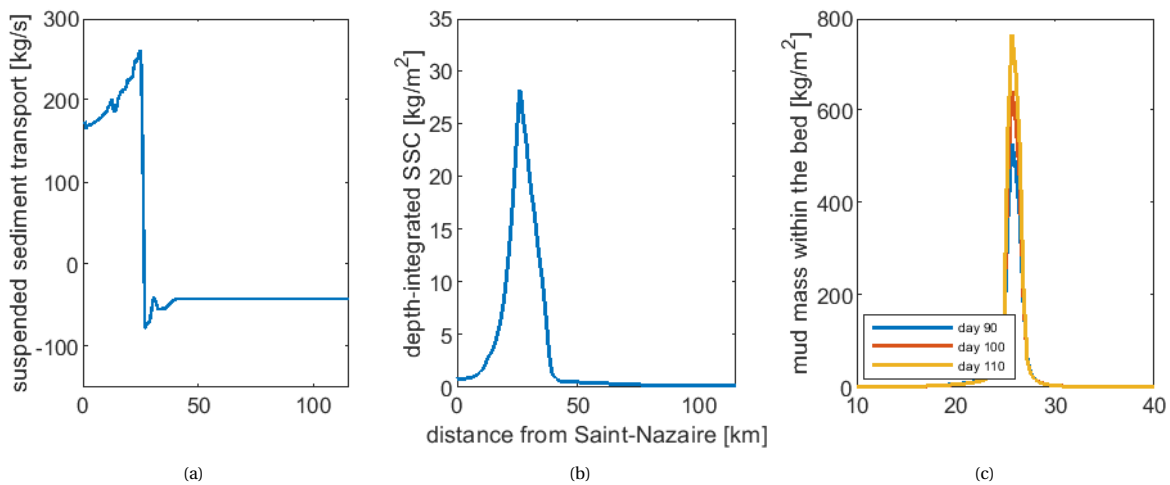


Figure 4.19: Mud transport for a baroclinic situation with $Q = 845 \text{ m}^3/\text{s}$. All parameters are tidally averaged.

The location and magnitude of the ETM depend on the river discharge. Salt intrudes less far for larger discharges, such that the ETM forms closer to the mouth and its extent is smaller. These results agree reasonably well with measured SSC in the estuary, see Figure 4.20 and Appendix B. The extent of the turbidity zone is underestimated for low discharges and its location is shifted somewhat in upstream direction compared to the observations.

Maximum depth-integrated SSC decrease for higher discharges, whereas for the amount of mud deposited on the bed a maximum is observed at $Q = 3000 \text{ m}^3/\text{s}$, see Figure 4.21. For $Q \leq 500 \text{ m}^3/\text{s}$, a maximum depth-integrated concentration of $33.5 \text{ kg}/\text{m}^2$ seems to be reached, after which SSC decrease rapidly for increasing discharge. This is mainly due to the exponential convergence of the estuary width. For higher discharges the ETM is located further downstream in a wider section of the estuary, leading to less lateral convergence of suspended sediment. This results in lower depth-integrated SSC.

The mass of mud within the bed is the result of two opposing influences. On the one hand, the extent over which deposition takes place is smaller for larger discharges. On the other hand, stratification increases for higher discharges, such that the longitudinal sediment transport gradient is larger and deposition is more efficient. Furthermore, the supply of riverine sediment increases for larger river flow. This leads to an increase in mud deposition within the estuary for discharges lower than $3000 \text{ m}^3/\text{s}$. For discharges higher than that, the turbidity zone is gradually pushed out of the estuary and mud deposition decreases. For $Q = 6000 \text{ m}^3/\text{s}$, the estuary becomes entirely ebb-dominant in terms of suspended sediment transport, see Appendix C.1, where a full overview of simulation results is provided. In all simulations, a steady growth of the bottom pool is reached after three months.

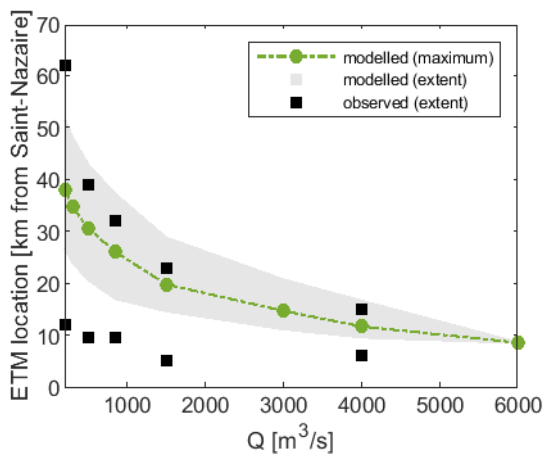


Figure 4.20: Location end extent of ETM for different discharges. Each green dot represents a model simulation. For model results, the extent is defined as the region where tidally averaged, depth-integrated SSC are larger than $5 \text{ kg}/\text{m}^2$ (the average water depth being approximately 10 m). For observations, the extent is defined as the region where SSC larger than $0.5 \text{ kg}/\text{m}^3$ have been measured 1 m below the water level.

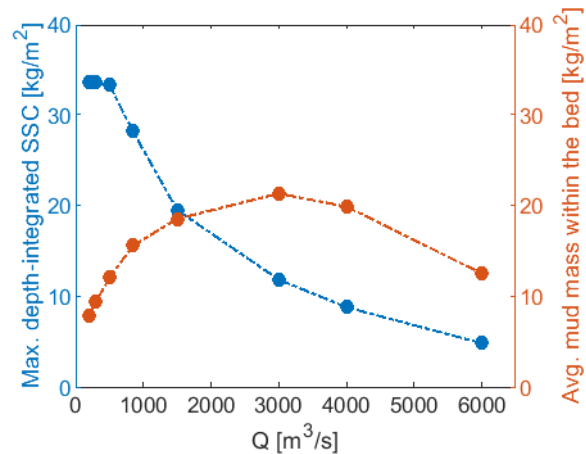


Figure 4.21: Suspended and deposited mud concentrations for different discharges. Dots represent outcomes of model simulations and are connected by lines. The blue line shows maximum SSC integrated over the water column and averaged over a tidal cycle. The red line shows mud mass within the bed after 110 days of simulation, averaged over a tidal cycle and over the area of the main channel and the transitional zone.

To investigate the contribution of tidal asymmetry to ETM formation, a simulation without an external M4 component is carried out, see Figure 4.22. The discharge is kept constant at $Q = 845 \text{ m}^3/\text{s}$. Without an external M4 tide, the estuary becomes significantly less flood-dominant, although a small M4 component is still generated internally.

It turns out that the external M4 tide contributes significantly to the magnitude of the ETM. Without an external M4 component, net sediment import in the gravitational circulation region is significantly smaller (4.22a) and depth-integrated SSC are more than 2 times lower (4.22b) compared to the reference scenario. The bottom pool grows much slower as well (4.22c). Remarkable is also the change in location of the ETM: without an external M4 tide the ETM forms more than 5 km closer to the mouth.

With the removal of the M4 component, not only the shape (spectral composition) of the tidal wave changes, but also its amplitude and therefore the amount of energy the wave contains. The changes in suspended sediment transport may be due to either of these effects. In order to separately investigate the influence of a change in tidal amplitude, a sensitivity analysis is performed on the amplitude of the M2 component

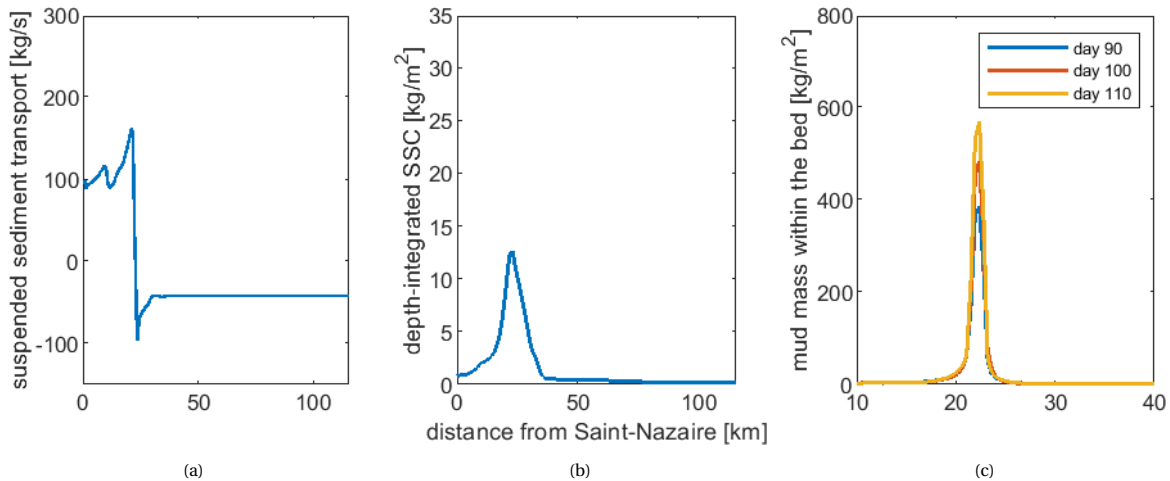


Figure 4.22: Mud transport for a baroclinic situation with $Q = 845 \text{ m}^3/\text{s}$, without an external M4 tide. All parameters are tidally averaged.

for the case where the M4 component is excluded, see Appendix C.2. In the analysis, the amplitude of the M2 tide is increased from 1.35 m to 1.95 m in increments of 0.05 m. From this set of simulations several notable results can be extracted, that will be discussed further in Section 4.3.4. For now the important result is that an increase of the M2 tidal amplitude leads to an increase in SSC. However, even for $a_{M2} = 1.95$ (which is effectively the addition of the M2 and M4 amplitudes from the reference scenario) SSC do not become nearly as high as for the reference scenario. It can be concluded that the spectral composition of the tidal wave indeed has a significant influence on the import of mud into the estuary.

It is however important to note that the tidal asymmetry does in itself not lead to the formation of an ETM in this model set-up. Although it is enhanced by the flood-dominance of the tide, an ETM can only exist due to the gravitational circulation. This is in contrast with earlier model studies for the Loire, in which it was hypothesized that the formation of the ETM is caused by tidal (duration) asymmetry, whereas the main effect of salinity gradients is to enhance concentrations near the tip of the salt wedge (Brenon and Le Hir, 1999; Le Hir and Thouvenin, 1992; Jalón-Rojas et al., 2016).

Furthermore, only one ETM is present in each simulation; no second ETM is detected in the freshwater zone landward of the salt wedge. For the Loire, the formation of such a secondary ETM has indeed not been reported. However, in many other macrotidal, flood-dominant estuaries, tidal transport mechanisms are often responsible for suspended sediment trapping in the freshwater zone, especially during low river flows (Burchard et al., 2018).

4.3.2. Consequences of historical deepening

Phase I: after deepening

Figure 4.23 shows suspended sediment transport parameters for the simulation representing the Loire shortly after deepening of the estuary. In this simulation, the depth is equal to the reference scenario (representing the current situation), but the bed is less smooth because the formation of fluid mud layers has yet to start. Furthermore, the effect of sediment on fluid density is switched off. The reader is referred to Section 3.6 for an extensive explanation of the scenario schematization.

Residual sediment import is significantly reduced with respect to the reference situation. An ETM still forms but maximum sediment concentrations are much smaller and there is no mud deposit to speak of. The decrease in mud import mainly occurs because the effect of sediment on fluid density is switched off. If this effect is switched on, turbulence is damped significantly and velocities increase, especially during flood. This process favors import of mud, which again leads to more turbulence damping.

Decreasing the Chézy coefficient from 60 to 53 $\text{m}^{1/2}/\text{s}$ leads to a slight decrease in tidal range and salt intrusion. Although current velocities decrease somewhat, bed shear stresses slightly increase due to the larger roughness coefficient. This leads to larger erosion and resuspension rates, such that the average mass of the bottom pool decreases somewhat whereas SSC slightly increase. Only if C is decreased further, for example to 40 $\text{m}^{1/2}/\text{s}$, the import of mud is reduced significantly. The bed shear stresses remain relatively

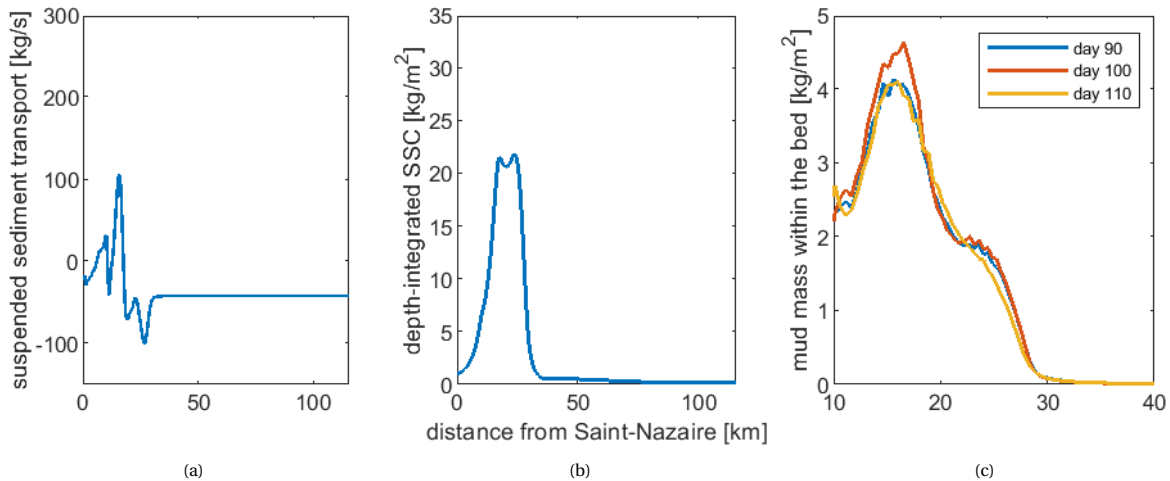


Figure 4.23: Mud transport for a baroclinic situation with $Q = 845 \text{ m}^3/\text{s}$. All parameters are tidally averaged.

large, such that a large percentage of mud is found in suspension. Hence, SSC decrease only slightly, whereas the maximum amount of mud contained in the bottom pool is reduced to little more than 200 kg/m^2 , see Figure 4.24. Notable is also the change in location of the ETM with respect to the simulation with $C = 53 \text{ m}^{1/2}/\text{s}$. Due to the limited salt intrusion, the ETM shifts from 25 to 21 km upstream of the mouth. However, switching off the effect of sediment on fluid density remains the most important contribution to the results of Figure 4.23.

This scenario gives an important clue that the decrease in hydraulic drag and damping of turbulence due to large mud concentrations has indeed played a large role in the evolution of the Loire estuary towards a hyper-turbid state.

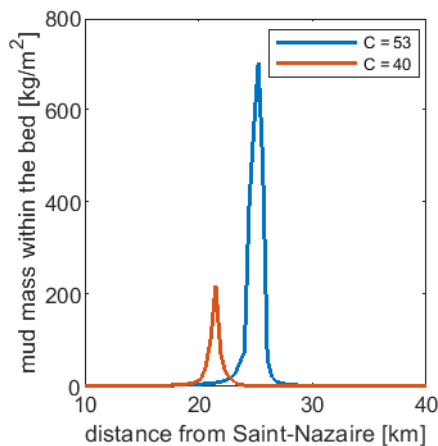


Figure 4.24: Mud deposit after 110 days of simulation, for 2 different Chézy coefficients. The unit of the Chézy value ($\text{m}^{1/2}/\text{s}$) is omitted due to space limitations.

Phase II: before deepening

The second scenario represents the historical situation before major dredging works took place and the estuary was much shallower. For this scenario, the estuary is somewhat more flood-dominant than the reference scenario representing the current situation, see Figure 4.25. This makes sense as the ratio a/h (tidal amplitude over water depth) is generally larger in the historical scenario: over the first 35 km upstream of Saint-Nazaire, the decrease in water depth with respect to the current situation is larger than the decrease in tidal amplitude. A large ratio of a/h is known to induce flood-dominance (Friedrichs and Aubrey, 1988). In that case the difference in water depth between flood and ebb is relatively large, and as the wave celerity in shallow water scales with the water depth, flood velocities will be larger than ebb velocities.

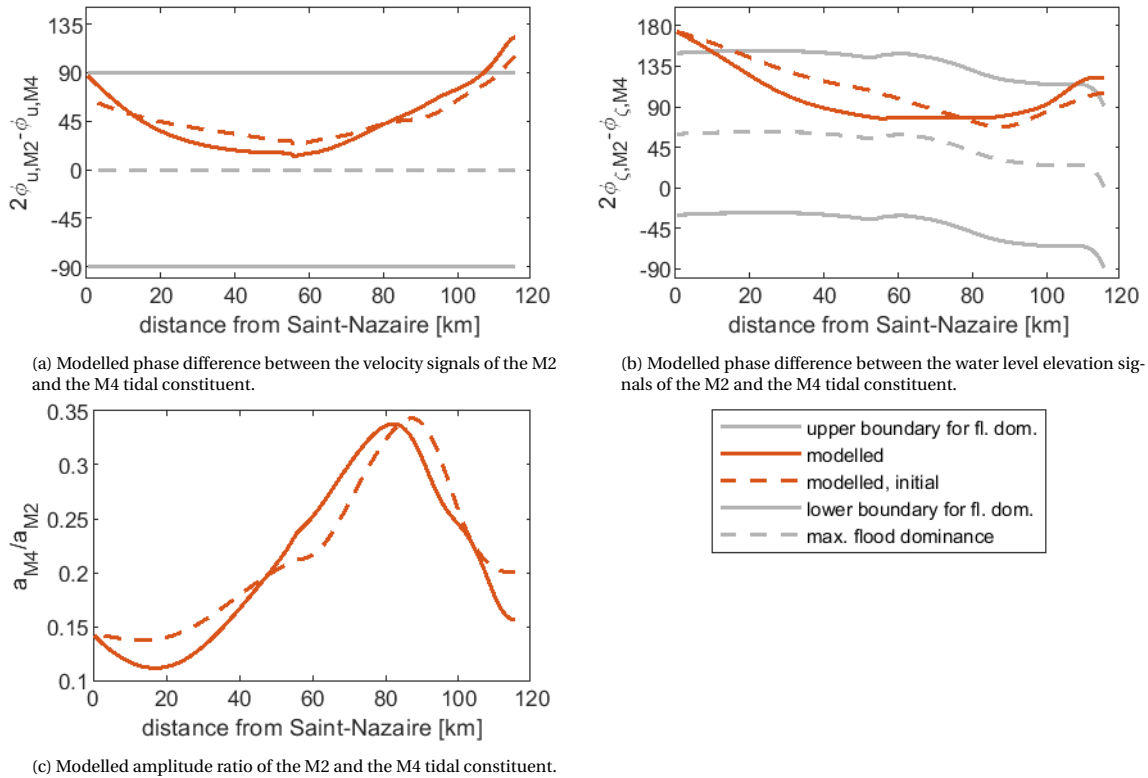


Figure 4.25: Indicators of the nature (Figures 4.25a and 4.25b) and strength (Figure 4.25c) of the tidal asymmetry, for $Q = 845 \text{ m}^3/\text{s}$.

However, it should be noted that in the period before deepening of the estuary took place, the tidal flat area was also much larger, which induces ebb-dominance. This aspect will be considered separately in the tidal flat restoration scenario (see Section 4.3.3). For now the focus is on the effect of deepening only.

Next to a slight change in tidal asymmetry, the main effect of the shallower estuary is damping of the tidal wave, see Figure 4.26. Instead of increasing, the tidal range now decreases in upstream direction, changing the estuary from amplified to damped. Furthermore, a decrease in salt intrusion length is observed, see Figure 4.27. Salt transport is governed by landward-directed dispersive or mixing-type transport due to tide-driven and density-driven processes, balanced by seaward-directed advection due to river discharge. Hence, a decrease in salt intrusion length may be due to a change in either of these three factors. The relative contribution of changes in the abovementioned dispersion and advection processes to the decrease in salt intrusion length is investigated further through the use of the analytical salt intrusion model for convergent estuaries by Kuijper and Van Rijn (2011). A drawback of these types of models is that all dispersive processes are represented by one longitudinal dispersion coefficient. This approach must be used as there is still a great lack of knowledge of dispersive processes in real estuaries (Jay et al., 1997). The relative contribution of tide- and density-driven processes to the total dispersion is therefore not straightforward to determine. By examining the influence of each parameter that changes in value between the current and the historical situation within the equation for the salt intrusion length, some conclusions can still be drawn.

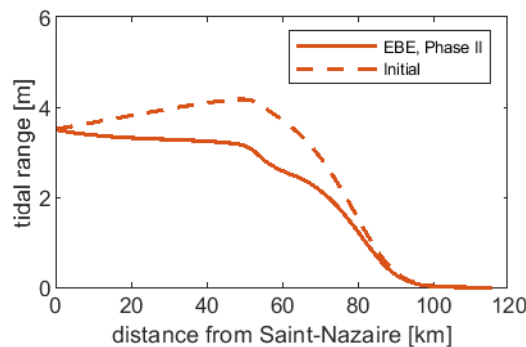


Figure 4.26: Modelled tidal range along the river-estuary for $Q = 845 \text{ m}^3/\text{s}$.

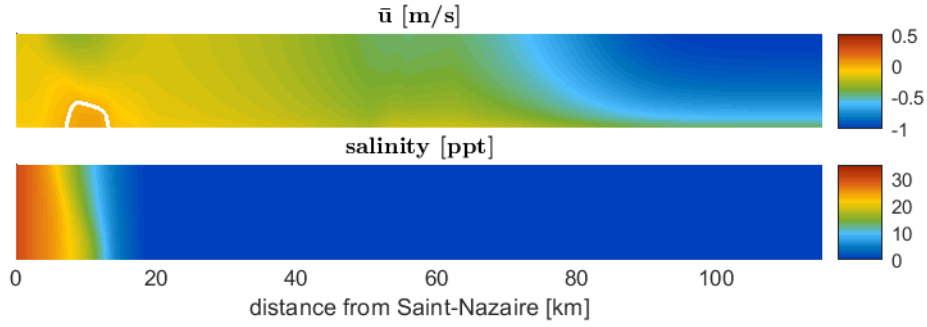


Figure 4.27: Mean horizontal velocity for an external M2 and M4 tide, a constant river discharge of $Q = 845 \text{ m}^3/\text{s}$ and a salinity of 35 ppt imposed at the seaward boundary. The zero-velocity contour is indicated in white. The lower plot shows tidally averaged salinity.

It is important to note that in general, the analytical model predicts much larger salt intrusion lengths than the numerical model. For the reference situation, the maximum salt intrusion length is about 30 km according to the numerical model, whereas the analytical model gives a length of about 80 km. Kuijper and Van Rijn (2011) also compared their analytical model results to an idealized model of a convergent estuary in Delft3D and arrived at the same conclusion. They attributed this discrepancy to the unrealistically smooth geometry of the schematized estuary, which would lead to an underestimation of large-scale mixing processes, thus limiting dispersion. As the analytical model was calibrated on data from real estuaries, the analytical model implicitly accounts for the irregularities present in these natural alluvial systems. This reasoning would indeed explain the observed discrepancy, and also the underprediction of salt intrusion lengths by the numerical model compared to observations in the Loire (see Section 3.5). However, it does not explain the fact that the numerical results are still much closer to the observations than the results of the analytical model. This is probably due to the poor analytical model performance for relatively short, strongly convergent estuaries (such as the Loire), as was already noticed by Kuijper and Van Rijn (2011). For these estuaries, in which the salt intrusion is limited, the analytical model indeed overpredicts intrusion lengths.

Despite the differences in absolute values of the salt intrusion length as predicted by the analytical and the numerical model, relative changes in the intrusion length as a result of changes in model parameters are in reasonable agreement. While the numerical model gives a decrease of 12 km (39%) in salt intrusion length with respect to the reference scenario, the analytical model predicts a decrease of 34 km (43%). The analytical model can therefore still be used to gain insight into the influence of advective and dispersive processes on salt intrusion.

In the analytical model, the largest influence on the decrease in salt intrusion length is the decrease in the following parameter, representing the relative importance of the propagation velocity of a density current with respect to the maximum tidal flow velocity:

$$\frac{v_{\Delta}}{\hat{u}_0} \quad (4.1)$$

where

$$v_{\Delta} = \sqrt{\frac{\Delta\rho}{\rho} g h_0} \quad (4.2)$$

with:

- $\Delta\rho$ density difference between sea and river water [kg/m^3]
- ρ density of fresh water [kg/m^3]
- g the gravitational acceleration [m/s^2]
- h_0 water depth at the estuary mouth [m]
- \hat{u}_0 amplitude of the tidal velocity [m/s]

Of the abovementioned parameters, h_0 is the only one that changes significantly, leading to a decrease in the value of v_{Δ}/\hat{u}_0 and a significant decrease in the dispersion coefficient D_0 and salt intrusion length L_{max} . This indicates that a decrease in the strength of the gravitational circulation is an important cause of the decrease in salt intrusion.

The same finding results from an analysis of salt transport mechanisms with the numerical model. To investigate the relative influence of tide- and density-driven processes on this transport, salt is substituted with a sediment fraction for the reference simulation and the historical deepening simulation. In this way, the effect of the constituent on the fluid density can easily be switched on and off, which for salt is not the case. The settling velocity of the sediment fraction is set to zero and its concentration at the boundary is set equal to the salinity used in the simulations with salt. Furthermore, the density of the sediment is such that the resulting fluid density (when density effects are included) is equal to that of salt water with the same constituent concentration. Results of these simulations are included in Appendix D.

When the effect of sediment on fluid density is switched off, tidal processes form the only mechanism that transports salt into the estuary. As it turns out, the influence of tidal processes on salt transport is similar for the reference situation and the historical situation (before deepening). Only when the effect of sediment on fluid density is switched on, thus taking the effect of density-driven processes into account as well, a large difference can be observed between the current (deep) and historical (shallow) situation. Whereas in the reference situation, density-driven processes have a strong impact on hydrodynamics and import of salt, in the historical situation the gravitational circulation is much weaker and leads to a significantly smaller intrusion length. These same differences are observed when comparing Figure 4.3 and 4.27.

Due to the decrease in salt intrusion length and strength of the gravitational circulation, the import of suspended sediment also stops. The amount of mud deposited on the bed remains stable and close to zero and maximum depth-integrated SSC are less than 2 kg/m^2 when averaged over a tidal cycle, see Figure 4.28. It can be concluded that human-induced deepening of the estuary has directly led to an increase in mud import through both tide- and density-driven processes. This initial response has set a feedback mechanism in motion, in which the import of mud is promoted further due to a decrease in bed roughness and damping of turbulence due to large SSC, as observed in Phase I of this Section.

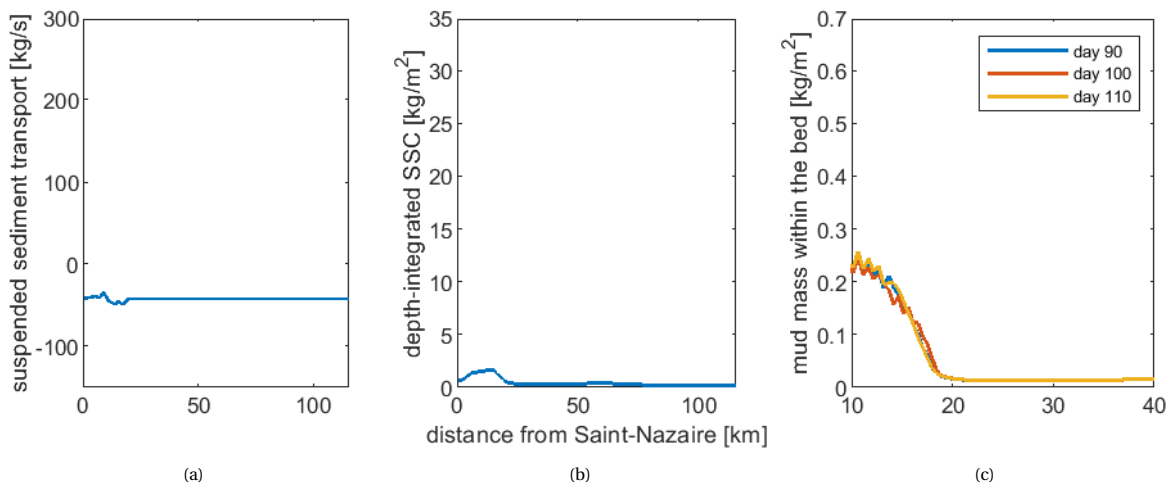


Figure 4.28: Mud transport for a baroclinic situation with $Q = 845 \text{ m}^3/\text{s}$. All parameters are tidally averaged.

4.3.3. Measures to decrease turbidity

The question remains if the current, hyper-turbid state of the Loire can be reversed. The most logical way to reach this goal would be to reverse the historical changes to the estuarine geometry, i.e. to increase the bed elevation and to bring back the intertidal area that has been reclaimed in the past. Both these interventions are simulated with the model. Of course, in practice these measures are very hard to realize on a large scale, due to the large costs involved and the practical limitations, for example because a minimum water depth must be maintained for navigation.

Estuarine bed elevation

The effectiveness of an increase in bed levels in the estuary is investigated by implementing the bed topography used in Phase II of the historical scenario in the current situation, without changing the Chézy coefficient and keeping the effect of sediment on fluid density switched on. As can be seen from a comparison between Figure 4.29 and 4.28, the results for this scenario are very similar to those of the historical scenario representing the situation before deepening (Phase II).

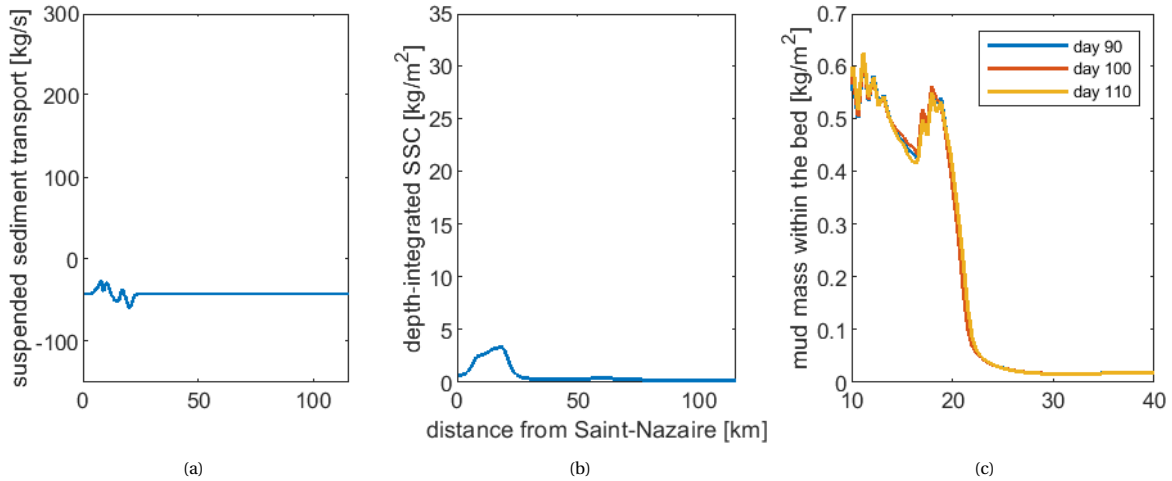


Figure 4.29: Mud transport for a baroclinic situation with $Q = 845 \text{ m}^3/\text{s}$. All parameters are tidally averaged.

Tidal flat restoration

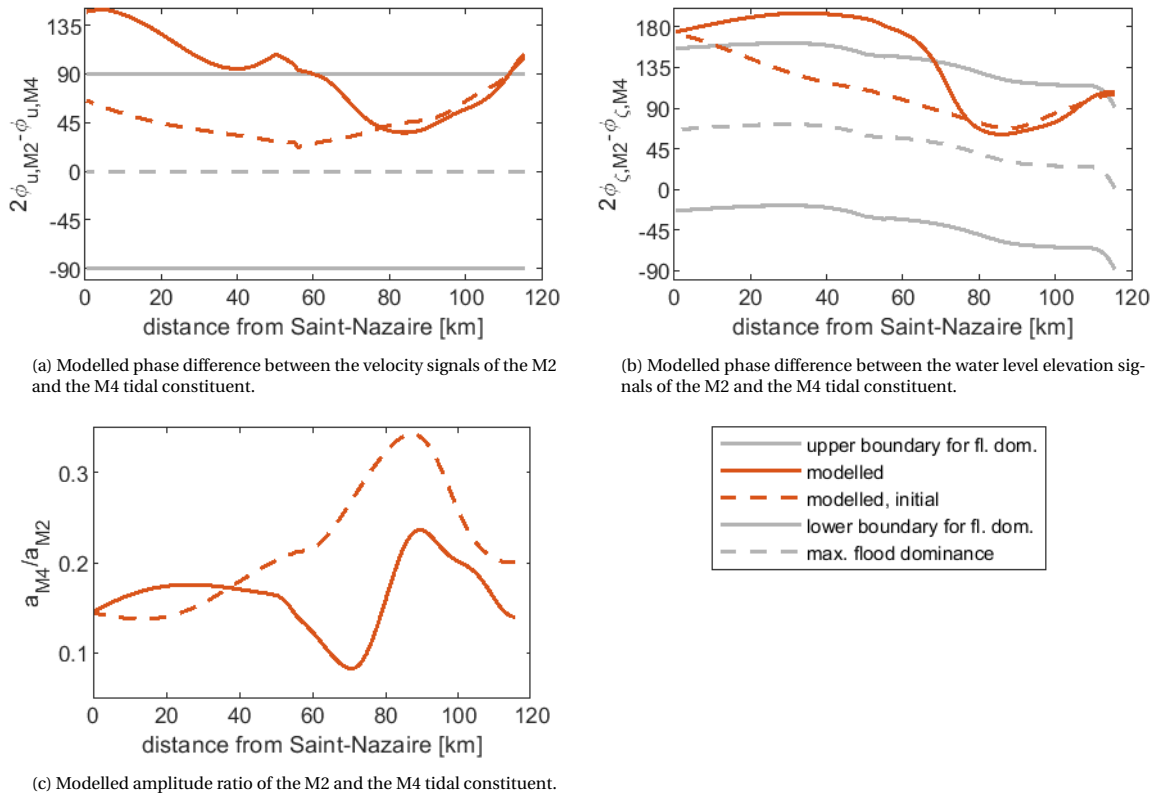


Figure 4.30: Indicators of the nature (Figures 4.30a and 4.30b) and strength (Figure 4.30c) of the tidal asymmetry, for $Q = 845 \text{ m}^3/\text{s}$.

When tidal flats are restored, ebb velocities increase whereas flood velocities are slightly damped. The tidal range along the estuary does not change significantly. The estuary turns from flood- into ebb-dominant, but it stays in the regime where HW slack is longer than LW slack ($0^\circ < \Delta\varphi_u < 180^\circ$), see Figure 4.30. For this scenario the salt intrusion length decreases with 3 km, which is again investigated further using the analytical salt intrusion model by Kuijper and Van Rijn (2011). For this scenario an even stronger decrease of the parameter $\nu\Delta/\hat{u}_0$ results (see Equation 4.1), as the cross-sectionally averaged depth in the mouth becomes much smaller due to the large area of shallow flats. In this case, this is the only parameter that has a negative (decreasing) influence on the salt intrusion length. All other parameters that change due to the new geometry

(tidal excursion length, cross-sectional area, river runoff velocity and tidal amplification factor, all increasing) lead to an increase in the intrusion length, but their influence is much weaker. An additional effect could be that velocities are now maximum during ebb instead of during flood. Since stratification and gravitational circulation are normally strongest during ebb due to tidal straining, increased tidal mixing during ebb is effective to weaken this circulation.

Hence, also in this case weakening of the gravitational circulation is the main cause of the decrease in salt intrusion length. The same is found from model simulations where salt is replaced with a sediment tracer, see Appendix D.3. Just as in the case of elevating estuarine bed levels (see Section 4.3.2), simulations in which the effect of sediment on fluid density is switched off (thus taking only tidal processes into account), do not show large differences in constituent concentration and mean horizontal velocities between the reference scenario and the situation with tidal flats. Only when density-driven processes are taken into account, it can be seen that the import of salt and the strength of the gravitational circulation is much smaller for the simulation with tidal flats than for the simulation without them, see also Figure 4.3 and 4.31.

Due to the intervention the estuary now starts exporting mud (Figure 4.32a), such that the maximum depth-integrated SSC reduce to about 3 kg/m^2 (4.32b) and mud deposits remain close to zero (4.32c).

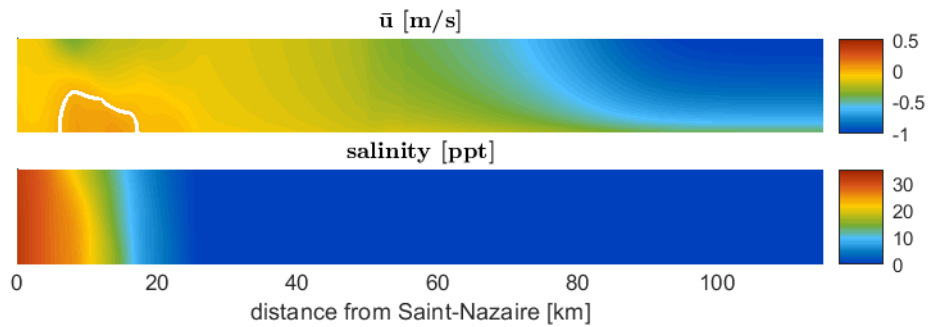


Figure 4.31: Mean horizontal velocity for an external M2 and M4 tide, a constant river discharge of $Q = 845 \text{ m}^3/\text{s}$ and a salinity of 35 ppt imposed at the seaward boundary. The zero-velocity contour is indicated in white. The lower plot shows tidally averaged salinity.

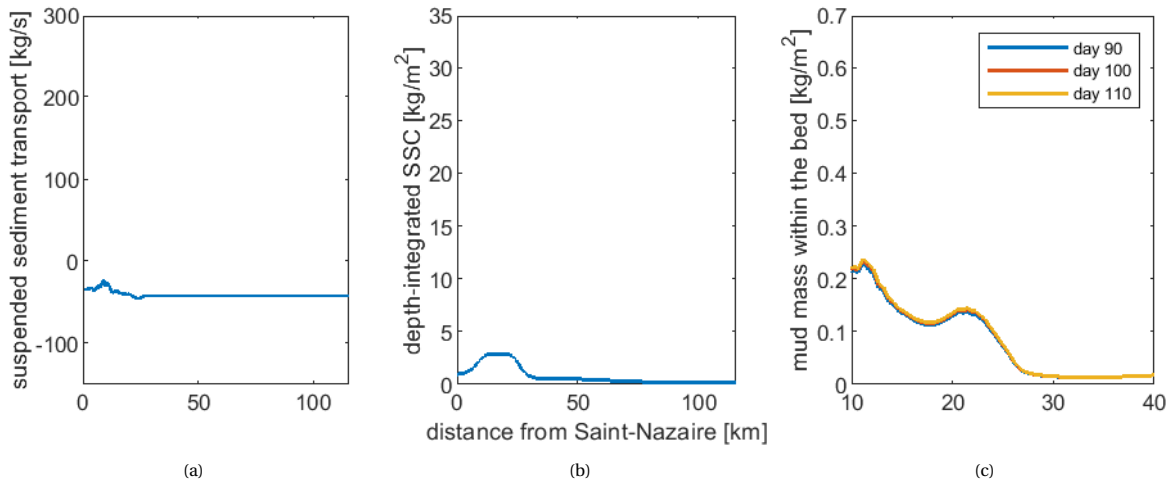


Figure 4.32: Mud transport for a baroclinic situation with $Q = 845 \text{ m}^3/\text{s}$. All parameters are tidally averaged.

4.3.4. Sensitivity to changes in boundary conditions: tidal schematization

M2 component

The results of a variation in the amplitude of the M2 component (as shown in Appendix C.2) were already partly discussed in Section 4.3.1 in relation to a scenario including an M4 component as well. A more careful investigation of this sensitivity analysis reveals some interesting results, that are summarized in Figure 4.33.

As can be seen from this figure, maximum depth-integrated SSC increase monotonically for increasing tidal amplitude. This is not unexpected, because an increase in tidal amplitude leads to larger tidal currents

in the estuary. In a more tidally energetic environment, more sediment can be kept in suspension. For the amount of mud deposited on the bed however, two regimes can be distinguished. For amplitudes smaller than 1.60 m, the sediment trapping efficiency of the estuary increases for increasing amplitude. Hence, both the mud deposit and SSC increase in this regime. For $a_{M2} = 1.60$ m a maximum is reached for the amount of mud deposited on the bed, after which it monotonically decreases for increasing amplitude. Apparently, in this regime the estuary does not become a more efficient sediment trap. Still, the conditions in the estuary become more energetic in the area where longitudinal convergence of suspended sediment occurs. As a result, SSC increase whereas the bottom pool decreases.

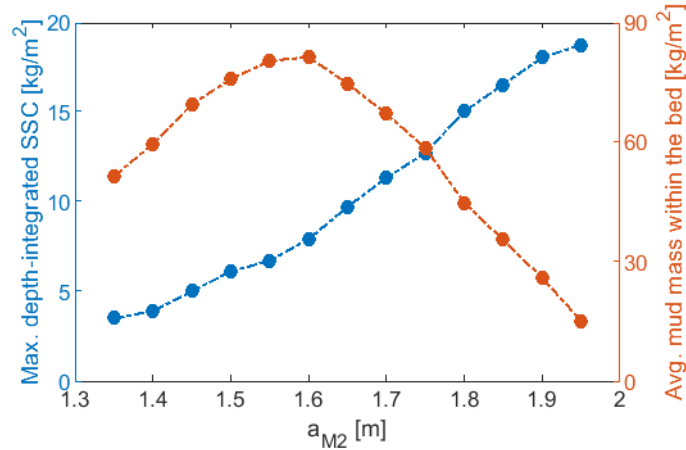


Figure 4.33: Suspended and deposited mud concentrations for different tidal amplitudes. The simulations (each represented by a pair of blue and red dots) only contain an M2 component, river discharge is set constant at $845 \text{ m}^3/\text{s}$. The blue line shows maximum SSC integrated over the water column and averaged over a tidal cycle. The red line shows mud mass within the bed after 110 days of simulation, averaged over a tidal cycle and over a distance of 15 km around the center of the ETM (15 to 30 km upstream of Saint-Nazaire, as the location of the ETM varies only little between different simulations).

M2, M4 and S2 component: inclusion of the spring-neap tidal cycle

As mentioned already in Section 3.3, it is well known that the spring-neap tidal cycle (resulting from the interaction between the M2 and S2 component) can have a significant influence on the residual transport of fine sediment (Allen et al., 1980; Fettweis et al., 1998). For simplicity, the S2 component was excluded from the analysis of the system behaviour and effectiveness of measures. To investigate the sensitivity of the results to this schematization, a simulation was carried out with a tidal boundary condition containing an M2 ($a_{M2} = 1.75$ m), M4 ($a_{M4} = 0.20$ m) and S2 component ($a_{S2} = 0.63$ m), as obtained from tidal analysis of water levels at Saint-Nazaire, see Section 3.5. The results of this simulation are compared with the reference scenario, see Figure 4.34 and 4.35.

Between the figures, several marked differences can be noted. Figure 4.34 shows a steady growth of the mass of sediment within the bed. When the S2 component is included, this growth is slower and more variable. Growth is fastest when water level amplitudes are decreasing, towards neap tide. When amplitudes are increasing the growth stops and the sediment mass even decreases slightly just before spring tide. This inverse relation between growth of the bottom pool and tidal amplitude (that was also observed for an M2 component only with $a_{M2} \geq 1.60$ m) reveals that gravitational circulation is a more important mechanism for sediment trapping than tidal pumping. During neap tides, gravitational circulation is dominant over tidal mixing processes and sediment is trapped efficiently. During spring tides, landward transport of sediment by tidal mixing increases, but the gravitational circulation is much weaker, leading to increased export. The net effect is a smaller growth of the sediment mass over the entire fortnightly cycle, compared to the scenario without the S2 component. Note that in these simulations the bed level is not updated, which means that the hydrodynamics are not affected by bed level changes. In reality velocities would increase in regions where large amounts of mud are deposited due to the decrease in water depth, thus enhancing erosion.

Furthermore, the amount of mud within the bed fluctuates more for larger tidal amplitudes, when both deposition and erosion fluxes are large. The same yields for SSC during spring tide, but of course the fluctuations are opposite from those of the deposits (SSC increase when deposits are decreasing).

Compared to the situation without S2 tide, SSC averaged over the entire spring-neap cycle are larger and residual import is smaller (see Appendix C.3), highlighting the importance of spring tides for resuspension and flushing of mud.

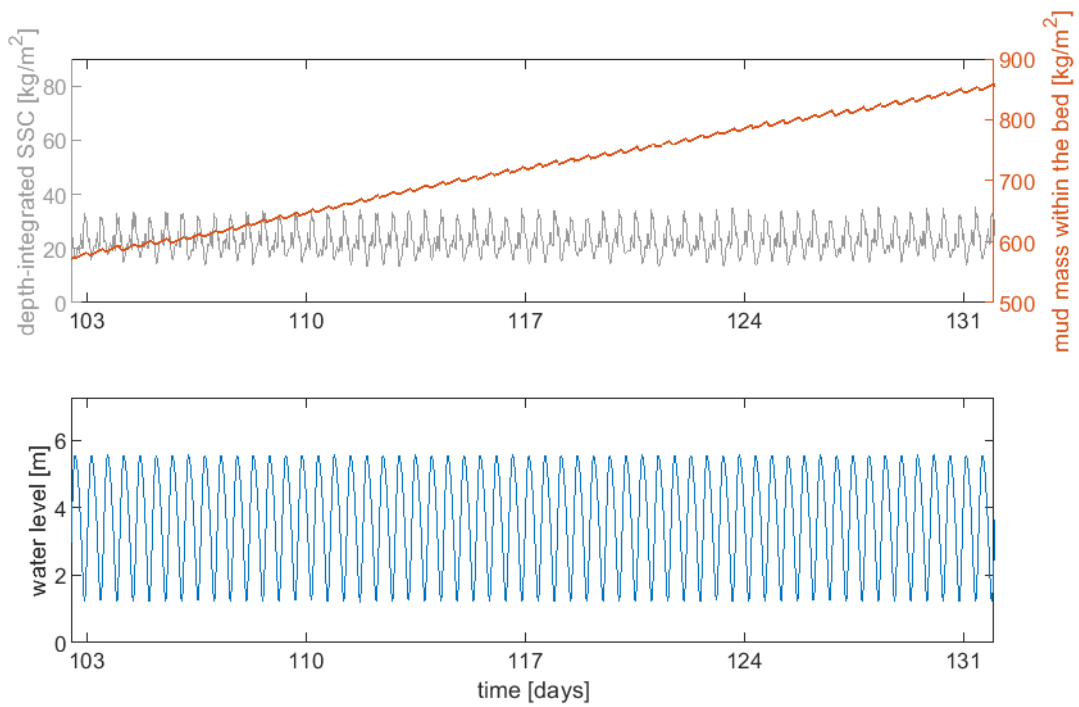


Figure 4.34: SSC and mud mass within the bed at the center of the turbidity maximum, 26 km upstream of the mouth. The bottom plot shows the water level record at the same location. The tide imposed at the downstream boundary contains an M2 and M4 component, as obtained from tidal analysis of water levels at Saint-Nazaire.

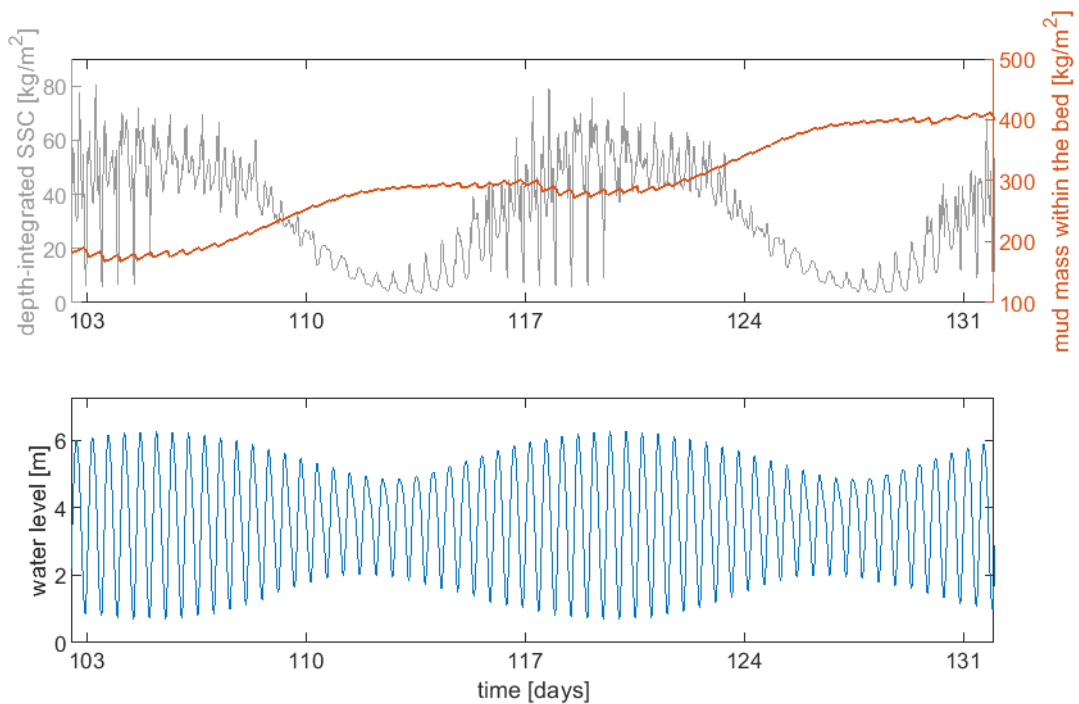


Figure 4.35: SSC and mud mass within the bed at the center of the turbidity maximum, 25 km upstream of the mouth. The bottom plot shows the water level record at the same location. The tide imposed at the downstream boundary contains an M2, M4 and S2 component, as obtained from tidal analysis of water levels at Saint-Nazaire. Note the different limits of the right vertical axis in the upper plots of Figure 4.34 and 4.35.

4.4. River-estuary interaction

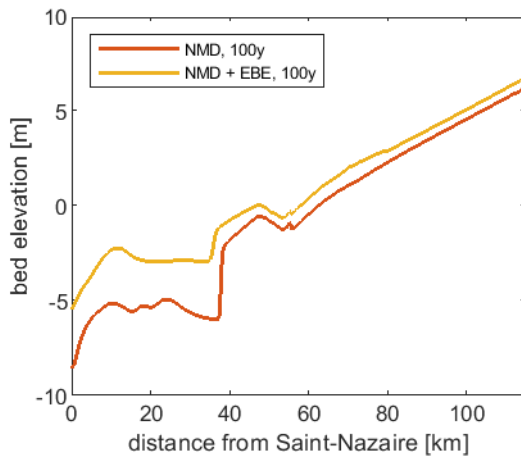


Figure 4.36: Effect of estuarine bed elevation (without maintenance dredging) in the estuary on bed level after $T = 100$ yr compared to a simulation without maintenance dredging.

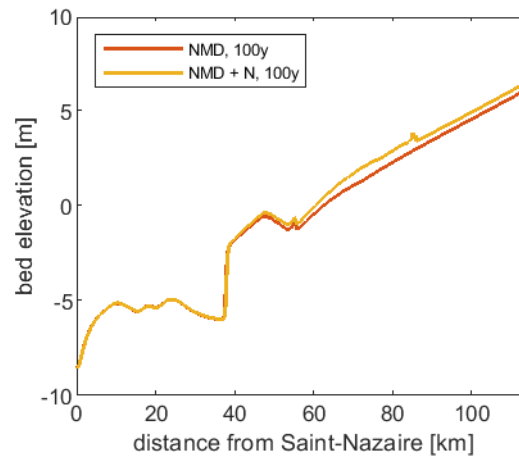


Figure 4.37: Effect of sediment nourishments (without maintenance dredging) in the river on bed level after $T = 100$ yr compared to a simulation without maintenance dredging.

One of the aims of this research is to investigate the interaction between the river and estuary section, as so far these sections have mostly been modelled separately. In order to assess the extent to which measures in the river influence the morphology of the estuary and vice versa, two simulations have been performed. In the first simulation the effect of increasing the bed elevation in the estuary on bed levels further upstream is assessed, see Figure 4.36. The second simulation concerns the effect of sediment nourishments in the river section on bed levels in the estuary, see Figure 4.37. These two scenarios represent the reversal of the two historical interventions that have taken place on the largest scale within the Loire river-estuary: deepening of the estuary and sand mining in the river.

In both simulations maintenance dredging is switched off. If this feature is not switched off, maintenance dredging acts as a barrier between the estuary and river section, as it keeps the bed level between km 30 and 50 fixed. Any additional sediment supply from downstream or upstream will then only lead to an increase in dredged volumes and not to a change in bed levels. The results of both simulations are therefore compared to a reference situation where maintenance dredging is switched off as well.

Results clearly show that an increase in bed levels in the estuary significantly affects bed levels throughout the entire domain, whereas sediment nourishments in the river do not influence bed levels in the estuary at all. These results may indicate that deepening of the estuary has been an important cause of autonomous, retrogressive erosion, whereas sand mining may have influenced the morphology of the river section in both upstream and downstream direction, but has not necessarily led to autonomous deepening of the estuary.

5

Discussion

5.1. Simplifications

Due to the high degree of schematization adopted in the model set-up, several drivers of the morphological development of the river-estuary are not taken into account. The representation of the tide at the seaward boundary with only an M2 and an M4 component has important consequences for the model results, as these were shown to be sensitive to changes in the tidal motion. Excluding the S2 component from the tidal signal imposed at the boundary is expected to be the most influential simplification in this respect. Spring-neap variations are significant in the Loire estuary, where the S2 component has the largest amplitude (0.63 m) after the M2 component (1.75 m), and have been shown to have considerable influence on sediment transport, in this research (Section 4.3.4) as well as in literature (e.g. Allen et al., 1980; Fettweis et al., 1998; Guo et al., 2014). Excluding these variations leads to an underestimation of SSC and an overestimation of mud deposition on the bed. The influence on the bed profile has not been investigated in this research, but was shown to be negligible for a similar model of the lower Fly river in Papua New Guinea (Canestrelli et al., 2014). However, Canestrelli et al. (2014) also showed that in general, including more tidal components leads to a lower equilibrium bed profile as tidal flushing increases. In the case of the Loire, including the N2 component ($a_{N2} = 0.37$ m) would then probably lead to the largest decrease in bed levels with respect to the reference situation.

The highly simplified representation of the river-estuary geometry introduces several discrepancies between model results and reality. Firstly, river bends are not included in the model, such that bend-induced spiral flow is neglected. The system is represented by a single channel with constant depth in lateral direction, ignoring the presence of islands and bars. Such variations are expected to be responsible for large-scale mixing processes (Kuijper and Van Rijn, 2011). Hence, the too smooth representation of the channel geometry can explain why salt intrusion is underpredicted for low discharges. Furthermore, channel and floodplain depth, width and slope are based on rough estimates using maps and figures of the study area (GIP Loire Estuaire, 2009; Brière et al., 2011a) and not on detailed data analyses. Cross-sectional areas are therefore not likely to coincide with reality, leading to discrepancies in flow velocities and water levels. Finally, the presence of tributaries is ignored, which together add a discharge to the domain in the order of 5% of the discharge from upstream. The sediment supply by these tributaries is however unknown, such that no statements can be made regarding the effect of ignoring tributaries on bed levels in the main channel.

Furthermore, wind and wind waves have been excluded from our analysis. Both these processes can influence estuarine morphology. As the Loire is a narrow, macrotidal estuary, wind waves play an important role only in the estuarine mouth zone (Dronkers, 2017). Excluding wind waves is therefore not expected to introduce large deviations. Wind can drive vertical circulations by inducing a shear stress at the water surface. In alluvial estuaries this mixing mechanism is considered less important than the tide- and density-driven processes (Savenije, 2012), but wind-induced resuspension can nonetheless lead to marked variations in SSC (De Jonge et al., 2014).

5.2. Consequences of numerical modelling approach

In this research an idealized modelling approach is taken on to assess the effects of both historical and future interventions. The model is calibrated qualitatively with observations that are representative for the current situation. This approach presents uncertainties regarding the validity of the results. Not only can recent observations not be precisely reproduced, the model is also not calibrated for the historical and future situations it has to represent. It is therefore good practice to perform an extensive sensitivity analysis on model results in order to obtain insight in the uncertainty of the conclusions that are drawn from these results (Schuttelaars et al., 2013). A start has been made with this by investigating the influence of changes in hydrodynamic boundary conditions. However, the vast majority of model parameters has not been analyzed systematically, such that the largest uncertainties in the results may not have been discovered yet. Especially the validity of the morphological parameters, such as the sediment transport formula used, is questionable without calibration.

The complex processes governing mud dynamics in the estuary are not represented well in the model. Some processes are simply not included in Delft3D, such as turbulence-induced flocculation or break-up of flocs (Deltares, 2014). Due to the low vertical grid resolution consolidation and entrainment of fluid mud layers cannot be represented accurately (Van Maren et al., 2015). Furthermore, the requirement of high computational efficiency poses limitations on the degree of complexity that can be used to represent morphodynamic features. For example, inclusion of multiple bed layers and multiple sediment fractions leads to a significant increase in computational time. Such additional features are therefore not included unless they are judged as essential to correctly represent the general morphodynamic behaviour of the river-estuary.

The same reasoning yields for sand-mud interaction processes. For simplicity and computational efficiency, it was decided to consider sand and mud separately and to neglect their interaction altogether. The main implication of this simplification is that the erosion of both fractions does not depend on the mud content, which would introduce a transition between non-cohesive and cohesive behaviour at a certain critical mud content (generally 5-10%) (Van Ledden et al., 2004).

The grid does not comply to generally recommended quality criteria for Delft3D models regarding smoothness and orthogonality (Deltares, 2014), see Figure 5.1. In the river section, the grid is completely orthogonal. The main deviation from purely orthogonal grid lines occurs in the grid cells representing the intertidal area in the estuary, because the model boundaries diverge exponentially while the grid lines in N-direction remain straight and orthogonal to the river axis. Moving closer to the mouth, the deviation from right angles increases, up to 7° at the seaward boundary. Grid cell dimensions vary smoothly in M-direction, but not in N-direction as the transitional cells are much smaller than the main channel and floodplain cells. Furthermore, the cell aspect ratio (N/M) is small in the river section with a maximum of 1.65, but becomes larger as we move closer to the mouth, with a maximum of 4.17 at the downstream model boundary. However, as the flow is predominantly in M-direction, this exceedance of recommended smoothness criteria is not expected to lead to large errors. Only when significant lateral circulations occur, for example due to differential advection of the along-channel density gradient between main channel and intertidal area, numerical errors may arise.

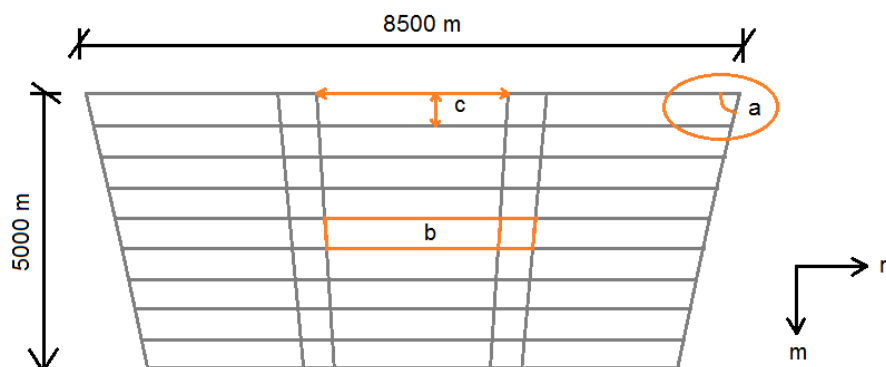


Figure 5.1: Orthogonality (a), ratio of neighbouring grid cell dimensions (b) and cell aspect ratio (c) at the estuary mouth. Figure is not to scale (n-dimension is exaggerated).

When the baroclinic pressure gradient is included, an anomaly occurs in the along-channel salinity profile, see Appendix A. During flood, a small body of water that is less saline than its surroundings is encapsulated near the water surface and shifts along the estuary as the tidal wave progresses in landward direction, coinciding with maximum flood velocities at each location. Due to the high degree of stratification in this area, turbulence is damped and velocities at the surface are amplified, whereas the velocities in the lower layers decrease slightly. The effect may occur because too little horizontal mixing takes place in the model due to the absence of topographic variations. As the effects are largest at the surface, where little sediment is present, the effect on sediment transport is expected to be limited.

The model geometry is characterized by steep bed slopes in lateral direction. The σ -layers that are used to discretize the vertical dimension can give rise to artificial mixing of salinity along these slopes. An alternative vertical grid coordinate system in Delft3D uses Z -layers, which have a fixed thickness throughout the domain, while the number of active layers varies with the depth. The horizontal grid lines are (nearly) parallel to density interfaces in areas with steep bed slopes, such that artificial mixing is reduced (Deltares, 2014). Although a Z -model would perform better in modelling vertical salinity stratification, its staircase representation of the bottom can lead to inaccuracies in the calculation of the bed shear stress and horizontal advection near the bed (Bijvelds, 2001), and therefore in the calculation of sediment transport. As the latter is of the utmost interest to this study, the use of σ -layers is preferred over the Z -model. An anti-creep correction is used to suppress artificial vertical diffusion.

5.3. Applicability to other river-estuaries

The simple geometrical representation of the river-estuary can easily be adapted for application to systems that are shaped by the same hydrodynamic forcing mechanisms, by changing the value of geometrical parameters such as the convergence length and width and depth at the mouth. Hence, the model is applicable to narrow, converging alluvial estuaries where tide and river discharge play a dominant role. See e.g. Dronkers (2017) for a list of estuaries that meet these criteria. Naturally, boundary conditions for flow and transport, sediment characteristics and roughness coefficients will need to be changed as well.

The Loire is not the only river-estuary that is affected by human-induced narrowing and deepening. In many estuaries worldwide and particularly in Western Europe, such interventions have led to similar consequences. Examples are the Ems, Weser and Elbe in Germany and the Scheldt in Belgium (Winterwerp and Wang, 2013). In some cases, such as the Ems (Van Maren et al., 2015), historical developments and consequences of human interventions have already been studied extensively. In others these aspects have not been investigated thoroughly yet, mostly due to a lack of data (Winterwerp et al., 2013). Applying the current model set-up, that does not need extensive calibration, to these estuaries as well can shed more light on the importance of different forcing mechanisms in each case.

Furthermore, bed degradation is an often encountered problem in rivers around the world. In this research, the effectiveness of commonly proposed countermeasures is investigated specifically for a tidal river. As the representation of the river section is so generic, qualitative results are expected to be applicable to other tidal rivers as well.

5.4. Relation to literature

Previous studies of the Loire estuary proposed that tidal (duration) asymmetry is the main driver of mud import and ETM formation (Brenon and Le Hir, 1999; Le Hir and Thouvenin, 1992; Jalón-Rojas et al., 2016). The evolution of the Loire towards a hyper-turbid state has been attributed to amplification of the tide and changes in tidal asymmetry (Winterwerp and Wang, 2013; Winterwerp et al., 2013). From the current research a different picture emerges. Model results reveal that gravitational circulation causes the formation of an ETM, whereas tidal asymmetry mainly enhances SSC further. Deepening and reclamation of intertidal area have, next to tidal amplification and increased flood-dominance, also led to enhanced gravitational circulation. Together, these processes have initiated the evolution towards hyper-turbid conditions and the formation of thick fluid mud layers in the estuary.

Furthermore, hyper-turbid conditions are often associated with the formation of a second ETM, driven by tidal mechanisms only. Model results do not show such a secondary maximum for any of the simulated conditions.

6

Conclusions and recommendations

6.1. Conclusions

1. How can the main processes influencing the morphology of the Loire river-estuary be included in a computationally efficient morphodynamic model?

The main hydrodynamic processes influencing the morphology of the Loire river-estuary are the river discharge, the tidal motion and the gravitational circulation. An idealized, three-dimensional morphodynamic model of the river-estuary was developed with the FLOW module of the Delft3D software suite (Deltares, 2014), in which these processes are included. The system geometry is represented with one flow-carrying channel, with elevated floodplains and intertidal areas on both sides. Grid cell sizes range from $600 \times 2500 \text{ m}^2$ to $200 \times 66 \text{ m}^2$. Over the first 50 km from the river mouth, the width of the estuary converges exponentially, after which the channel width is kept constant up to the landward model boundary, at 115 km upstream of the mouth. The converging section is called the estuary in this research, whereas the part with constant width is referred to as the river section.

Due to the low grid resolution and the use of a morphological factor, the development of the sandy bed over a period of 100 years can be simulated in about 1 day. ETM formation and the deposition of mud on the estuary bed over a period of several months can be simulated in a few hours, without the use of a morphological factor.

2. How do hydrodynamic processes affect the morphology of the Loire river-estuary, according to the developed model?

The current geometry of the estuary (lacking the presence of large intertidal areas) induces a flood-dominant tidal signal, which promotes import of sediment, when the effects of river discharge and the baroclinic pressure gradient are disregarded. River discharge introduces a mean seaward-directed velocity, but also enhances the flood-dominance of the tide by preferential damping of the ebb tide. Upstream of the estuary sediment transport is in seaward direction due to the dominance of river discharge over the tidal motion. Moving along the estuary in seaward direction, the influence of river discharge decreases due to width divergence, whereas the tide gains influence.

Without the baroclinic pressure gradient, net sand transport in the estuary mouth is directed landward for discharges lower than $1375 \text{ m}^3/\text{s}$, whereas net mud transport is directed seaward for all considered discharges ($200 \leq Q \leq 6000 \text{ m}^3/\text{s}$). In the mouth of the estuary, the baroclinic pressure gradient introduces a mean landward-directed velocity near the bed and amplifies the mean seaward-directed velocity near the surface. Only when this pressure gradient is included, net sand and mud transport in the estuary mouth are landward-directed for almost all discharges ($Q = 6000 \text{ m}^3/\text{s}$ being an exception for mud). Gravitational circulation causes the formation of an ETM at the tip of the salt wedge, which is strengthened further by the flood-dominance of the tide. The ETM forms closer to the mouth and has a smaller extent for larger discharges. Maximum SSC in the main channel decrease for increasing discharge, whereas the growth of the mud pool at the bed is maximum for $Q = 3000 \text{ m}^3/\text{s}$.

3. How did historical interventions affect the morphology of the Loire river-estuary?

Large-scale human interventions in the river have led to both an increase in transport capacity and a decrease in sediment supply. As a result, autonomous bed degradation takes place in the main channel of the lower Loire river. Secondary channels do not degrade at an equal rate and are increasingly cut off from the main channel, further enhancing flow velocities and erosion in the main channel.

Deepening of the estuary has led to amplification of the tidal range, whereas reclamation of intertidal area is the cause of the increase in flood-dominance of the tide, according to the model. Both interventions have enhanced the gravitational circulation. These effects have promoted the import of fine sediment into the estuary. Due to damping of turbulence by high SSC and smoothing of the estuary bed by fluid mud, the hydraulic drag decreases. This in turn leads to further strengthening of the gravitational circulation and deformation of the tide. Due to this feedback mechanism, that has been reported in literature and confirmed by model results, the Loire estuary has reached a hyper-turbid state that is hard to reverse. However, contrary to what has been suggested before, strengthening of the gravitational circulation plays a large role in this mechanism. With these findings, the feedback mechanism as depicted in Figure 2.4 can be updated for the Loire, see Figure 6.1.

Furthermore, model results indicate that historical deepening of the estuary has led to retrogressive erosion in the river section.

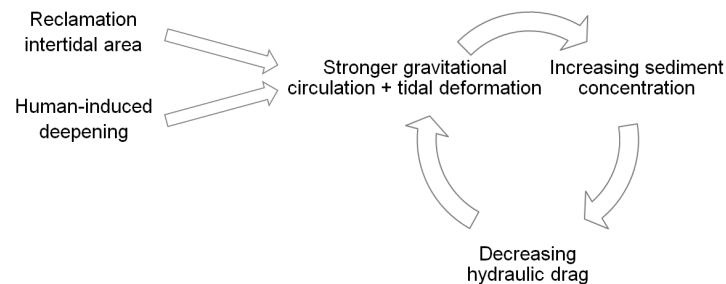


Figure 6.1: Feedback mechanism induced by historical interventions in the Loire estuary, adapted from Figure 2.4.

4. Which types of measures can mitigate the negative consequences of historical interventions?

To mitigate bed degradation, measures are considered that decrease the transport capacity of the flow, increase the sediment supply or do both. Sediment nourishments induce sedimentation both upstream and downstream of the nourishment location. The removal of groynes reduces flow velocities and hence the transport capacity in the main channel, leading to significant sedimentation along and upstream of the modified reach relative to the reference scenario. Restoration of a side channel has the same effect, but only when the side channel carries flow, which usually only happens above a certain discharge threshold. Release of sediment that is trapped in groyne fields or previously abandoned side channels does not lead to significant additional sedimentation within the main channel. A fixed bed layer with higher roughness than the natural river bed stabilizes the bed at the location of the intervention and induces sedimentation upstream of the structure due to backwater effects. However, just downstream of the structure a deep erosion pit arises. Cessation of maintenance dredging in the upstream part of the estuary increases the supply of sediment to the estuary, but also leads to sedimentation throughout the river section relative to the reference scenario.

To decrease the import of mud into the estuary, two measures have been investigated. Increasing bed levels in the main channel of the estuary leads to damping of the tidal wave, but does not affect the tidal asymmetry significantly. Restoring tidal flats, on the other hand, turns the tide from flood- into ebb-dominant but does not affect the tidal range. In both cases, a decrease of the salt intrusion length and a significant weakening of the gravitational circulation occurs, leading to a tidally averaged export of fine sediment and very low mud concentrations.

5. How sensitive are model results to changes in boundary conditions?

As a result of climate change, the mean water level at the downstream boundary is expected to rise and the average discharge imposed at the upstream boundary will most likely decrease. The main effect of these gradual changes on the sand profile is a steeper bed slope in the river section after 100 years. The difference with the reference scenario is of the same order of magnitude as the effects of human interventions. It is therefore important to account for these processes when assessing the effects of measures on a centennial scale.

SSC and growth of the mud pool on the bed are sensitive to the amplitude of the M2 tidal component and the spectral composition of the tide. SSC increase for increasing tidal amplitude, whereas the growth of the bottom pool shows a maximum for $a_{M2} = 1.60$ m, if no M4 component is included. Taking the spring-neap tidal cycle into account by including an S2 component leads to larger SSC and less growth of the bottom pool when averaging over a complete spring-neap tidal cycle.

6.2. Recommendations

6.2.1. Management of the Loire river-estuary

To mitigate bed degradation, sediment nourishments appear to be effective already on a decadal timescale, whereas the removal of groynes effectively induces sedimentation on a centennial scale according to the model. A combination of these two measures could be a feasible option to mitigate bed degradation both in the short and the long term. Further investigation is required to determine an optimal configuration of these mitigating measures and to assess the morphological response of the river-estuary in more detail.

In general, it is advised to consider a large computational domain and large temporal scales when assessing measures, as they can have far-reaching effects both in time and space. On a centennial timescale, the influence of climate change on the river hydrograph and the water level at sea should be taken into account. Furthermore, it is advised to assess the combined effect of planned measures instead of studying them in isolation, as the effect of a combination of certain measures is not the same as the sum of effects of the individual measures.

The SYVEL monitoring network provides the possibility to further expand measurements in the estuary. Firstly, current velocity measurements at multiple locations along the estuary would benefit the analysis of hydrodynamic processes and the calibration of numerical models. Tidal analyses can now be performed on water level measurements only, while the phase difference between surface elevation and velocity is unknown. When combined with measurements of SSC, the analysis of sediment transport mechanisms can be improved as well.

Furthermore, only at one observation point (Donges) salinity and SSC are measured continuously near the surface as well as near the bottom, instead of only near the surface. If this would be done at the other 5 measuring locations as well, the degree of stratification of the entire estuary could be assessed for different hydrodynamic conditions, as well as its influence on suspended sediment transport.

6.2.2. Further research

Fluid mud dynamics and sand-mud interaction processes have been neglected in this study, but could alter results significantly. On the one hand, the high computational efficiency required for this study limits possibilities to include these processes. On the other hand, underlying mechanisms are not yet sufficiently understood and included in modelling software. In general, modelling efforts regarding estuaries and tidal basins would benefit from an improved understanding and model representation of sand-mud interaction processes and fluid mud dynamics. For this study, results regarding mud deposition and ETM formation could be improved by increasing grid resolution and using a different modelling approach that is better suited for these purposes, for example the fluid mud feature within Delft3D. Sand-mud interaction could be represented better if the bed is modelled with multiple layers.

With few modifications (see Section 5.3), the model can be applied to comparable river-estuaries affected by deepening and narrowing. For many of these cases, consequences of human interventions have not been investigated thoroughly yet due to a lack of historical data. The developed model can then be used to explore the importance of different forcing and feedback mechanisms in a qualitative way.

It is highly recommended to extend the sensitivity analysis of model parameters further. To start with, sensitivity to changes in morphological parameters, such as the sediment transport formula, grain size and settling velocity should be investigated, as these parameters are highly uncertain. The effect of including more tidal constituents should be looked into as well, not only for SSC but also for the long-term development of the bed profile. A simplified representation of the tidal motion imposed at the downstream boundary may not be justified when a significant river flow is present, as in this way river-tide interactions are underestimated. It should be investigated which simplifications of the tide are justified in these situations, if any. Furthermore, parameters associated with the schematization of future interventions (such as dimensions of structures) should be varied, as the effectiveness of a certain measure can be highly dependent on the chosen configuration. Now, the comparison of different measures is based on just one simulation per measure, whereas another set of configurations might lead to a different outcome of this comparison.

In order to improve model results for transport of salt, it is recommended to extend the model domain further downstream, where variations in salinity are negligible. In that way, boundary conditions for salinity can be imposed more easily and salt intrusion can be modelled more accurately. However, downstream of the current model boundary (Saint-Nazaire), wind and waves could become important for sediment transport as well. Hence, it might be necessary to include wind and waves in the model if the domain is extended in downstream direction.

Furthermore, it is expected that the near absence of topographic variations in the model leads to an underestimation of large-scale mixing processes, such that salt intrusion may be underestimated. Further research is needed to confirm this hypothesis.

Bibliography

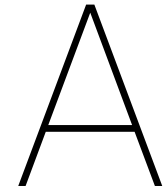
- Allen, G. P., Salomon, J. C., Bassoullet, P., Du Penhoat, Y., and De Grandpré, C. (1980). Effects of tides on mixing and suspended sediment transport in macrotidal estuaries. *Sedimentary Geology*, 26(1-3):69–90.
- Bagnold, R. A. (1977). Bed load transport by natural rivers. *Water Resources Research*, 13(2):303–312.
- Berkhof, A., Kabout, J., Loeve, R., Van de Paverd, M., and Verhoeven, D. (2018). MIRT Onderzoek Duurzame Bodemligging Rijntakken; Eindrapportage. Technical report, Arcadis, in opdracht van het Ministerie van Infrastructuur en Milieu.
- Bijvelds, M. (2001). *Numerical modelling of estuarine flow over steep topography*. PhD thesis, Delft University of Technology.
- Blom, A. (2016). Bed degradation in the Rhine River. *WaterViewer, Delft University of Technology*.
- Bosboom, J. and Stive, M. J. F. (2015). *Coastal Dynamics I; lecture notes CIE4305*. Delft Academic Press, Delft.
- Brenon, I. and Le Hir, P. (1999). Modelling the turbidity maximum in the Seine estuary (France): Identification of formation processes. *Estuarine, Coastal and Shelf Science*, 49:525–544.
- Brière, C., Giardino, A., and Winterwerp, J. C. (2011a). Analyse de la morphologie du chenal de Nantes et étude de sa restauration; Phase 1: Evolutions passées et fonctionnement actuel. Technical report, Deltares, Delft.
- Brière, C., Giardino, A., and Winterwerp, J. C. (2011b). Analyse de la morphologie du chenal de Nantes et étude de sa restauration; Phase 2: Proposition de leviers d'interventions pour la restauration du lit. Technical report, Deltares, Delft.
- Brière, C., Giardino, A., and Winterwerp, J. C. (2012). Analyse de la morphologie du chenal de Nantes et étude de sa restauration; Phase 3: Etude de l'impact d'une interventions à l'amont de Nantes sur les caractéristiques de la marée. Technical report, Deltares, Delft.
- Burchard, H. and Baumert, H. (1998). The formation of estuarine turbidity maxima due to density effects in the salt wedge. A hydrodynamic process study. *Journal of Physical Oceanography*, 28(2):309–321.
- Burchard, H., Schuttelaars, H. M., and Ralston, D. K. (2018). Sediment trapping in estuaries. *Annual Review of Marine Science*, 10(14):1–25.
- Cai, H., Savenije, H. H. G., and Toffolon, M. (2014). Linking the river to the estuary: Influence of river discharge on tidal damping. *Hydrology and Earth System Sciences*, 18(1):287–304.
- Canestrelli, A., Lanzoni, S., and Fagherazzi, S. (2014). One-dimensional numerical modeling of the long-term morphodynamic evolution of a tidally-dominated estuary: The Lower Fly River (Papua New Guinea). *Sedimentary Geology*, 301:107–119.
- Chernetsky, A. S., Schuttelaars, H. M., and Talke, S. A. (2010). The effect of tidal asymmetry and temporal settling lag on sediment trapping in tidal estuaries. *Ocean Dynamics*, 60(5):1219–1241.
- Cheviet, C., Violeau, D., and Guesmia, M. (2002). Numerical simulation of cohesive sediment transport in the Loire estuary with a three-dimensional model including new parametrisations. In Winterwerp, J. C. and Kranenburg, C., editors, *Fine sediment dynamics in the marine environment*, pages 529–543, Delft, the Netherlands.
- Codiga, D. L. (2011). Unified tidal analysis and prediction using the UTide Matlab functions. Technical report, Graduate School of Oceanography, University of Rhode Island, Narragansett, RI.
- Crosato, A. (2010). *Morphological response at the reach scale - lecture notes*. Unesco-IHE, Delft.

- Dayon, G., Boé, J., Martin, É., and Gailhard, J. (2018). Impacts of climate change on the hydrological cycle over France and associated uncertainties. *Comptes Rendus - Geoscience*, 350(4):141–153.
- De Jonge, V. N., Schuttelaars, H. M., Van Beusekom, J. E. E., Talke, S. A., and De Swart, H. E. (2014). The influence of channel deepening on estuarine turbidity levels and dynamics, as exemplified by the Ems estuary. *Estuarine, Coastal and Shelf Science*, 139:46–59.
- De Vriend, H. J. (2006). *River Engineering - lecture notes*. Delft University of Technology.
- De Vries, M. (1959). Transients in bed-load transport (basic considerations). Technical report, Waterloopkundig Laboratorium, Delft.
- Deltares (2014). 3D/2D modelling suite for integral water solutions; Delft3D-FLOW manual.
- Dronkers, J. (2017). Convergence of estuarine channels. *Continental Shelf Research*, 144(6):120–133.
- Engelund, F. and Hansen, E. (1967). *A monograph on sediment transport in alluvial streams*. Teknisk Forlag, Copenhagen.
- Ferret, Y., Donato, V., and Pouvreau, N. (2018). Historical sea level data rescue to assess long-term sea level evolution. In *Sea Level Futures Conference*, Liverpool. Service Hydrographique et Océanographique de la Marine (SHOM).
- Fettweis, M., Sas, M., and Monbaliu, J. (1998). Seasonal, neap-spring and tidal variation of cohesive sediment concentration in the Scheldt estuary, Belgium. *Estuarine, Coastal and Shelf Science*, 47(1):21–36.
- Friedrichs, C. T., Armbrust, B. D., and De Swart, H. E. (1998). Hydrodynamics and equilibrium sediment dynamics of shallow, funnel-shaped tidal estuaries. *Physics of Estuaries and Coastal Seas*, pages 315–327.
- Friedrichs, C. T. and Aubrey, D. G. (1988). Non-linear tidal distortion in shallow well-mixed estuaries: a synthesis. *Estuarine, Coastal and Shelf Science*, 27:521–545.
- Frings, R. M., Döring, R., Beckhausen, C., Schüttrumpf, H., and Vollmer, S. (2014). Fluvial sediment budget of a modern, restrained river: The lower reach of the Rhine in Germany. *Catena*, 122:91–102.
- Galay, V. J. (1983). Causes of river bed degradation. *Water Resources Research*, 19(5):1057–1090.
- Gasowski, Z. (1994). L'enfoncement du lit de la Loire / The entrenchment of the Loire's river bed. *Revue de géographie de Lyon*, 69(1):41–45.
- GIP Loire Estuaire (2003). Mise en eau des annexes hydrauliques; cahier indicateurs.
- GIP Loire Estuaire (2009). La Loire de la Maine à la mer; carte à l'échelle 1:50 000.
- GIP Loire Estuaire (2011). Les dragages d'entretien dans l'estuaire; cahier indicateurs.
- GIP Loire Estuaire (2013). Les amplitudes de l'onde de marée; cahier indicateurs.
- GIP Loire Estuaire (2014). La dynamique du bouchon vaseux; cahier indicateurs.
- GIP Loire Estuaire (2017). Bulletin SYVEL; Système de veille dans l'estuaire de la Loire; Réseau de mesure en continu: Synthèse 2007-2016.
- GIP Loire Estuaire (2018). Rééquilibrage du lit de la Loire de Nantes à l'océan. <http://www.loire-estuaire.org/accueil/les-actions/reequilibrage-du-lit-de-la-loire/reequilibrage-du-lit-de-la-loire-de-nantes-a-locean>, accessed 2018-11-05.
- Godin, G. (1985). Modification of river tides by the discharge. *Journal of Waterway, Port, Coastal and Ocean Engineering*, 111(2):257–274.
- Gölz, E. (1994). Bed degradation - Nature, causes, countermeasures. *Water Science and Technology*, 29(3):325–333.
- Grinsted, A., Jevrejeva, S., Riva, R. E., and Dahl-Jensen, D. (2015). Sea level rise projections for Northern Europe under RCP8.5. *Climate Research*, 64(1):15–23.

- Guo, L. (2014). *Modeling estuarine morphodynamics under combined river and tidal forcing*. PhD thesis, Delft University of Technology, UNESCO-IHE Institute for Water Education.
- Guo, L., Van der Wegen, M., Roelvink, J. A., and He, Q. (2014). The role of river flow and tidal asymmetry on 1-D estuarine morphodynamics. *Journal of Geophysical Research: Earth Surface*, 119:2315–2334.
- Guo, L., Van der Wegen, M., Roelvink, J. A., and He, Q. (2015a). Exploration of the impact of seasonal river discharge variations on long-term estuarine morphodynamic behavior. *Coastal Engineering*, 95:105–116.
- Guo, L., Van der Wegen, M., Roelvink, J. A., Wang, Z. B., and He, Q. (2015b). Long-term, process-based morphodynamic modeling of a fluvio-deltaic system, part I: The role of river discharge. *Continental Shelf Research*, 109:95–111.
- Habersack, H., Hein, T., Stanica, A., Liska, I., Mair, R., Jäger, E., Hauer, C., and Bradley, C. (2015). Challenges of river basin management: Current status of, and prospects for, the River Danube from a river engineering perspective. *Science of the Total Environment*, 543:828–845.
- Hu, K., Ding, P. X., Wang, Z. B., and Yang, S. (2009). A 2D/3D hydrodynamic and sediment transport model for the Yangtze Estuary, China. *Journal of Marine Systems*, 77(1-2):114–136.
- Huijts, K. M. H., Schuttelaars, H. M., De Swart, H. E., and Valle-Levinson, A. (2006). Lateral entrapment of sediment in tidal estuaries: An idealized model study. *Journal of Geophysical Research: Oceans*, 111(12):1–14.
- Hydratec (2013). *Stratégie de reconquête du lit de la Loire entre les Ponts-de-Cé et l'agglomération Nantaise; Définition du programme d'action 2012-2020*. Technical report, GIP Loire Estuaire.
- Jalón-Rojas, I., Schmidt, S., Sottolichio, A., and Bertier, C. (2016). Tracking the turbidity maximum zone in the Loire estuary (France) based on a long-term, high-resolution and high-frequency monitoring network. *Continental Shelf Research*, 117:1–11.
- Jay, D. A., Geyer, W. R., Uncles, R. J., Vallino, J., Largier, J., and Boynton, W. R. (1997). A review of recent developments in estuarine scalar flux estimation. *Estuaries*, 20(2):262–280.
- Jay, D. A. and Musiak, J. D. (1994). Particle trapping in estuarine tidal flows. *Journal of Geophysical Research*, 99(C10):20445–20461.
- Koenig, F., Quick, I., and Vollmer, S. (2012). Defining quantitative morphological changes in large rivers for a sustainable and effective sediment management applied to the River Elbe; Germany. In *Proceedings of the 10th International Conference on Hydrosience & Engineering*, pages 1–11, Orlando, Florida.
- Kuijper, K. and Van Rijn, L. C. (2011). Analytical and numerical analysis of tides and salinities in estuaries; part II: salinity distributions in prismatic and convergent tidal channels. *Ocean Dynamics*, 61(11):1743–1765.
- Lanzoni, S. and Seminara, G. (1998). On tide propagation in convergent estuaries. *Journal of Geophysical Research*, 103(C13):30793–30812.
- Lanzoni, S. and Seminara, G. (2002). Long-term evolution and morphodynamic equilibrium of tidal channels. *Journal of Geophysical Research*, 107(C1):3001–3013.
- Larue, J.-P. (2004). Morphodynamique fluviale actuelle d'origine anthropique: exemples dans le bassin de la Loire (France) / Human impacts on present day fluvial morphodynamics: examples from the Loire river basin (France). *Géomorphologie: relief, processus, environnement*, 10(2):127–138.
- Le Hir, P. and Thouvenin, B. (1992). Modélisation mathématique simplifiée de la masse turbide dans l'estuaire de la Loire. *Journées Génie Civil - Génie Côtier*, pages 141–158.
- Liefveld, W. M., Emond, D., and Van der Valk, M. (2011). Kribverlaging Waal fase 3 en Langsdammen Wamel en Ophemert; Toetsing in het kader van de Flora- en faunawet, de Natuurbeschermingswet 1998 en de Ecologische Hoofdstructuur. Technical report, Bureau Waardenburg.
- Maquet, J. (1974). Aménagement de l'estuaire de la Loire. *La Houille Blanche*, 60(1-2):79–89.

- Migniot, C. (1993). Bilan de l'hydrologie et de l'hydrosédimentaire de l'estuaire de la Loire au cours des deux dernières décennies; Synthèse. Technical report.
- Mosselman, E. and Le, T. B. (2016). Five common mistakes in fluvial morphodynamic modeling. *Advances in Water Resources*, 93:15–20.
- Mosselman, E., Van Vuren, S., Yossef, M., Ottevanger, W., and Sloff, K. (2007). Case studies Duurzame Vaardiepte Rijndelta. Technical report, Deltares.
- Niessen, I. and Becker, A. (2018). Nourishments as part of the future Dutch river management: insights from a pilot. In *NCR Days 2018; The Future River*, pages 34–35, Delft, the Netherlands.
- Pérard, C. (2018). Assistance à maîtrise d'ouvrage pour le programme de rééquilibrage du lit de la Loire entre les Ponts-de-Cé et Nantes – Phase I; Rapport de présentation des études au Conseil Scientifique de l'Estuaire de la Loire du 13 février 2018. Technical report, Voies Navigables de France.
- Richardson, J. F. and Zaki, W. N. (1954). Sedimentation and fluidization: Part I. *Transactions of the Institution of Chemical Engineers*, 32:35–53.
- Rijkswaterstaat Oost-Nederland (2016). Duurzame Vaardiepte Rijntakken (DVR2); Studie naar problematiek en mogelijke aanpak van bodemerrosie en aanzanding in het zomerbed van de Rijntakken in Oost-Nederland. Technical report.
- Roelvink, J. A. (2006). Coastal morphodynamic evolution techniques. *Coastal Engineering*, 53(2-3):277–287.
- Rudolph, M. (2018). *Measures for mitigating the ongoing bed degradation in the Rhine river - A first assessment using idealized models of the Waal branch*. MSc thesis.
- Sanford, L. P. and Halka, J. P. (1993). Assessing the paradigm of mutually exclusive erosion and deposition of mud, with examples from upper Chesapeake Bay. *Marine Geology*, 114(1-2):37–57.
- Savenije, H. H. G. (2012). *Salinity and tides in alluvial estuaries; Second completely revised edition*.
- Schuttelaars, H. M., De Jonge, V. N., and Chernetsky, A. (2013). Improving the predictive power when modelling physical effects of human interventions in estuarine systems. *Ocean and Coastal Management*, 79:70–82.
- Schuttelaars, H. M. and De Swart, H. E. (2000). Multiple morphodynamic equilibria in tidal embayments. *Journal of Geophysical Research*, 105(C10):105–118.
- Sloff, K., Van der Sligte, R., and Ottevanger, W. (2014). Morfologische Pakket som Waal; Morfologische effecten Ruimte-voor-de-Riviermaatregelen. Technical report, Deltares, Delft.
- Van de Kreeke, J. and Robaczewska, K. (1993). Tide-induced residual transport of coarse sediment; Application to the Ems estuary. *Netherlands Journal of Sea Research*, 31(3):209–220.
- Van der Wegen, M., Dastgheib, A., and Roelvink, J. A. (2010). Morphodynamic modeling of tidal channel evolution in comparison to empirical PA relationship. *Coastal Engineering*, 57(9):827–837.
- Van Ledden, M., Wang, Z. B., Winterwerp, H., and De Vriend, H. (2004). Sand-mud morphodynamics in a short tidal basin. *Ocean Dynamics*, 54(3-4):385–391.
- Van Maren, D. S., Winterwerp, J. C., and Vroom, J. (2015). Fine sediment transport into the hyper-turbid lower Ems River: the role of channel deepening and sediment-induced drag reduction. *Ocean Dynamics*, 65(4):589–605.
- Van Rijn, L. C. (1984). Sediment transport, part II: Suspended load transport. *Journal of Hydraulic Engineering*, 110(11):1613–1641.
- Voies Navigables de France (2016a). Bellevue; Fiche 1; Présentation du projet.
- Voies Navigables de France (2016b). Oudon-Anetz; Fiche 1; Présentation du projet.

- Voies Navigables de France (2018). Programme de Rééquilibrage du lit de la Loire entre les Ponts-de-Cé et Nantes. Technical report, Direction Territoriale Bassin de la Seine - Unité Territoriale Loire.
- Wang, Z. B., Jeuken, C., and De Vriend, H. J. (1999). Tidal asymmetry and residual sediment transport in estuaries; A literature study and application to the Western Scheldt. Technical report, WL| Delft Hydraulics.
- Winterwerp, J. C. (2010). Fine sediment transport by tidal asymmetry in the high-concentrated Ems River: Indications for a regime shift in response to channel deepening. *Ocean Dynamics*, 61(2-3):203–215.
- Winterwerp, J. C. (2016). Net sediment transport by tidal asymmetry in the hyper-turbid Ems River. *Physics of Estuaries and Coastal Seas Conference*, pages 2–3.
- Winterwerp, J. C. and Wang, Z. B. (2013). Man-induced regime shifts in small estuaries - I: theory. *Ocean Dynamics*, 63(11-12):1279–1292.
- Winterwerp, J. C., Wang, Z. B., Van Braeckel, A., Van Holland, G., and Kösters, F. (2013). Man-induced regime shifts in small estuaries - II: a comparison of rivers. *Ocean Dynamics*, 63(11-12):1293–1306.
- Wright, N. and Crosato, A. (2011). The hydrodynamics and morphodynamics of rivers. In Wilderer, P., editor, *Treatise on water science*, volume 2, pages 135–156. Academic Press, Oxford.



Velocity under baroclinic forcing

Adding a baroclinic pressure gradient to the system of equations changes the vertical velocity profiles considerably, see Figure A.1.

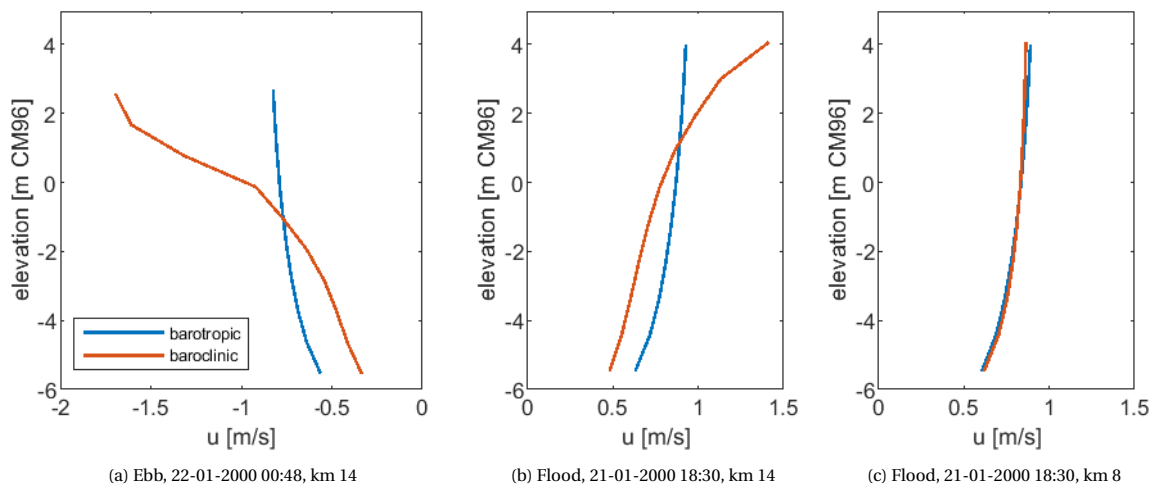


Figure A.1: Vertical profiles of horizontal velocity half the period of a tidal cycle apart. Profiles during flood are shown for 2 different locations along the main channel of the estuary.

During ebb, the changes in the vertical profile from barotropic to baroclinic are as expected, see Figure A.1a. Due to the gravitational circulation, velocities decrease in magnitude near the bed and increase in magnitude near the surface. Due to stable stratification during ebb, an additional straining of the velocity profile occurs, increasing the velocity gradient over the vertical further.

During flood, however, the resulting velocity profiles including the baroclinic pressure gradient are remarkable at certain moments in space and time. On the basis of the gravitational circulation, an increase in velocities would be expected near the bed, whereas surface velocities are expected to decrease. Due to unstable stratification the profile would become even more uniform over the vertical. Most of the time the resulting velocity profiles are indeed according to these expectations, as can be seen in Figure A.1c, which shows the velocity profile during flood at a distance of 8 km from the mouth. As the velocity profile is already relatively uniform in a barotropic situation, differences between the barotropic and baroclinic profile are marginal.

However, when at that same moment, the velocity profile at a location 6 km further landward is assessed, an effect similar to that during ebb is observed: near-bed velocities decrease, whereas surface velocities are amplified. This effect only occurs over a limited distance (about 5 to 10 km), but it shifts along the estuary as the tidal wave progresses, coinciding with maximum flood velocities at each location. At the location where the straining effect occurs, the salinity profile along the estuary shows an anomaly, see Figure A.2.

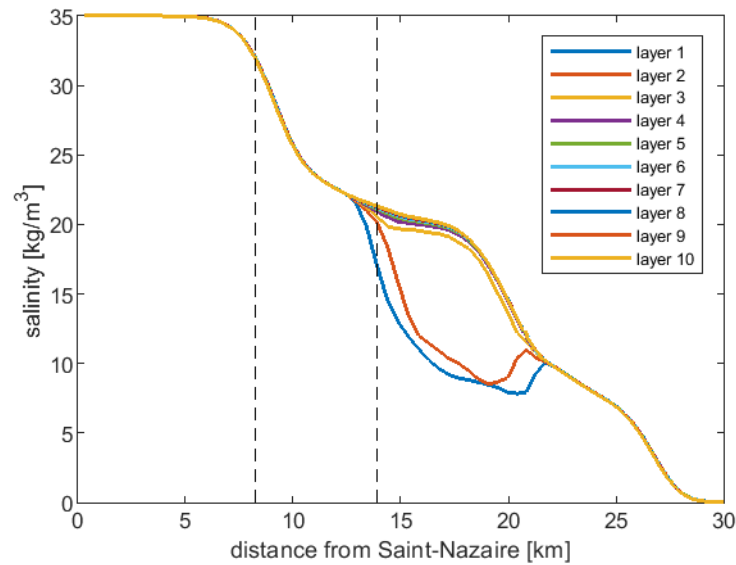


Figure A.2: Flood, 21-01-2000 18:30. Salinity in each σ -layer, with layer 1 at the surface and layer 10 at the bottom. The dashed vertical lines show the location at which the flood velocity profiles shown in Figure A.1 are taken.

Where normally the horizontal salinity gradient is negative (salinity decreasing in landward direction), here the salinity shows a strong decrease and subsequent increase in landward direction in the upper layers in the vertical. The estuary is well-mixed both seaward and landward of this short stratified region. Hence, a small body of water that is less saline than its surroundings is encapsulated near the water surface. Due to the high degree of stratification turbulence is damped at this location and velocities are amplified with respect to the barotropic situation, whereas the velocities in the lower layers decrease slightly.

The anomaly mostly affects velocities near the surface. As sediment is mainly found in the bed and the lower part of the water column, the influence on estuarine morphology is expected to remain limited, especially because the anomaly only occurs within a limited space and period. However, its effect should be kept in mind when interpreting morphological model results.

B

Overview of measured SSC

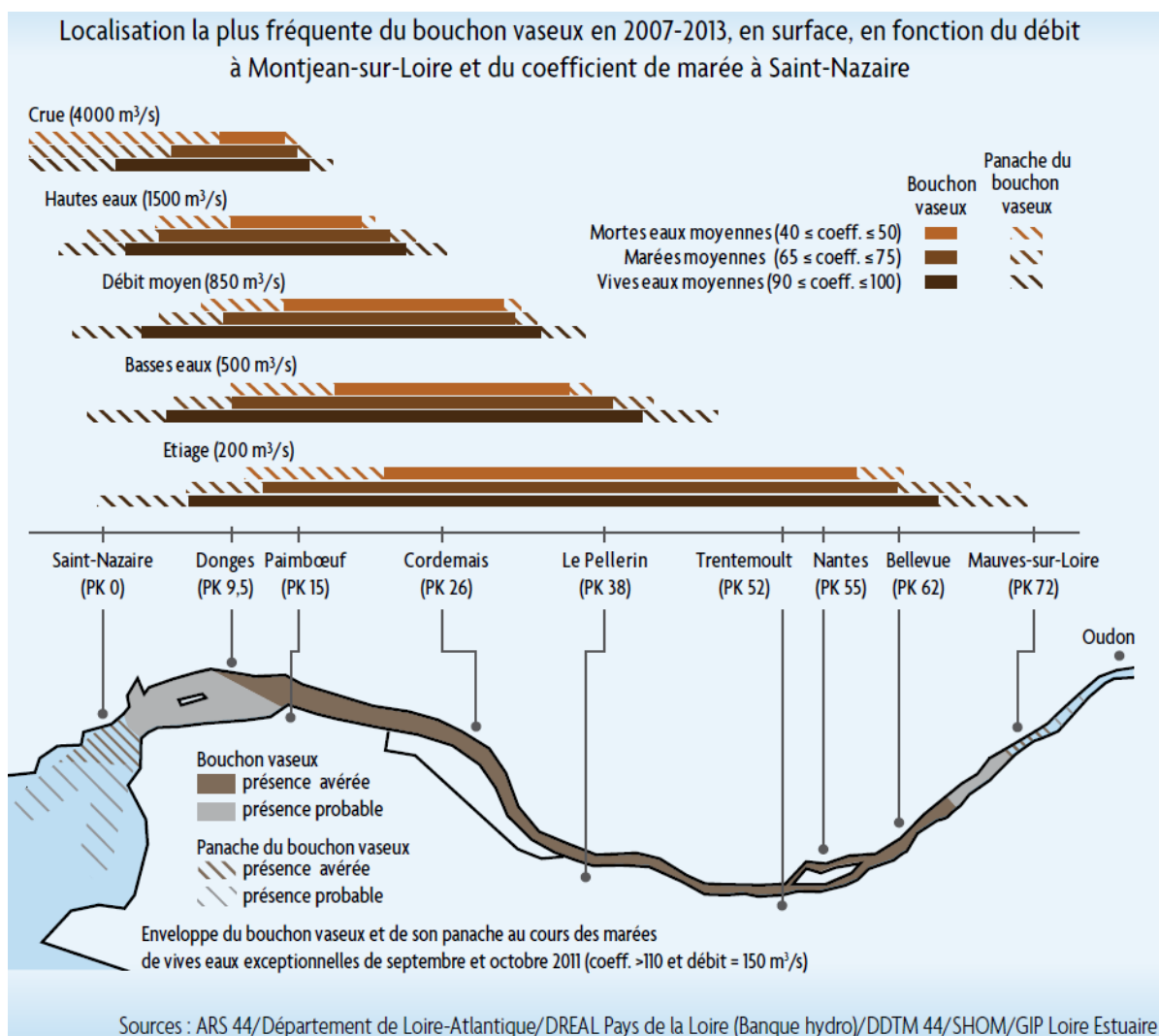


Figure B.1: SSC for different discharges and tidal conditions (spring tide, mean tide and neap tide), measured in the period 2007-2013. Fully colored bars ('bouchon vaseux') indicate concentrations between 0.5 and 30 kg/m³. Dashed bars ('panache du bouchon vaseux') indicate concentrations between 0.1 and 0.5 kg/m³. The lower figure indicates SSC during a low discharge event (Q = 150 m³/s) with spring tide. Brown-colored areas indicate measured concentrations between 0.5 and 30 kg/m³. Grey indicates areas where concentrations larger than 0.5 kg/m³ were probably present, but not measured. The same division yields for the dashed areas, but now for concentrations between 0.1 and 0.5 kg/m³. Measurements were taken every 30 minutes at 6 locations along the estuary, at 1 m below the water surface. Source: GIP Loire Estuaire (2014).

C

Mud simulation results

C.1. Discharge

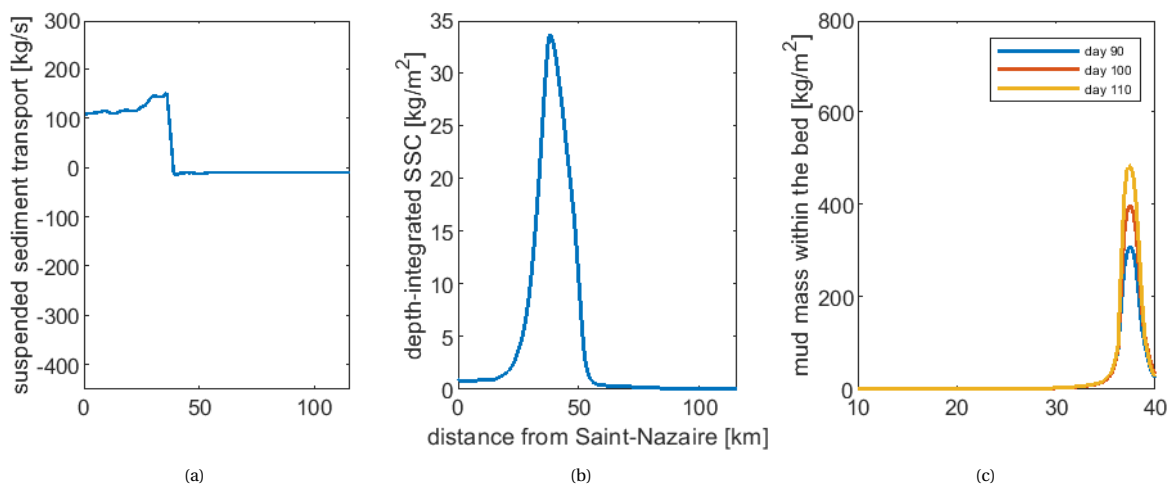


Figure C.1: $Q = 200 \text{ m}^3/\text{s}$

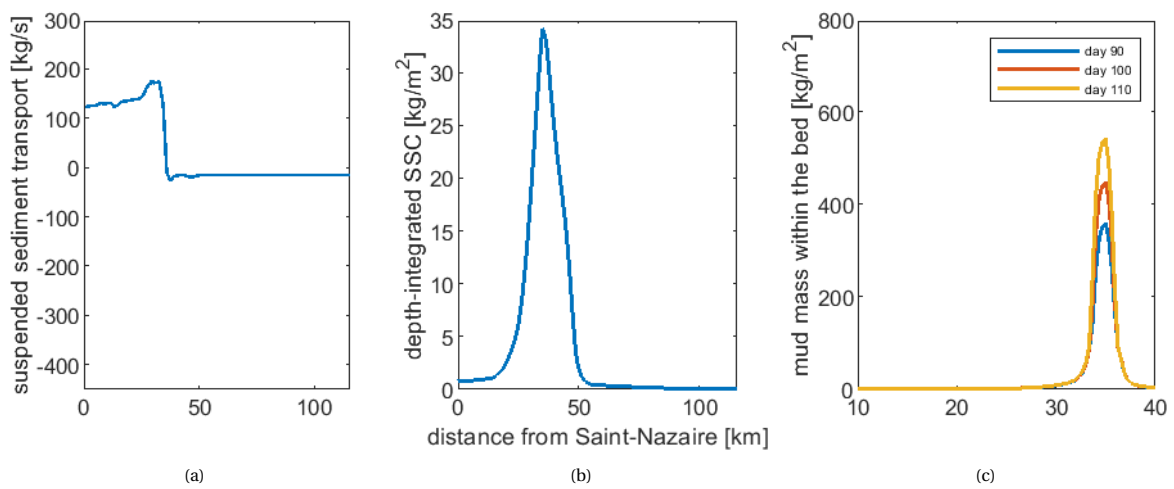


Figure C.2: $Q = 300 \text{ m}^3/\text{s}$

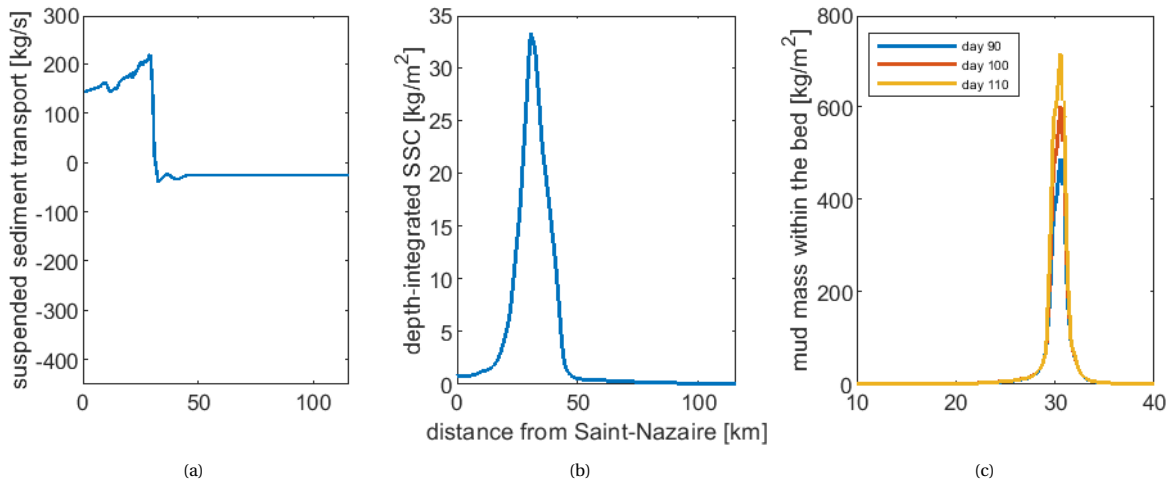


Figure C.3: $Q = 500 \text{ m}^3/\text{s}$

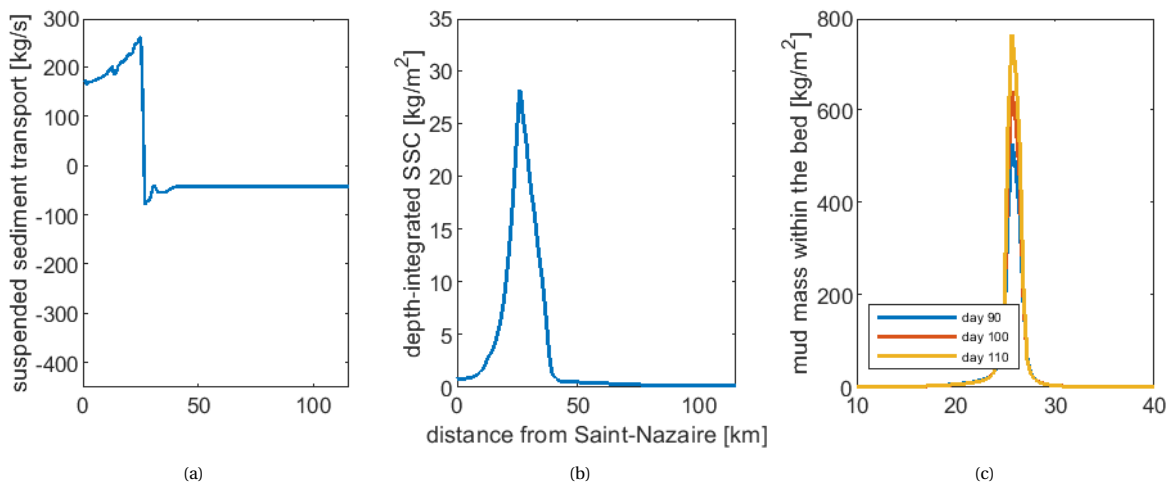


Figure C.4: $Q = 845 \text{ m}^3/\text{s}$

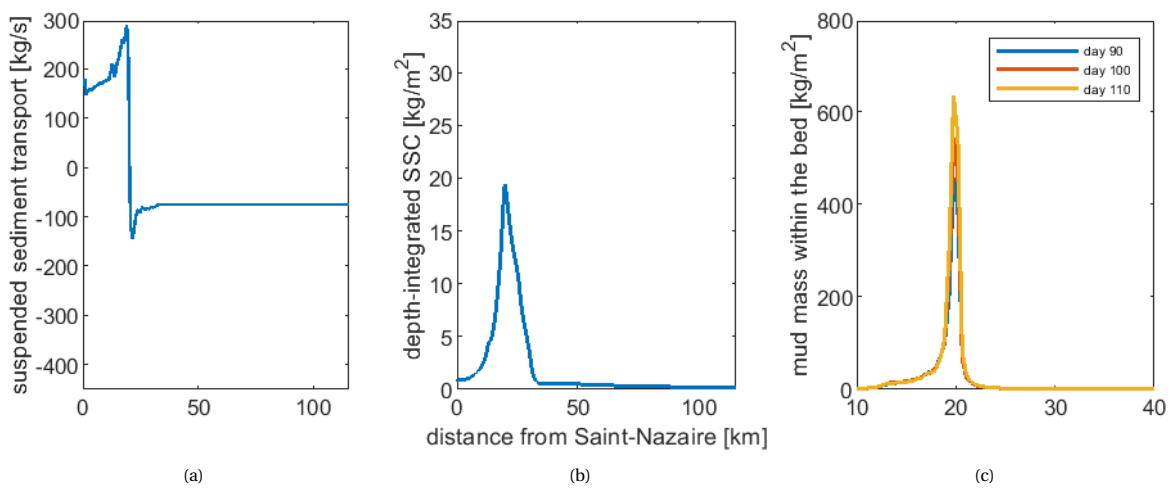
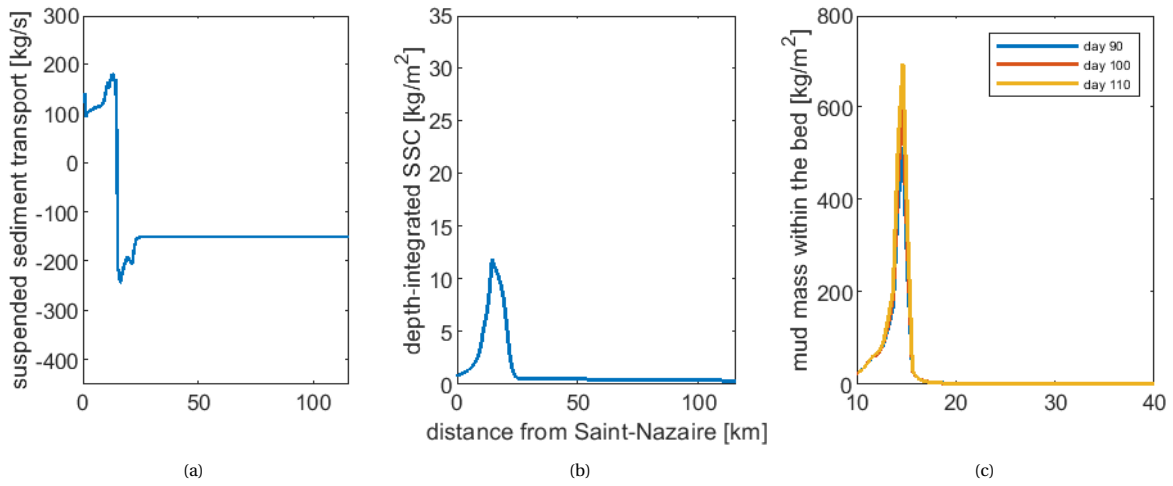
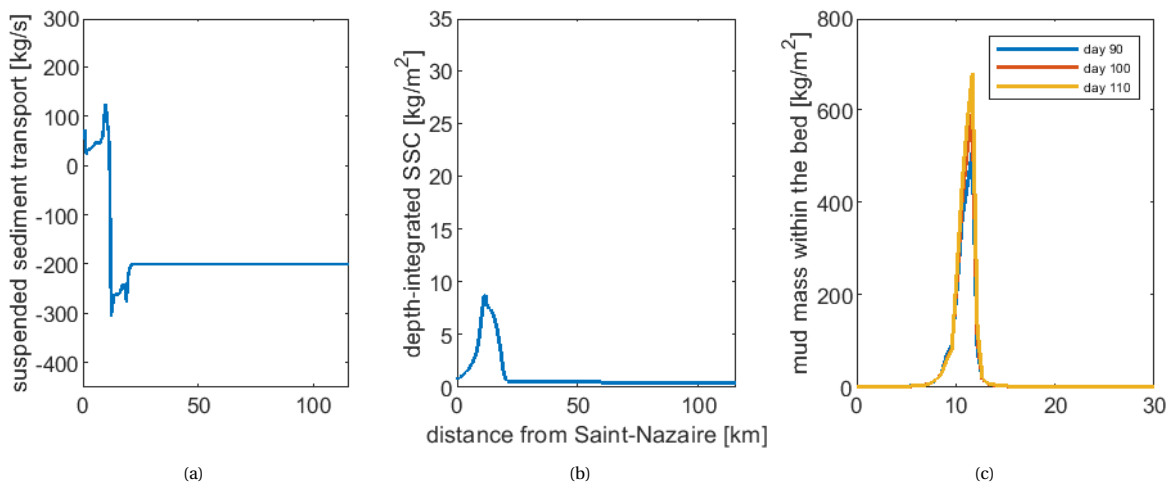
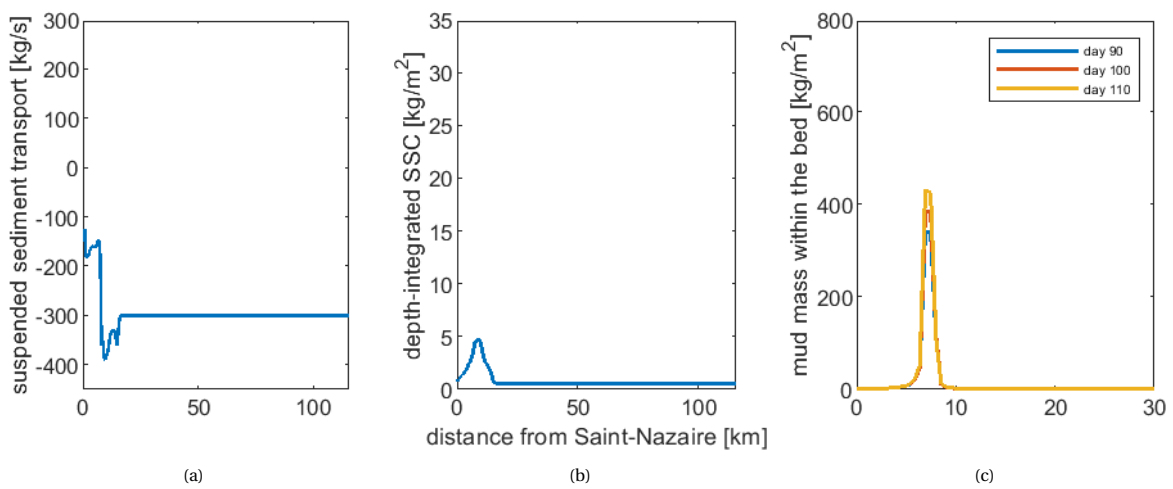
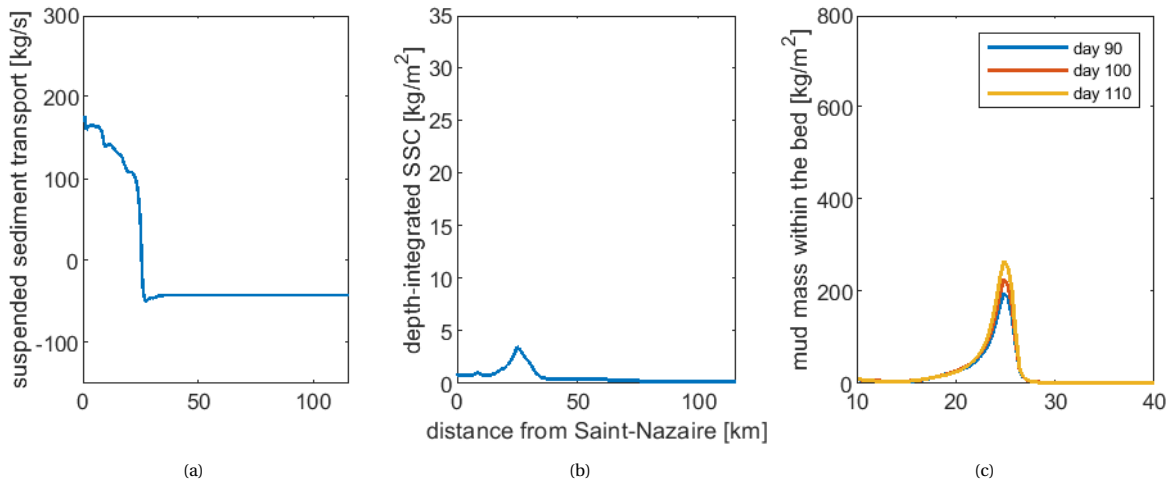
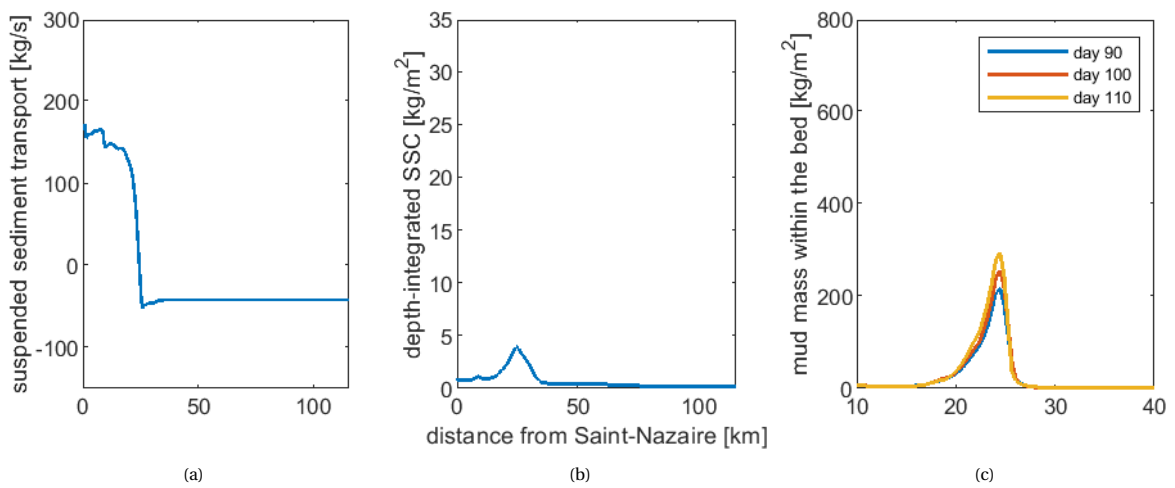
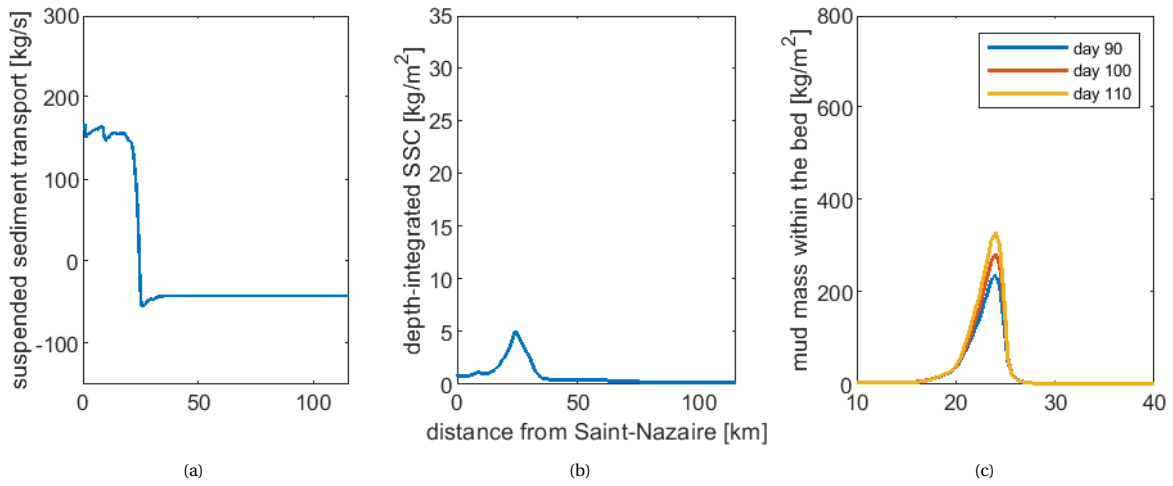
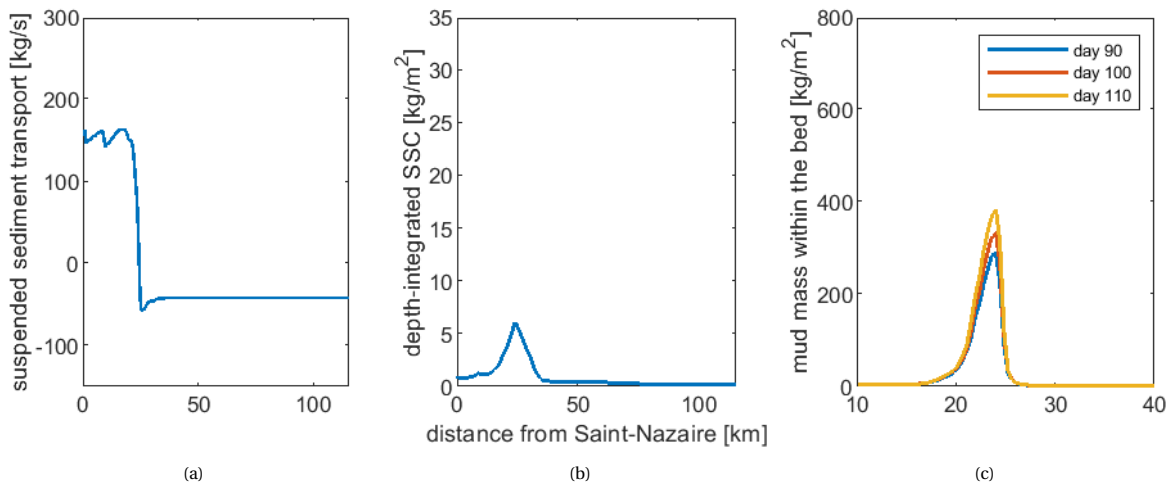
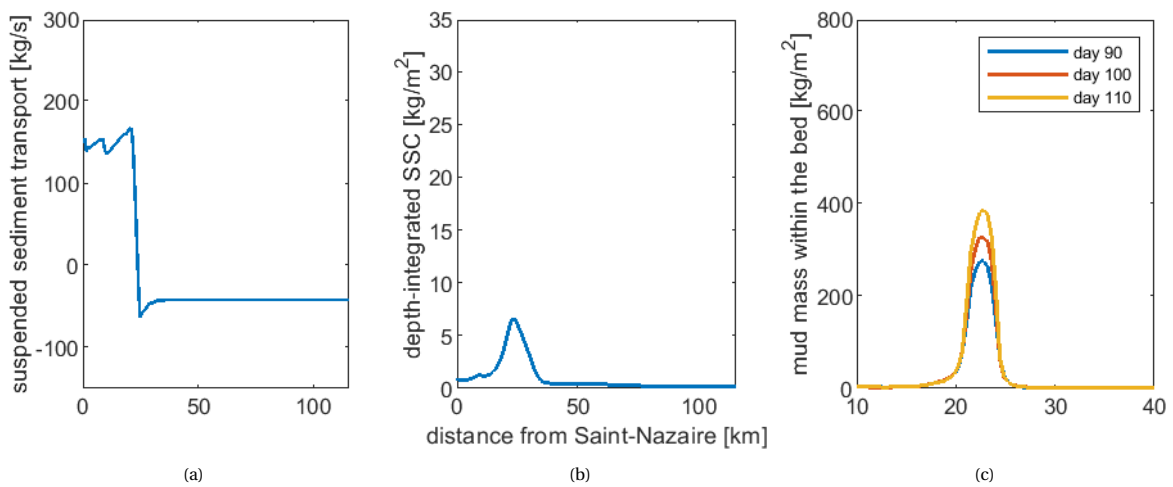


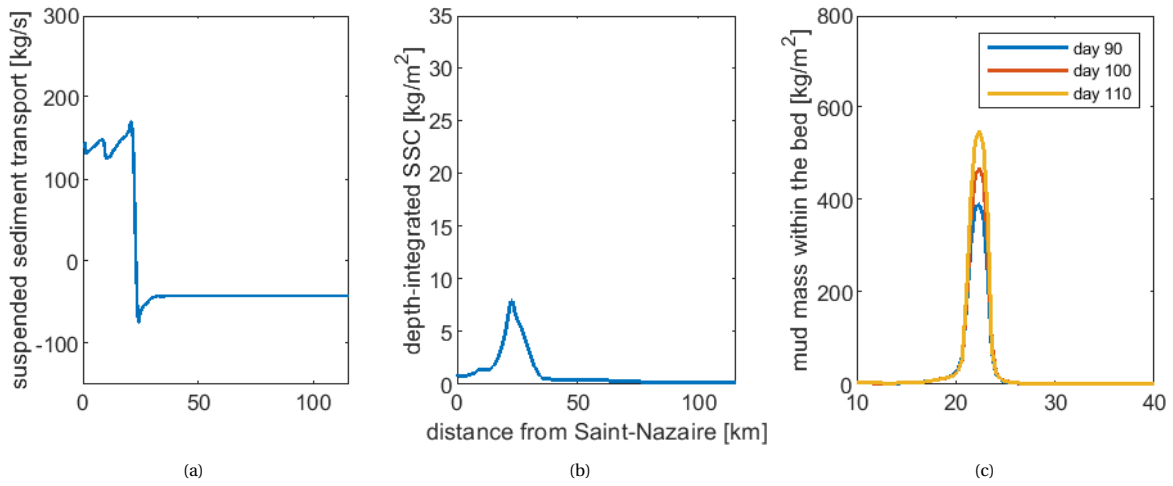
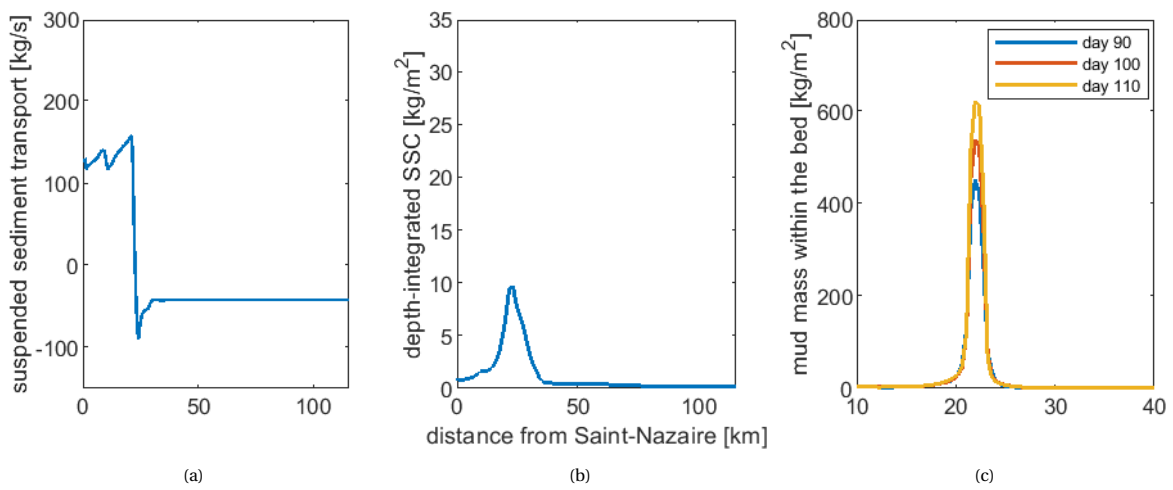
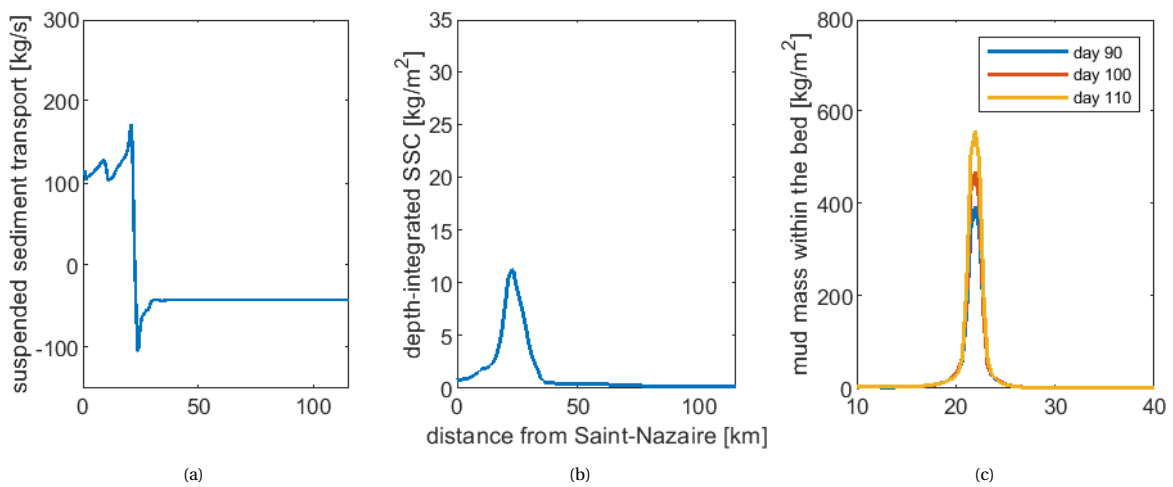
Figure C.5: $Q = 1500 \text{ m}^3/\text{s}$

Figure C.6: $Q = 3000 \text{ m}^3/\text{s}$ Figure C.7: $Q = 4000 \text{ m}^3/\text{s}$ Figure C.8: $Q = 6000 \text{ m}^3/\text{s}$

C.2. M2 component

Figure C.9: $a_{M2} = 1.35$ mFigure C.10: $a_{M2} = 1.40$ m

Figure C.11: $a_{M2} = 1.45$ mFigure C.12: $a_{M2} = 1.50$ mFigure C.13: $a_{M2} = 1.55$ m

Figure C.14: $a_{M2} = 1.60$ mFigure C.15: $a_{M2} = 1.65$ mFigure C.16: $a_{M2} = 1.70$ m

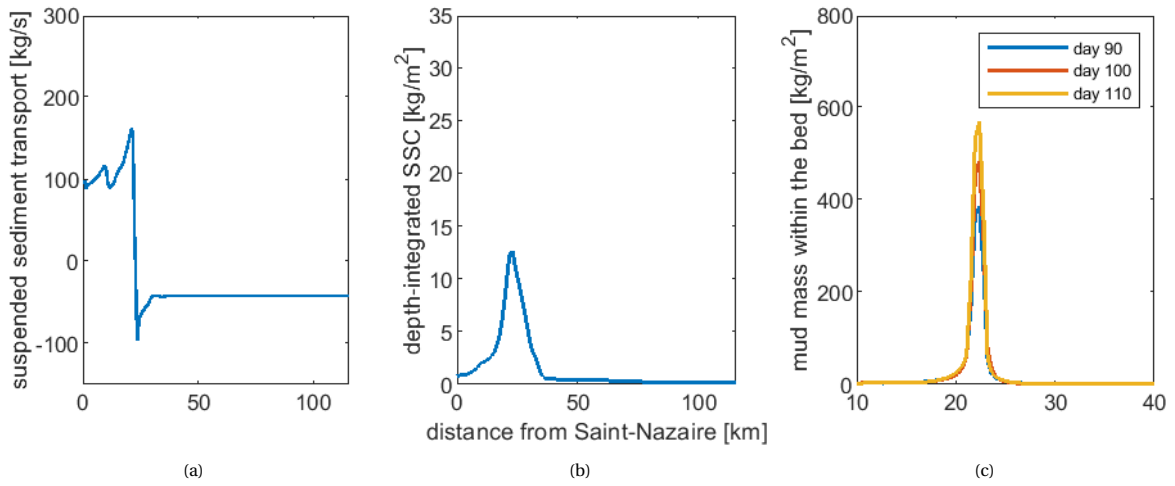


Figure C.17: $a_{M2} = 1.75$ m

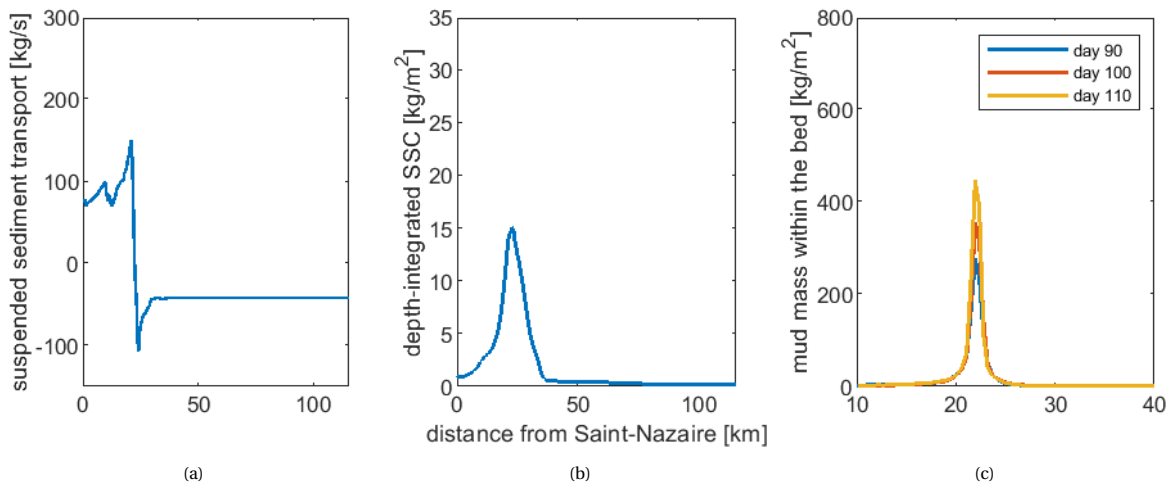


Figure C.18: $a_{M2} = 1.80$ m

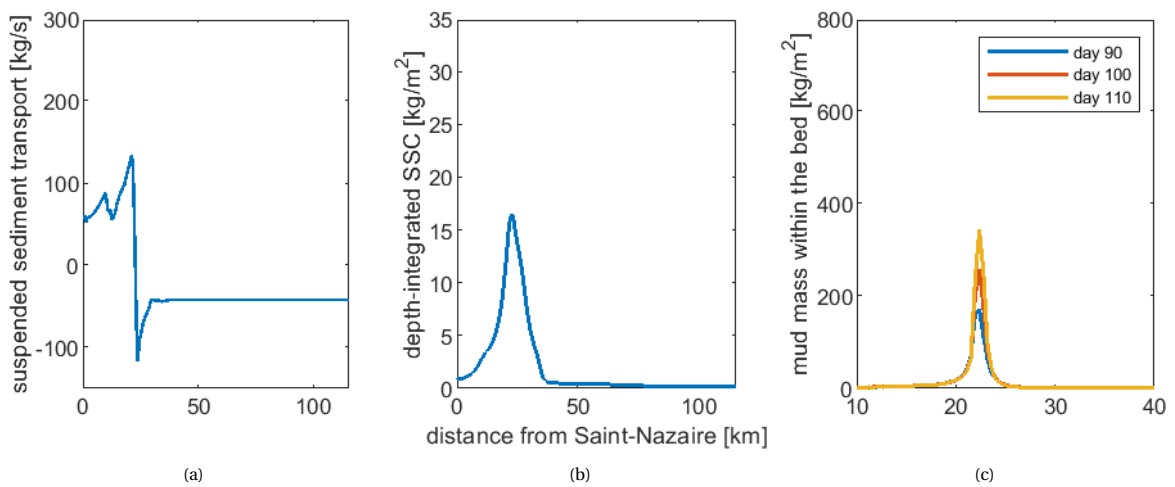
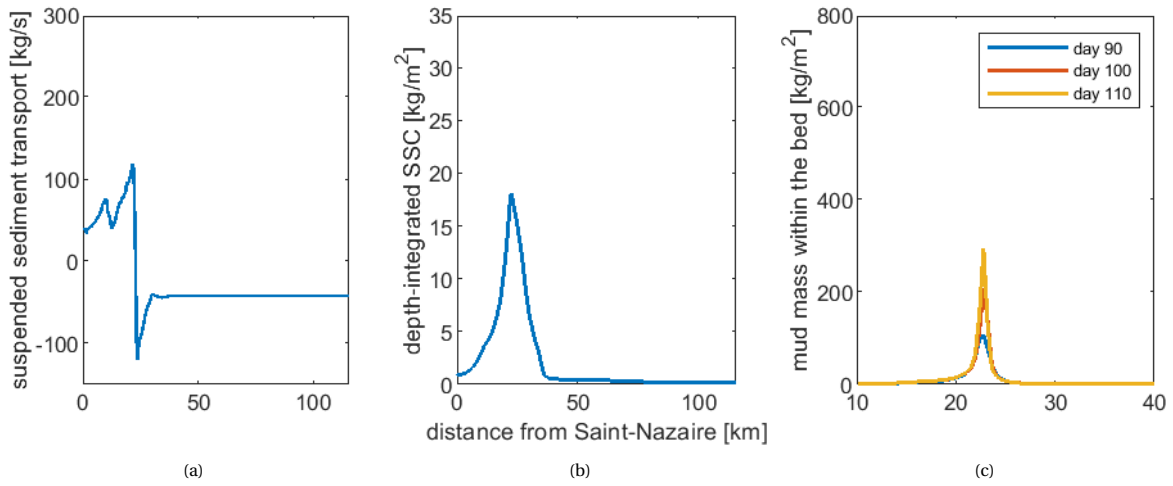
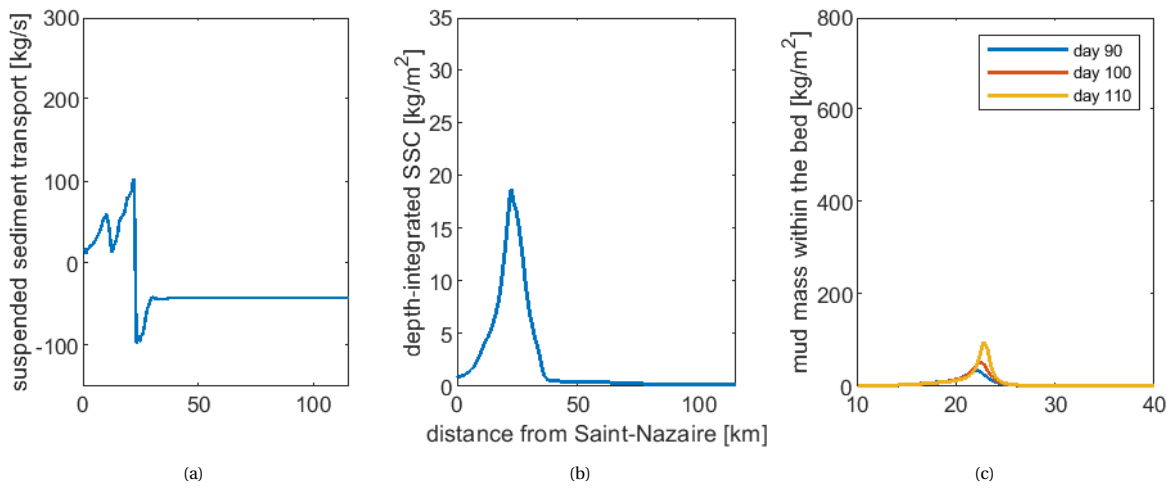


Figure C.19: $a_{M2} = 1.85$ m

Figure C.20: $a_{M2} = 1.90$ mFigure C.21: $a_{M2} = 1.95$ m

C.3. M2, M4 and S2 component

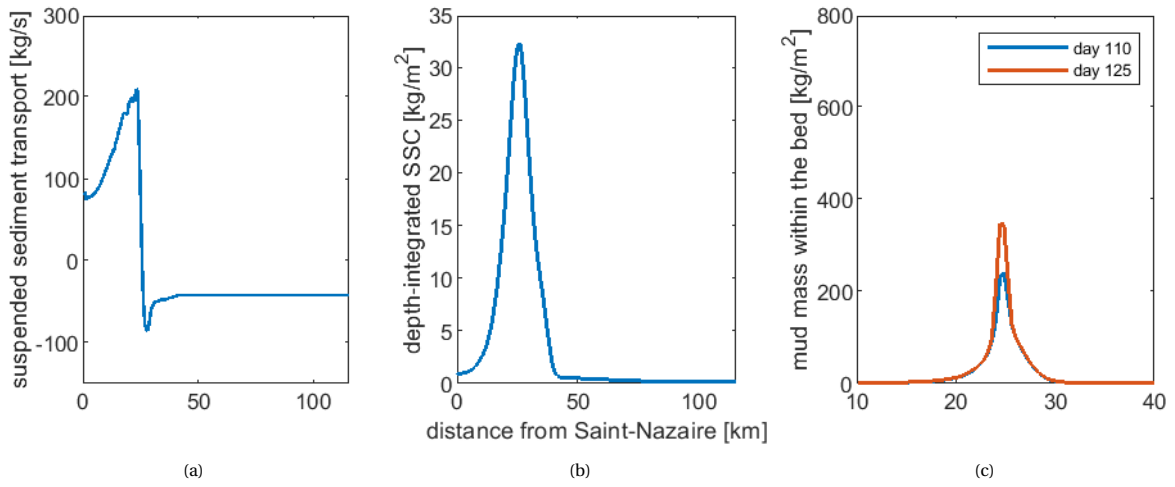
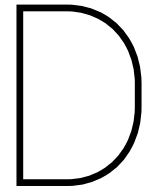


Figure C.22: $a_{M2} = 1.75$ m, $a_{M4} = 0.2$ m, $a_{S2} = 0.63$ m. All parameters are averaged over an entire spring-neap tidal cycle.



Analysis of salt transport with sediment tracer simulations

To investigate the relative influence of tide- and density-driven processes on the transport of salt, simulations are carried out in which salt is replaced with a sediment fraction that mimics the salt behaviour. The settling velocity of the sediment fraction is set to zero and its concentration at the boundary is set equal to the boundary condition for salinity used in the simulations with salt. Furthermore, the density of the sediment is such that the resulting fluid density (when density effects are included) is equal to that of salt water with the same concentration.

The advantage of this substitution is that the effect of sediment on fluid density can be switched off, which cannot be done easily for salt. In this way, the effect of tidal processes on the import of salt can be assessed separately from the effect of density-driven processes.

With this sediment tracer, simulations are carried out for the reference (current) situation (Section D.1), a situation where bed levels in the estuary are raised by 3 m (Section D.2) and a situation where tidal flats are restored (Section D.3). For each situation, first, the results of an ordinary simulation with salt are shown. Subsequently, results are shown for a simulation where salt is replaced with sediment, while keeping the effect of sediment on fluid density switched on. These results are the same as those of the ordinary simulation, proving that the sediment works well as a tracer for salt. Finally, the results of a simulation where the effect of sediment on fluid density is switched off are given. In this simulation, density-driven processes are excluded from the mechanisms for salt transport, such that only tidal processes can lead to import of salt. The difference between the simulations with and without density effects thus shows the influence of density-driven processes.

D.1. Reference simulation: current situation

When comparing Figure D.2 and D.3, it can be seen that density-driven processes have a significant impact on hydrodynamics and the import of salt. With density-driven processes included, mean velocities in the estuary are highly affected and salt intrudes about 15 km further than when these processes are excluded. These results show that in the current state of the estuary, the gravitational circulation has a large influence on salt and sediment transport.

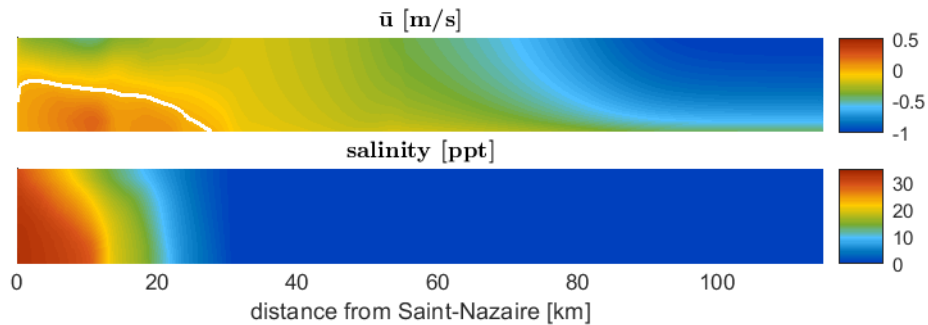


Figure D.1: Mean horizontal velocity and tidally averaged salinity for the reference scenario, representing the current state of the river-estuary. The zero-velocity contour is indicated in white.

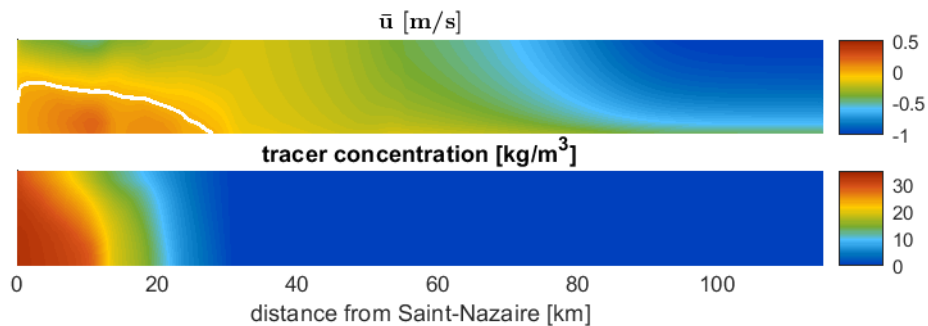


Figure D.2: Mean horizontal velocity and tidally averaged sediment concentration for the reference scenario, where salt is replaced by a sediment fraction. The effect of sediment on fluid density is switched on.

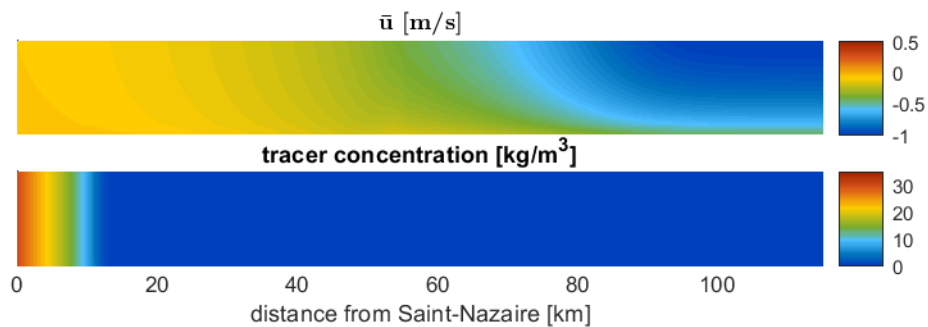


Figure D.3: Mean horizontal velocity and tidally averaged sediment concentration for the reference scenario, where salt is replaced by a sediment fraction. The effect of sediment on fluid density is switched off.

D.2. Estuarine bed elevation

When bed levels in the estuary are raised by 3 m, transport of salt by tidal processes is not affected much, as can be seen from a comparison between Figure D.3 and D.6. In both the current (deep) and historical (shallow) situation, tidal processes lead to a salt intrusion of about 10 km. However, where in the current situation (Section D.1) the inclusion of density-driven processes leads to a significant increase in salt intrusion length and a change in the direction of mean near-bed velocities in the estuary, in the historical (shallow) situation these processes have a much smaller influence. Salt intrusion increases by a few km only and only over a small area mean horizontal velocities become landward-directed (see Figure D.4 and D.5). It can be concluded that the influence of the gravitational circulation on the transport of salt and sediment has increased largely after the estuary was deepened in the past.

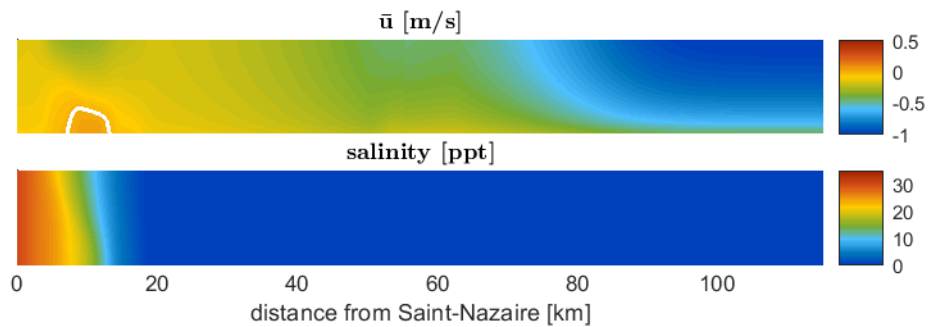


Figure D.4: Mean horizontal velocity and tidally averaged salinity for a simulation where bed levels in the estuary are raised by 3 m, representing the state of the river-estuary before deepening had taken place. The zero-velocity contour is indicated in white.

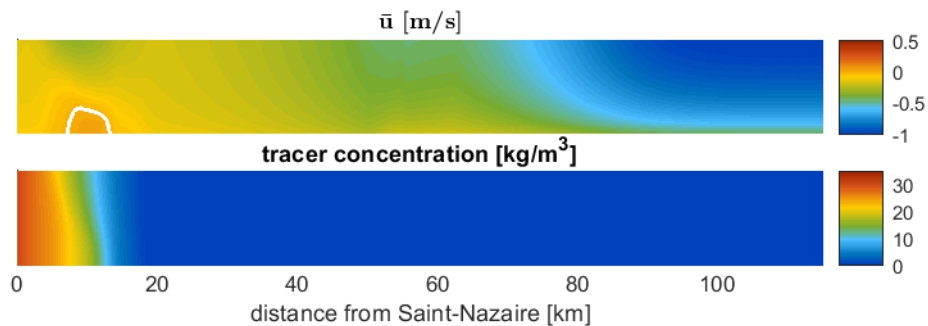


Figure D.5: Mean horizontal velocity and tidally averaged sediment concentration for the shallow estuary scenario, where salt is replaced by a sediment fraction. The effect of sediment on fluid density is switched on.

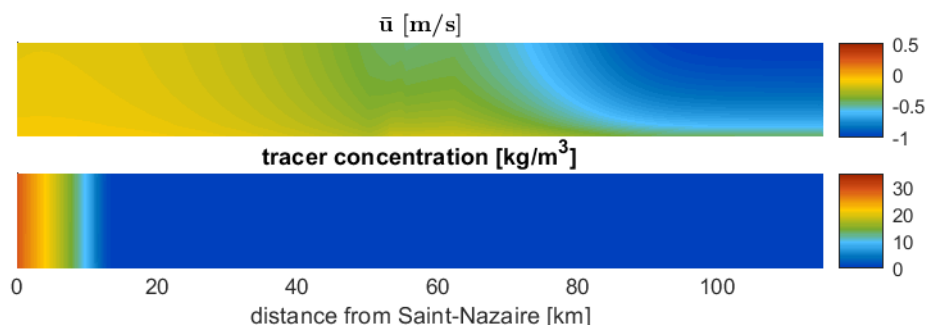


Figure D.6: Mean horizontal velocity and tidally averaged sediment concentration for the shallow estuary scenario, where salt is replaced by a sediment fraction. The effect of sediment on fluid density is switched off.

D.3. Tidal flat restoration

In a situation where tidal flats in the estuary are restored, the same conclusions can be drawn as for the situation where bed levels in the main channel are raised (Section D.2). With respect to the current situation (Section D.1), the influence of tidal processes on salt intrusion has not changed significantly (compare Figure D.3 and D.9), whereas the influence of density-driven processes is smaller in the tidal flat restoration scenario than in the current situation (compare Figure D.2 and D.8). The difference with the current situation is somewhat smaller than for the situation where bed levels are raised, but it is nevertheless significant. Hence, it can be concluded that both reclamation of intertidal area and deepening of the estuary have led to an increased influence of the gravitational circulation on the import of salt and sediment, whereas the influence of the tide on these processes has not changed significantly.

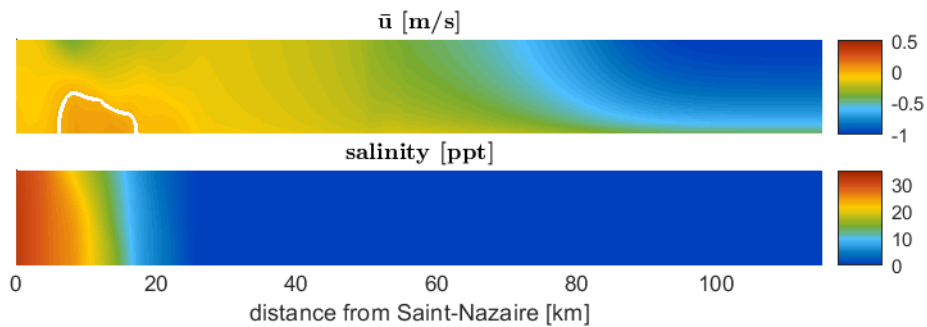


Figure D.7: Mean horizontal velocity and tidally averaged salinity for a simulation where tidal flat area in the estuary is restored. The zero-velocity contour is indicated in white.

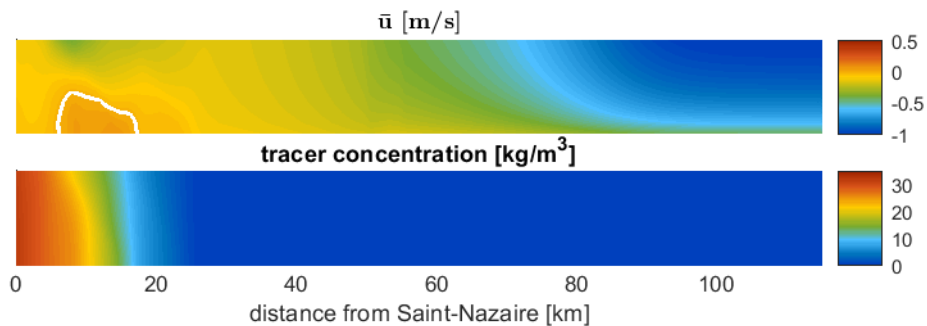


Figure D.8: Mean horizontal velocity and tidally averaged sediment concentration for the tidal flat restoration scenario, where salt is replaced by a sediment fraction. The effect of sediment on fluid density is switched on.

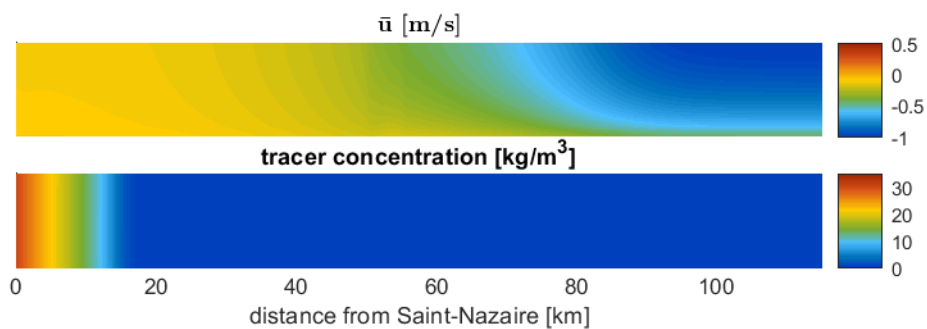


Figure D.9: Mean horizontal velocity and tidally averaged sediment concentration for the tidal flat restoration scenario, where salt is replaced by a sediment fraction. The effect of sediment on fluid density is switched off.